VIRGINIA DIVISION OF MINERAL RESOURCES PUBLICATION 78

GEOCHEMISTRY AND RADIOACTIVITY IN THE POWHATAN AREA, VIRGINIA

Jan Krason, Stanley S. Johnson, Patrick D. Finley,
and John D. Marr, Jr.

COMMONWEALTH OF VIRGINIA

DEPARTMENT OF MINES, MINERALS AND ENERGY
DIVISION OF MINERAL RESOURCES

Robert C. Milici, Commissioner of Mineral Resources and State Geologist

CHARLOTTESVILLE, VIRGINIA
1988

VIRGINIA DIVISION OF MINERAL RESOURCES PUBLICATION 78

GEOCHEMISTRY AND RADIOACTIVITY IN THE POWHATAN AREA, VIRGINIA

Jan Krason, Stanley S. Johnson, Patrick D. Finley,
and John D. Marr, Jr.

COMMONWEALTH OF VIRGINIA

DEPARTMENT OF MINES, MINERALS AND ENERGY
DIVISION OF MINERAL RESOURCES

Robert C. Milici, Commissioner of Mineral Resources and State Geologist

CHARLOTTESVILLE, VIRGINIA
1988

FRONT COVER: Typical field environment in the project area. The beaver pond shown is on a tributary of Fighting Creek just south of drill site 2. Ponds of this type are common in the Fighting Creek drainage area. The drill rig shown was utilized for coring operations (rig shown at drill site 1).

VIRGINIA DIVISION OF MINERAL RESOURCES PUBLICATION 78

GEOCHEMISTRY AND RADIOACTIVITY IN THE POWHATAN AREA, VIRGINIA

Jan Krason, Stanley S. Johnson, Patrick D. Finley,
and John D. Marr, Jr.

COMMONWEALTH OF VIRGINIA

DEPARTMENT OF MINES, MINERALS AND ENERGY
DIVISION OF MINERAL RESOURCES

Robert C. Milici, Commissioner of Mineral Resources and State Geologist

CHARLOTTESVILLE, VIRGINIA
1988

DEPARTMENT OF MINES, MINERALS AND ENERGY
RICHMOND, VIRGINIA
O. GENE DISHNER, Director

Commonwealth of Virginia
Department of Purchases and Supply
Richmond

Copyright 1988
Commonwealth of Virginia

Portions of this publication may be quoted if credit is given to the Virginia Division of Mineral Resources. It is recommended that reference to this report be made in the following form:
Krason, Jan, Johnson, S.S., Finley, P.D., and Marr, J.D., Jr., 1988,
Geochemistry and radioactivity in the Powhatan area, Virginia: Virginia Division of Mineral Resources Publication 78, 60 p.

CONTENTS

	Page
Abstract	1
Introduction	1
Data base	3
Aeroradiometric surveys	3
Ground geochemical and radioactivity surveys	3
Drilling and sampling	3
Geology	9
Regional geology	9
Petrography	11
Surficial geology	15
Ground radioactivity	16
Survey grid	16
Radioactivity survey	17
Geochemistry	17
Analytical methods	18
Reliability of data	18
Distribution of elements	19
Uranium	19
Thorium	23
Cobalt and vanadium	27
Elemental relationships	27
Correlation analysis	29
Core samples	29
Stream sediment	31
Soil	31
Core data analysis	31
Drill hole P-1	31
Drill hole P-2	31
Rare-earth elements	33
Summary of geochemistry	42
Discussion	43
Conclusions	48
Acknowledgments	48
References cited	48
Appendix I: Geologic log: Drill hole P-1	50
Appendix II: Geologic log: Drill hole P-2	53
Appendix III: Representative thin section descriptions	57

ILLUSTRATIONS

Plate

1. Soil-sample and drill-hole locations ..... in pocket
2. Location of supplemental, gravel, bedrock, and water samples ..... in pocket
3. Contour map of total-count ground radioactivity ..... in pocket
4. Contour map of uranium concentration ..... in pocket
5. Contour map of thorium concentration ..... in pocket
6. Contour map of the ratio of uranium to thorium ..... in pocket
7. Contour map of the ratio of thorium to uranium ..... in pocket
8. Contour map of vanadium concentration ..... in pocket
9. Contour map of cobalt concentration ..... in pocket

Figure Page

1. Location of study area 1
2. Aeroradiometric contour map of the southwest quadrant of the Powhatan 15-minute quadrangle 2
3. Regional geologic map of the Powhatan study area, Virginia 21
4. Radioactivity and geochemical profile A-A′ 23
5. Radioactivity and geochemical profile B-B′ 24
6. Radioactivity and geochemical profile C-C′ 24
7. Radioactivity and geochemical profile D-D′ 25
8. Radioactivity and geochemical profile E-E′ 25
9. Histogram of uranium content in all samples 26
10. Histogram of uranium content in core, stream sediment, and soil 27
11. Cumulative probability plot for uranium 28
12. Histogram of radiometric uranium content in all samples analyzed 29
13. Histogram of radiometric uranium content in stream sediment, rock chips, and soil 30
14. Histogram of thorium content in all samples 33
15. Histogram of thorium content in core, stream sediment, and soil 34
16. Cumulative probability plot for thorium 35
17. Histogram of radiometric thorium content in all samples analyzed 36
18. Histogram of radiometric thorium content in stream sediment, rock chips, and soil 37
19. Thorium and uranium content and thorium to uranium ratios of cores from drill hole P-1 39
20. Thorium and uranium content and thorium to uranium ratios of cores from drill hole P-2 40
21. Aeroradiometric profile ML-95 44
22. Aeroradiometric profile ML-96 45
23. Aeroradiometric profile ML-97 and geologic cross section 46
24. Photomicrograph of a quartz-feldspar-biotite-garnet gneiss 58
25. Photomicrograph of hydrothermal pyrite vein 59
26. Photomicrograph of microbreccia vein 59
27. Photomicrograph of monazite crystal in a matrix consisting of sericitized orthoclase and quartz 59
28. Photomicrograph of orthoclase crystal surrounded by rim of biotite and microcline 60
29. Photomicrograph of pyroxene (?) crystal with biotite inclusions 60

TABLES

Page

1. Geochemical analyses of soil, stream sediment, and rock samples 4
2. Geochemical analyses of core samples from drill hole P-1 10
3. Detection limit and method of analyses (samples P-1-15 through P-1-18 and P-2-15 through P-2-21) 12
4. Detection limit and method of analyses (samples P-1-1 through P-1-14 and P-2-1 through P-2-14) 13
5. Mineralogy of selected samples from drill hole P-1 14
6. Geochemical analyses of core samples from drill hole P-2 14
7. Mineralogy of selected samples from drill hole P-2 16
8. Geochemical analyses of supplementary samples 18
9. Analysis of water samples 20
10. Modal analyses of samples from drill hole P-1 22
11. Modal analyses of samples from drill hole P-2 22
12. Gamma-ray spectrometer survey 32
13. Correlation matrix of selected geochemical values of stream sediment samples 38
14. Correlation matrix of selected geochemical values of soil samples 38
15. Correlation matrix of radioactive and selected rare-earth elements in 11 core samples 41
16. Relative distribution of selected rare-earth elements in core samples and Amelia County monazite 42

GEOCHEMISTRY AND RADIOACTIVITY IN THE POWHATAN AREA, VIRGINIA

Jan Krason[1], Stanley S. Johnson[2], Patrick D. Finley[1] and John D. Marr, Jr.[2]

ABSTRACT

Anomalous radioactivity resulting from thorium and uranium was detected in a 1974 aeroradiometric survey in an area of crystalline rocks in the Piedmont just southwest of Powhatan, Virginia. Geological, geochemical, and ground radiometric surveys of a 3.8-square-mile area were done during 1976 through 1978. The geochemical survey included samples of soil, stream sediment, and rock outcrops. The samples (336) were analyzed for uranium, thorium, cobalt, vanadium, molybdenum, and 11 of these samples were analyzed for gold. Total-count ground radioactivity readings define a distinct northeastward-trending linear anomaly. The radiometric anomaly lies on the axis of the Goochland anticline.

In 1986 two core holes were drilled at sites where ground radioactivity, 20 and 80 times regional background, had been measured in 1976 through 1978 and confirmed in 1986. The holes were cored to depths of 140 and 160 feet. Selected samples of core were analyzed geochemically for as many as 49 elements. A petrographic analysis was made of selected samples of core. In the fall of 1986, additional soil, stream gravel, and water samples were collected from the area for analysis.

The results of the surveys and analyses indicate that the radioactivity is mainly caused by the thorium that is present in monazite. The monazite is present in the Maidens gneiss. In one thin section, it constitutes 10.3 percent. The part of the Maidens gneiss which coincides with the radiometric anomaly lies along the crest of the Goochland anticline, suggesting structural control of the surface distribution of the zone enriched in monazite. Resistant monazite grains were probably concentrated in the residual soil and in stream sediments after weathering of the gneiss.

INTRODUCTION

The Powhatan study area is located about 30 miles west of Richmond, Virginia. The survey area is bounded on the north and west by State Highway 13, and to the northeast by the town of Powhatan. The southern boundary is along State Road 718, and State Road 620 defines the eastern boundary (Plate 1). Powhatan County is located within the Piedmont physiographic province, a moderately high plateau underlain by weathered crystalline rocks that is intricately dissected by many streams. The upland areas between the streams are moderately wide with gently rolling topography, and the drainage pattern is dendritic and irregularly branched. The highest elevation in the project area, greater than 390 feet, occurs near the intersection of U.S. highways 60 and 522. The lowest elevation, less than 230 feet, is at Fighting Creek, in the southeastern part of the Powhatan 7.5-minute quadrangle.

In 1976 the area was chosen for uranium mineral exploration by Wyoming Mineral Corporation based on the results of a 1974 aeroradiometric survey flown by the Virginia Division of Mineral Resources (Virginia Division of Mineral Resources, 1975). This survey indicated high radioactivity anomalies attributed to thorium and uranium in an area southwest of Powhatan (Figures 1 and 2). The airborne data indicate that total-count anomalies near Powhatan were approximately twice the regional background that was established by the survey.

To assess the uranium potential of the Powhatan anomalies, Geoexplorers International, Inc. conducted a detailed geological, geochemical, and ground radioactivity survey from 1976 through 1978 for Wyoming Mineral Corporation. The Division of Mineral Resources added to the data base in 1986 by core drilling and by additional geological and geochemical surveys. The Division's interest in the area was based on potential uranium enrichment and on possible environmental problems that might be caused by the radioactivity and its potential impact on the increased residential growth in the county.

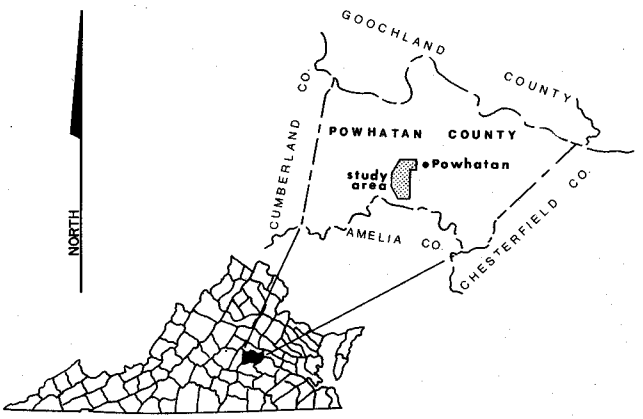

Figure 1. Location of study area in Powhatan County, Virginia.

1. Geoexplorers International, Inc., 5701 E. Evans Ave., Denver, Colorado 80222
2. Virginia Division of Mineral Resources, McCormick Road, Charlottesville, Virginia 22903

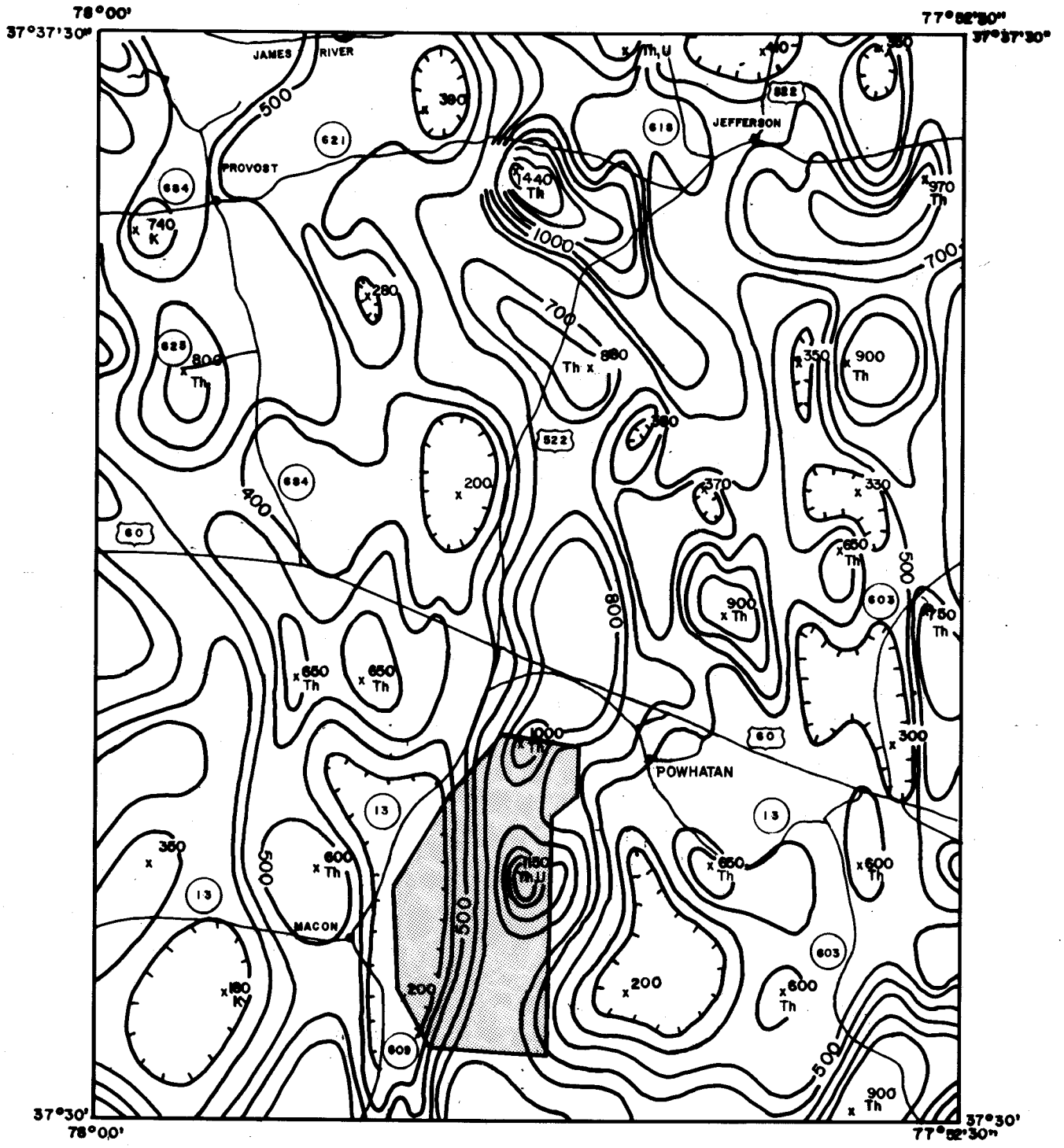

Figure 2. Aeroradiometric contour map of the southwest quadrant of the Powhatan 15-minute quadrangle. Survey: flown June, 1974, contour interval 50 and 100 cps; flight-line spacing 0.5 mile, altitude 500 feet A.M.T.; radionuclides: K-potassium 40, Th-thorium (^{208}Tl), U-uranium (^{214}Bi); study area is shaded; contour map modified from open-file map of Powhatan quadrangle, Virginia Division of Mineral Resources, 1975.

DATA BASE

Aeroradiometric Surveys

The 1974 aeroradiometric survey, flown by LKB Resources, Inc., under contract to the Virginia Division of Mineral Resources, utilized a four-channel, gamma-ray spectrum analyzer installed in a modified twin-engine Aero Commander 680E aircraft. The airborne detector used in this survey contained a sensor with a crystal volume of 256 cubic inches. The thallium-activated sodium iodide crystals were coupled to photomultiplier tubes. The window settings for the spectrometer were established in accordance with the manufacturer's recommendations. A 35-mm continuous strip camera was used to record the flight path of the aircraft. The distance from aircraft to ground was continuously recorded by radar and differential-pressure altimeters. The survey was flown in an east-west direction at an altitude of 500 feet. The flight lines were spaced at 0.5 mile, and sufficient tie lines were flown to cover the survey area. The flight path was recovered by matching images on the 35-mm tracking camera film with 1:24,000 scale, U.S. Geological Survey topographic maps. Total-count aeroradiometric maps were hand-contoured and the associated uranium (^{214}Bi), potassium (^{40}K), or thorium (^{208}Tl) highs were labeled as determined by visual inspection of the analog charts. The final maps were produced at a scale of 1:62,500, with a 1:250,000 composite (Virginia Division of Mineral Resources, 1975).

In 1975 the U.S. Energy Research and Development Administration (ERDA) released the results of an aeroradiometric and aeromagnetic survey that included parts of Triassic basins in South Carolina, North Carolina, and Virginia. The survey also covered the Powhatan area. This survey was part of the aerial radiometric survey program of the National Uranium Resource Evaluation Program (NURE). This survey utilized 3320 cubic inches of sensing crystal with computer-controlled airborne equipment. The flight lines were flown in an east-west direction at 400 feet above ground and were spaced at 2-mile intervals. The survey data were released as flight-line profiles at a scale of 1:250,000 (Geodata International, Inc., 1975).

Ground Geochemical and Radioactivity Surveys

In 1976 Wyoming Mineral Corporation contracted Geoexplorers International, Inc. to perform a reconnaissance survey of the Powhatan radiometric anomalies as part of an exploration program for potential uranium deposits in the eastern United States. Eight samples of soil and stream sediment were collected in the reconnaissance phase of the program. The analyses of these samples showed that the main radioactivity source was thorium (1400 ppm in stream sediment) but also indicated as much as 28 ppm of uranium in the stream sediment (60 ppm by radiometric assay) and 20 ppm of uranium and 480 ppm of thorium in the residual soil. The uranium values reported from the original eight reconnaissance samples were considered to be anomalous because of the high mobility of uranium in warm and humid climatic conditions, such as those that exist in the Piedmont of Virginia, whereas thorium is usually considered stable.

Additional detailed aeroradiometric data were obtained over the area in 1977 by Wyoming Mineral Corporation to complement those obtained by the Division of Mineral Resources in 1974. The airborne data from the 1974, 1975, and 1977 surveys indicate elevated radioactivity at the Powhatan site and areas to the north and south when compared with adjacent areas.

A detailed geological investigation was undertaken by Geoexplorers International over an area of approximately 4 square miles just southwest of Powhatan (Figure 2). The detailed 1977 investigations were based on the results obtained from the reconnaissance samples and the additional airborne data. In addition to the geologic investigation, systematic and detailed ground radiometric and geochemical surveys were done over the project area.

A total of 336 samples were collected in 1977 and 1978 and were analyzed for uranium, thorium, cobalt, vanadium, molybdenum; also 11 samples were analyzed for gold (Table 1). Samples of soil, stream sediment, and rock outcrops were analyzed, and these data are presented and discussed in this report.

Drilling and Sampling

In June 1986 two NX-diameter core holes (P-1 and P-2, Plate 1) were drilled to obtain samples. The core holes were drilled in areas where the total-count ground radioactivity was 80 times (P-1) and 20 times (P-2) the average background (Plate 3). The drilling sites were selected solely on the basis of ground radioactivity.

The cores from these two holes were logged and sampled (Appendices I and II). Eighteen samples from P-1 were selected for geochemical analyses (Tables 2, 3, and 4), six samples were analyzed by X-ray diffraction, and 13 thin sections were made for petrographic analysis (Table 5). Twenty-one samples from P-2 were selected for geochemical analyses (Table 6), 12 samples were analyzed by X-ray diffraction, and 26 thin sections were made for petrographic analysis (Table 7). Additional geological observations and geochemical samples, including water samples and ground radioactivity

Table 1. Geochemical analyses of soil, stream sediment, and rock samples.

Sample Number	Location Latitude ° ' "	Longitude ° ' "	Co	V_2O_5	U	U_3O_8	eU	Th	eTh	Mo	Au
4901 G	37 32 07.5	77 56 54.4	4	165	3.5	4.0		90		<1	.04
4902 S	37 32 04.5	77 56 50.6	8	170	1.3	1.5		100		<1	
4903 G	37 32 03.1	77 56 53.0	18	375	2.5	3.0		85		<1	.07
4904 S	37 32 00.8	77 56 54.9	25	680	1.7	2.0		115		<1	
4905 S	37 32 01.0	77 56 56.5	19	365	2.1	2.5		100		<1	
4906 S	37 31 58.4	77 56 55.7	12	265	2.1	2.5		75		<1	
4907 S	37 31 55.5	77 56 53.5	12	220	2.1	2.5		60		<1	
4908 S	37 31 54.5	77 56 49.1	15	280	1.7	2.0		95		<1	
4909 S	37 31 51.0	77 56 49.6	12	410	1.3	1.5		100		1	
4910 S	37 32 01.0	77 56 31.0	10	190	2.5	3.0		80		<1	
4911 S	37 32 01.6	77 56 35.0	16	230	4.2	5.0		100		<1	
4912 S	37 32 02.5	77 56 39.0	7	190	4.2	5.0		80		<1	
4913 S	37 32 03.2	77 56 43.0	9	250	3.4	4.0		70		<1	
4914 S	37 32 06.8	77 56 44.3	13	430	3.8	4.5		95		1	
4915 S	37 32 09.7	77 56 43.0	14	320	3.8	4.5		85		1	
4916 S	37 31 54.9	77 56 32.5	13	270	2.1	2.5		75		<1	
4917 S	37 31 55.5	77 56 36.4	15	230	3.4	4.0		75		<1	
4918 S	37 31 56.3	77 56 40.5	17	290	5.4	7.0		70		<1	
4919 S	37 31 57.0	77 56 44.5	25	220	2.1	2.5		60		<1	
4920 S	37 31 51.6	77 56 53.7	12	270	3.4	4.0		105		<1	
4921 G	37 31 52.0	77 56 56.3	15	280	7.2	8.5		115		<1	.04
4922 S	37 31 52.9	77 57 01.6	17	290	2.1	2.5		85		<1	
4923 S	37 31 53.0	77 57 05.8	25	300	2.1	2.5		100		<1	
4924 S	37 31 54.2	77 57 09.8	35	560	2.1	2.5		95		<1	
4925 S	37 31 55.0	77 57 13.7	15	260	2.1	2.5		95		<1	
4926 S	37 31 48.4	77 56 34.0	13	190	2.5	3.0		85		<1	
4927 S	37 31 49.0	77 56 38.0	19	270	2.5	3.0		50		<1	
4928 S	37 31 49.7	77 56 42.1	14	310	2.5	3.0		75		<1	
4929 S	37 31 50.5	77 56 45.9	12	270	4.7	5.5		85		<1	
4930 G	37 31 46.0	77 56 50.9	10	120	18.7	22.0		100		3	
4931 S	37 31 44.0	77 56 47.5	30	350	2.5	3.0		85		<1	
4932 S	37 31 43.4	77 56 43.5	30	410	3.4	4.0		85		<1	
4933 S	37 31 42.6	77 56 39.7	30	300	3.4	4.0		85		<1	
4934 S	37 31 42.0	77 56 35.6	12	180	2.5	3.0		65		<1	
4935 S	37 31 35.5	77 56 37.4	20	320	3.8	4.5		85		<1	
4936 S	37 31 36.1	77 56 41.3	14	260	5.0	6.0		90		<1	
4937 G	37 31 36.6	77 56 45.4	18	250	6.4	7.5		100		<1	.04
4938 S	37 31 37.5	77 56 49.0	25	330	2.1	2.5		80		2	
4939 S	37 31 38.0	77 56 58.0	20	200	2.1	2.5		85		<1	
4940 S	37 31 38.5	77 56 57.1	30	230	2.5	3.0		75		<1	
4941 S	37 31 39.5	77 57 00.9	15	220	2.1	2.5		80		<1	
4942 S	37 31 33.0	77 57 02.5	15	270	2.1	2.5		95		<1	
4943 S	37 31 32.4	77 56 58.6	13	230	2.5	3.0		75		<1	
4944 S	37 31 31.7	77 56 54.8	13	280	2.5	3.0		90		<1	
4945 S	37 31 31.1	77 56 50.5	20	160	2.1	2.5		85		<1	
4946 S	37 31 30.5	77 56 46.7	25	260	2.1	2.5		85		<1	
4947 S	37 31 30.0	77 56 42.6	18	160	3.8	4.5		90		<1	
4948 G	37 31 26.6	77 56 39.3	16	130	3.8	4.5		90		<1	.08
4949 S	37 31 21.0	77 56 38.2	15	240	6.4	7.5		85		<1	
6801 S	37 32 01.5	77 56 27.0	12	155	3.8	4.5	10	80	50	<1	
6802 S	37 31 54.3	77 56 28.6	15	155	4.7	5.5	< 10	75	50	<1	
6803 S	37 31 48.9	77 56 29.7	13	95	5.4	7.0	140	85	660	<1	
6804 S	37 31 49.1	77 56 30.2	12	150	3.8	4.5	60	75	230	<1	
6805 S	37 31 49.1	77 56 29.5	12	117	2.5	3.0	60	50	230	<1	
6806 G	37 31 49.8	77 56 29.6	14	200	4.2	5.0	50	90	170	<1	
6807 S	37 31 47.8	77 56 30.1	16	320	2.5	3.0	< 10	70	30	1	
6808 S	37 31 41.0	77 56 31.8	12	315	3.4	4.0	< 10	75	40	2	
6809 S	37 31 37.9	77 56 32.5	9	130	4.7	5.5	30	80	100	<1	
6810 S	37 31 34.9	77 56 33.2	17	165	5.4	7.0	20	90	50	2	
6811 S	37 31 28.8	77 56 34.5	10	315	4.2	5.0	20	70	50	2	
6812 S	37 31 23.4	77 56 35.7	15	155	5.5	6.5	20	100	60	<1	

Sample Number	Location Latitude ° ' "	Longitude ° ' "	Co	V_2O_5	U	U_3O_8	eU	Th	eTh	Mo	Au
6813 S	37 31 21.0	77 56 36.4	30	280	1.7	2.0	< 10	45	20	12	
6814 S	37 31 16.0	77 56 37.5	15	140	4.2	5.0	< 10	80	40	1	
6815 S	37 31 10.0	77 56 38.9	11	270	5.5	6.5	10	75	30	1	
6816 S	37 31 07.6	77 56 39.4	15	190	5.0	6.0	< 10	75	20	<1	
6817 S	37 31 05.1	77 56 40.0	30	200	5.0	6.0	10	95	50	<1	
6818 S	37 31 01.2	77 56 41.0	25	250	3.4	4.0	10	90	40	<1	
6820 G	37 32 08.8	77 56 25.1	25	200	8.8	10.0	80	85	250	1	
6821 S	37 32 13.2	77 56 24.0	14	190	5.0	6.0	10	75	50	<1	
6822 S	37 32 19.0	77 56 22.5	7	195	6.8	8.0	20	80	50	1	
6823 S	37 32 26.0	77 56 20.7	12	340	4.2	5.0	< 10	90	50	3	
6824 G	37 32 29.0	77 56 20.0	17	230	5.5	6.5	20	80	120	1	.07
6825 S	37 32 32.1	77 56 19.4	9	220	4.7	5.5	10	75	30	<1	
6826 S	37 32 38.4	77 56 17.5	19	210	3.8	4.5	10	95	60	1	
6827 G	37 32 38.9	77 56 17.1	10	180	11.4	13.5	90	90	350	1	
6828 S	37 32 45.1	77 56 16.0	12	270	5.0	6.0	10	80	40	1	
6829 S	37 32 51.8	77 56 14.5	7	120	[illegible]	5.0	< 10	80	40	<1	
6830 S	37 32 52.8	77 56 21.9	14	380	2.1	2.5	< 10	90	30	2	
6831 G	37 32 51.3	77 56 22.0	15	180	13.1	15.5	150	95	610	<1	.07
6832 S	37 32 46.6	77 56 23.8	10	280	3.4	4.0	10	75	20	2	
6833 S	37 32 39.7	77 56 25.7	10	245	3.4	4.0	10	80	20	1	
6834 S	37 32 33.3	77 56 27.0	18	250	3.9	4.5	< 10	75	20	1	
6835 G	37 32 31.0	77 56 27.5	18	240	9.3	11.0	10	75	80	1	.06
6836 S	37 32 27.0	77 56 28.7	12	205	2.1	2.5	20	90	60	1	
6837 S	37 32 20.2	77 56 26.2	9	155	4.2	5.0	10	90	50	<1	
6838 S	37 32 14.7	77 56 31.7	12	300	3.8	4.5	< 10	75	20	1	
6839 S	37 32 08.2	77 56 33.3	14	215	2.1	2.5	< 10	90	20	<1	
6840 S	37 32 08.1	77 56 39.5	15	240	1.7	2.0	< 10	90	40	<1	
6841 S	37 32 07.5	77 56 29.5	9	130	4.2	5.0	30	95	250	<1	
6842 S	37 32 08.9	77 56 37.0	13	215	4.7	5.5	10	85	40	<1	
6843 S	37 32 11.5	77 56 41.5	13	180	2.1	2.5	< 10	90	30	<1	
6844 S	37 32 14.2	77 56 44.0	10	200	2.1	2.5	< 10	95	30	<1	
6845 S	37 32 15.7	77 56 47.7	10	210	1.7	2.0	10	95	30	<1	
6846 S	37 32 16.6	77 56 51.6	12	135	2.1	2.5	< 10	80	20	<1	
6847 S	37 32 20.5	77 56 51.5	13	170	1.7	2.0	< 10	80	20	<1	
6848 S	37 32 23.0	77 56 52.5	13	180	1.7	2.0	< 10	95	30	<1	
6849 S	37 32 14.9	77 56 53.5	11	155	1.7	2.0	< 10	65	20	<1	
6899 G	37 31 38.0	77 56 24.5	7	125	40.7	48.0	70	115	290	2	
6900 G	37 31 38.5	77 56 26.7	9	160	15.3	18.0	40	85	160	<1	
6901 S	37 31 39.0	77 56 26.5	20	210	3.4	4.0	20	60	80	<1	
6902 S	37 31 40.7	77 56 28.3	10	330	3.4	4.0	< 10	65	40	<1	
6903 S	37 31 34.4	77 56 29.4	12	195	2.1	2.5	< 10	65	20	1	
6904 S	37 31 33.9	77 56 26.6	12	230	2.1	2.5	< 10	50	30	<1	
6905 G	37 31 33.6	77 56 25.5	14	205	6.8	8.0	< 10	80	40	<1	
6906 S	37 31 33.1	77 56 21.3	17	260	4.2	5.0	20	70	80	<1	
6907 S	37 31 32.5	77 56 17.3	25	195	2.5	3.0	10	65	50	<1	
6908 S	37 31 31.9	77 56 13.4	16	195	3.4	4.0	10	75	50	<1	
6909 S	37 31 28.5	77 56 11.7	10	210	3.4	4.0	20	80	50	1	
6910 S	37 31 25.0	77 56 10.7	10	195	2.1	2.5	10	70	40	<1	
6911 S	37 31 22.0	77 56 07.5	14	245	2.5	3.0	20	80	60	1	
6912 S	37 31 16.6	77 56 05.4	11	310	2.1	2.5	10	80	40	<1	
6913 S	37 31 10.4	77 56 00.0	15	265	2.1	2.5	10	100	60	<1	
6914 S	37 30 55.4	77 57 14.0	15	175	1.7	2.0	< 10	90	40	<1	
6915 S	37 30 58.3	77 57 08.2	12	150	1.7	2.0	10	95	40	<1	
6916 S	37 31 01.7	77 57 04.5	17	200	2.1	2.5	< 10	100	30	<1	
6917 S	37 31 03.4	77 57 01.3	12	250	2.1	2.5	< 10	75	30	<1	
6918 S	37 31 03.2	77 57 53.2	14	210	2.1	2.5	< 10	95	40	<1	
6919 S	37 31 03.5	77 56 41.1	18	240	3.4	4.0	< 10	75	40	<1	
6920 S	37 31 03.2	77 56 36.8	19	150	4.2	5.0	20	90	130	<1	
6920 S	37 31 03.2	77 56 36.8	35	275	11.0	13.0		105		1	
6921 S	37 31 02.0	77 56 33.1	65	385	5.5	6.5	20	105	290	1	
6922 S	37 31 01.9	77 56 32.3	80	360	6.8	8.0	30	100	3180	1	
6923 R	37 31 01.5	77 56 33.0	20	115	3.8	4.5	10	25	80	4	

Sample Number	Location Latitude ° ' "	Longitude ° ' "	Co	V_2O_5	U	U_3O_8	eU	Th	eTh	Mo	Au
6924 S	37 31 02.7	77 56 28.8	25	330	3.8	4.5	20	65	10	1	
6925 S	37 31 03.0	77 56 24.3	14	210	8.0	9.5	40	85	180	<1	
6926 S	37 31 03.0	77 56 20.5	20	230	6.8	8.0	20	90	80	<1	
6927 G	37 31 01.0	77 56 16.0	20	245	3.0	3.5	20	85	80	1	
6928 S	37 30 59.9	77 56 17.5	9	420	1.7	2.0	< 10	45	40	2	
6929 S	37 30 56.5	77 56 17.3	13	310	2.1	2.5	< 10	80	40	<1	
6930 S	37 30 53.0	77 56 18.6	9	185	4.7	5.5	20	80	60	<1	
6931 S	37 30 50.5	77 56 22.4	18	270	3.4	4.0	< 10	65	60	1	
6932 S	37 30 47.4	77 56 25.0	6	140	6.0	7.0	10	75	70	1	
6933 S	37 30 44.5	77 56 25.7	8	210	6.0	7.0	10	75	50	<1	
6934 S	37 30 42.3	77 56 26.5	6	180	6.0	7.0	< 10	90	50	<1	
6935 S	37 30 39.9	77 56 26.4	7	210	4.7	5.5	< 10	80	50	1	
6936 G	37 31 02.1	77 56 10.5	25	245	3.4	4.0	< 10	85	30	1	
6937 S	37 31 02.6	77 56 13.0	17	350	3.4	4.0	< 10	80	30	1	
6938 S	37 31 04.0	77 56 16.0	17	325	3.4	4.0	20	70	110	1	
6939 S	37 31 06.0	77 56 19.4	20	260	5.5	6.5	20	80	100	<1	
6940 S	37 31 08.9	77 56 23.3	25	245	5.0	6.0	< 10	70	40	<1	
6941 S	37 31 07.2	77 56 27.3	13	345	3.4	4.0	20	60	30	2	
6942 S	37 31 08.0	77 56 31.3	10	180	5.5	6.5	30	85	60	<1	
6943 S	37 31 08.7	77 56 35.2	8	180	6.0	7.0	20	80	660	<1	
6944 S	37 31 08.8	77 56 37.1	8	315	4.2	5.0	20	80	50	1	
6945 S	37 32 00.0	77 56 23.0	8	125	2.1	2.5	< 10	75	30	1	
6946 S	37 31 58.8	77 56 15.2	9	150	3.8	4.5	20	75	60	<1	
6850 G	37 32 12.2	77 56 57.2	70	300	3.4	4.0	< 10	80	20	<1	.07
6851 S	37 31 16.3	77 56 42.0	7	185	4.2	5.0	10	65	30	<1	
6852 S	37 31 16.9	77 56 48.0	30	250	2.5	3.0	< 10	80	30	1	
6853 S	37 31 17.5	77 56 49.8	15	340	3.8	4.5	< 10	85	20	1	
6854 S	37 31 15.5	77 56 54.1	18	280	1.7	2.0	10	95	10	1	
6855 S	37 31 12.8	77 56 59.5	20	310	2.5	3.0	< 10	90	10	1	
6856 S	37 31 06.0	77 57 01.0	20	250	2.1	2.5	< 10	110	20	<1	
6857 S	37 31 05.3	77 56 56.5	17	215	3.8	4.5	< 10	90	10	<1	
6858 S	37 31 04.3	77 56 52.8	16	205	1.7	2.0	< 10	95	10	<1	
6859 S	37 31 03.7	77 56 49.0	17	240	4.7	5.5	< 10	85	30	<1	
6860 S	37 31 03.4	77 56 45.0	30	245	3.0	3.5	< 10	80	40	<1	
6861 S	37 32 14.0	77 56 28.0	7	120	6.0	7.0	10	90	50	<1	
6862 S	37 32 15.3	77 56 35.6	9	110	5.4	7.0	20	80	30	<1	
6863 S	37 32 15.9	77 56 39.5	7	150	2.5	3.0	10	75	30	<1	
6864 S	37 32 16.5	77 56 43.7	9	185	1.7	2.0	< 10	75	10	<1	
6865 S	37 31 59.5	77 56 18.8	20	240	4.7	5.5	20	90	50	<1	
6866 S	37 31 58.2	77 56 11.4	10	150	3.4	4.0	20	115	30	<1	
6867 S	37 31 56.9	77 56 03.1	16	175	1.7	2.0	< 10	100	30	1	
6868 G	37 31 56.0	77 55 57.1	13	230	2.1	2.5	20	90	20	1	
6869 S	37 31 46.1	77 55 48.9	20	230	3.4	4.0	20	110	70	<1	
6870 G	37 31 45.2	77 55 51.2	15	190	3.4	4.0	20	95	60	<1	.05
6871 S	37 31 41.7	77 55 42.5	16	270	1.7	2.0	10	85	50	1	
6872 S	37 31 39.5	77 55 38.8	15	220	3.4	4.0	10	80	50	<1	
6873 G	37 31 38.0	77 55 34.0	16	250	2.1	2.5	< 10	85	30	1	.02
6874 S	37 31 53.4	77 56 24.7	9	190	5.0	6.0	< 10	85	40	1	
6875 S	37 31 53.0	77 56 21.9	13	245	3.4	4.0	< 10	75	30	<1	
6876 S	37 31 50.0	77 56 19.0	11	180	3.4	4.0	30	85	190	<1	
6877 S	37 31 47.7	77 56 15.2	25	325	1.7	2.0	< 10	90	50	<1	
6878 S	37 31 43.0	77 56 11.1	14	245	2.1	2.5	< 10	85	30	<1	
6879 S	37 31 48.2	77 56 00.0	20	255	1.7	2.0	< 10	80	30	<1	
6880 S	37 31 43.7	77 56 00.7	13	215	3.4	4.0	< 10	75	50	1	
6881 G	37 31 43.0	77 56 00.6	5	95	9.3	11.0	< 10	95	20	<1	
6882 S	37 31 41.5	77 55 57.5	20	300	1.7	2.0	< 10	85	30	<1	
6883 S	37 31 45.7	77 56 26.5	9	95	4.2	5.0	10	65	70	1	
6884 G	37 31 45.2	77 56 27.0	7	110	8.9	10.5	10	90	50	<1	
6885 S	37 31 43.5	77 56 22.8	13	150	3.8	4.5	10	80	50	<1	
6886 G	37 31 43.1	77 56 21.6	40	290	4.2	5.0	50	75	160	2	
6887 S	37 31 40.1	77 56 19.5	11	140	2.5	3.0	20	95	70	<1	
6888 S	37 31 39.0	77 56 15.8	11	300	1.7	2.0	10	90	50	1	

Sample Number	Location Latitude ° ' "	Longitude ° ' "	Co	V_2O_5	U	U_3O_8	eU	Th	eTh	Mo	Au
6889 S	37 31 38.2	77 56 12.0	9	370	2.5	3.0	10	75	40	2	
6890 S	37 31 37.0	77 56 03.9	12	245	3.4	4.0	< 10	65	30	1	
6891 S	37 31 32.0	77 56 05.0	20	210	2.5	3.0	< 10	70	40	1	
6892 G	37 31 31.6	77 56 05.6	12	180	6.8	8.0	10	85	50	1	
6893 S	37 31 30.8	77 56 05.3	25	175	3.4	4.0	10	80	50	<1	
6894 S	37 31 31.4	77 56 10.2	9	200	3.4	4.0	20	80	70	<1	
6895 S	37 31 34.4	77 56 12.2	12	210	2.1	2.5	10	80	60	<1	
6896 S	37 31 36.0	77 56 16.4	11	195	3.4	4.0	10	65	40	<1	
6897 S	37 31 36.2	77 56 20.3	5	120	6.0	7.0	20	65	40	<1	
6898 G	37 31 36.4	77 56 22.6	7	125	4.7	5.5	< 10	75	30	<1	
6947 S	37 32 06.2	77 56 21.4	10	95	3.8	4.5	20	70	40	<1	
6948 S	37 32 04.0	77 56 17.7	13	155	5.5	6.5	20	75	60	<1	
6949 G	37 32 03.9	77 56 17.0	85	230	4.7	5.5	80	75	350	<1	
6950 S	37 32 02.9	77 56 14.0	13	130	3.4	4.0	20	75	60	1	
6951 S	37 32 11.8	77 56 20.3	11	155	5.5	6.5	30	75	90	2	
6952 G	37 32 10.0	77 56 16.4	13	120	12.3	14.5	70	95	270	<1	
6953 S	37 32 10.5	77 56 13.3	11	130	3.0	3.5	20	75	70	<1	
6954 S	37 32 14.5	77 56 18.4	11	110	6.4	7.5	20	70	60	1	
6955 S	37 32 12.8	77 56 15.9	15	145	7.0	8.5	10	75	40	<1	
6956 S	37 32 13.1	77 56 11.6	15	265	3.0	3.5	10	70	10	1	
6957 S	37 32 12.6	77 56 08.0	12	120	4.2	5.0	10	80	50	<1	
6958 G	37 32 11.9	77 56 07.3	12	120	8.5	10.0	340	95	1380	<1	
6959 G	37 32 13.2	77 56 03.4	12	145	10.1	12.0	30	95	130	<1	
6960 G	37 32 06.7	77 55 57.2	6	125	14.4	17.0	40	115	80	<1	
6961 G	37 32 06.6	77 55 56.0	12	210	10.1	12.0	250	150	1240	1	
6962 G*	37 32 08.7	77 55 55.0	8	90	53.4	63.0	800	835	4040	2	
6963 G	37 32 02.5	77 55 57.0	16	215	7.6	9.0	60	90	300	1	
6964 S	37 32 02.6	77 55 59.0	35	300	3.0	3.5	20	75	80	2	
6965 S	37 32 03.1	77 56 01.9	20	160	3.0	3.5	< 10	80	40	<1	
6966 S	37 32 03.6	77 56 05.6	25	330	3.4	4.0	< 10	70	30	2	
6967 S	37 32 04.3	77 56 09.5	12	165	2.1	2.5	10	75	50	4	
6968 S	37 32 05.0	77 56 13.6	25	150	3.0	3.5	< 10	165	80	1	
6969 S	37 32 05.7	77 56 17.5	5	130	4.2	5.0	30	85	70	<1	
6970 S	37 32 04.7	77 56 22.4	11	165	5.0	6.0	20	75	30	4	
6971 G	37 32 17.4	77 56 23.5	13	185	3.8	4.5		80		1	
6972 S	37 32 19.3	77 56 17.9	25	265	3.0	3.5		65		1	
6973 S	37 32 18.4	77 56 14.5	25	310	7.0	8.5		75		1	
6974 G	37 32 21.7	77 56 09.5	16	205	15.7	18.5		90		1	
6975 S	37 32 17.9	77 56 10.5	18	240	3.4	4.0		70		<1	
6976 S	37 32 17.1	77 56 06.4	9	125	7.0	8.5		95		1	
6977 S	37 32 16.6	77 56 02.6	25	310	2.1	2.5		70		1	
6978 S	37 32 16.0	77 55 58.7	15	190	3.4	4.0		75		1	
6979 S	37 32 17.9	77 55 54.0	13	305	3.0	3.5		75		2	
6980 G	37 32 18.2	77 55 52.0	15	180	1.7	2.0		85		<1	
6981 S	37 32 19.0	77 55 49.0	11	130	3.0	3.5		95		<1	
6982 S	37 32 19.0	77 55 45.5	16	270	3.8	4.5		100		2	
6983 S	37 32 20.0	77 55 41.3	25	235	3.0	3.5		85		2	
6984 S	37 32 24.1	77 55 36.0	13	250	2.1	2.5		80		1	
6985 S	37 32 32.0	77 55 35.6	16	150	2.1	2.5		75		<1	
6986 G	37 32 33.2	77 55 37.5	14	215	4.2	5.0		80		1	
6987 S	37 32 34.0	77 55 36.1	6	90	3.0	3.5		80		<1	
6988 G	37 32 33.1	77 55 42.9	18	245	3.0	3.5		80		2	
6989 S	37 32 33.6	77 55 46.8	13	135	0.8	1.0		75		<1	
6990 G	37 32 34.0	77 55 48.3	25	240	6.4	7.5		95		2	
6991 S	37 32 34.9	77 55 53.8	30	225	3.0	3.5		85		<1	
6992 S	37 32 35.2	77 55 58.0	11	155	1.7	2.0		85		1	
6993 S	37 32 34.9	77 56 02.8	15	120	2.5	3.0		80		<1	
6994 S	37 32 28.5	77 55 55.5	15	155	2.1	2.5		75		<1	
6995 S	37 32 27.5	77 56 00.0	16	210	1.7	2.0		100		<1	
6996 S	37 32 28.0	77 56 03.7	18	185	1.7	2.0		80		1	
6997 S	37 32 27.9	77 56 08.0	12	80	1.7	2.0		75		<1	
6998 G	37 32 28.1	77 56 13.5	14	180	6.0	7.0		110		<1	

Sample Number	Location Latitude ° ' "	Longitude ° ' "	Co	V_2O_5	U	U_3O_8	eU	Th	eTh	Mo	Au
9501 S	37 32 28.5	77 56 17.0	14	125	3.4	4.0	20	75	50	<1	
9502 S	37 31 15.3	77 56 33.7	20	175	3.0	3.5	20	70	70	1	
9503 S	37 31 14.6	77 56 29.8	20	220	1.3	1.5	< 10	85	30	1	
9504 S	37 31 19.3	77 56 35.0	20	200	3.4	4.0	130	80	560	1	
9506 S	37 31 24.3	77 56 32.4	9	225	1.7	2.0	< 10	70	30	<1	
9507 G	37 31 27.5	77 56 27.5	10	130	0.8	1.0	50	95	220	<1	
9508 S	37 31 21.0	77 56 28.4	16	105	3.4	4.0	20	70	60	1	
9509 S	37 31 17.3	77 56 26.1	9	80	6.4	7.5	30	80	90	2	
9510 S	37 31 13.7	77 56 26.0	25	130	3.4	4.0	20	80	90	<1	
9511 S	37 31 10.5	77 56 27.0	45	345	4.7	5.5	30	80	90	<1	
9513 S	37 30 29.2	77 55 49.0	11	185	3.0	3.5	20	70	60	2	
9514 R	37 30 26.0	77 55 46.1	9	105	3.0	3.5	20	65	50	1	
9515 G	37 30 24.2	77 55 44.0	12	125	3.4	4.0	< 10	80	30	<1	
9516 S	37 30 22.5	77 55 43.6	16	310	1.3	1.5	< 10	75	20	2	
9517 G	37 30 20.2	77 55 40.5	12	165	0.8	1.0	60	115	240	<1	
9518 S	37 30 34.5	77 56 47.9	5	150	5.5	6.5	70	105	260	<1	
9519 S	37 30 30.4	77 56 48.0	25	210	3.4	4.0	80	80	370	<1	
9520 G	37 30 31.5	77 56 48.8	7	205	6.0	7.0	40	80	150	2	
9521 S	37 30 23.8	77 56 50.5	17	245	3.0	3.5	< 10	75	50	2	
9522 G	37 30 16.5	77 56 52.5	15	180	5.5	6.5	30	85	150	<1	
9523 S	37 30 15.3	77 56 52.7	8	180	3.0	3.5	< 10	75	50	<1	
9524 S	37 30 07.9	77 56 54.5	14	120	2.1	2.5	10	70	50	<1	
9525 S	37 30 01.9	77 56 55.9	9	150	1.7	2.0	< 10	85	30	<1	
9527 S	37 31 01.0	77 57 10.4	11	215	1.3	1.5	< 10	95	20	<1	
9528 S	37 31 01.8	77 57 14.3	25	260	0.8	1.0	< 10	100	20	1	
9529 S	37 31 02.5	77 57 19.6	10	130	3.0	3.5	< 10	90	20	<1	
9530 S	37 31 03.6	77 57 26.2	5	95	1.7	2.0	< 10	80	30	<1	
9531 S	37 31 04.4	77 57 31.2	5	65	1.7	2.0	< 10	70	30	<1	
9532 S	37 30 59.5	77 57 02.5	60	215	1.3	1.5	< 10	85	20	1	
9533 S	37 30 59.0	77 56 58.4	20	170	1.7	2.0	< 10	100	40	1	
9534 S	37 30 58.3	77 56 54.4	9	185	3.4	4.0	10	75	30	1	
9535 S	37 30 57.6	77 56 50.6	10	260	1.7	2.0	< 10	85	20	<1	
9536 S	37 30 57.2	77 56 46.5	8	125	4.7	5.5	20	80	70	<1	
9537 S	37 30 57.6	77 56 42.6	8	135	4.2	5.0	20	90	60	<1	
9538 S	37 30 55.9	77 56 38.6	5	75	11.0	13.0	20	90	40	<1	
9539 G	37 30 56.1	77 56 37.2	10	140	7.6	9.0	30	105	110	<1	
9540 R	37 30 55.5	77 56 37.3	6	45	3.4	4.0	80	80	350	1	
9541 S	37 30 55.4	77 56 34.5	17	130	5.4	7.0	10	90	30	<1	
9542 S	37 30 54.7	77 56 30.5	18	145	3.4	4.0	< 10	80	20	<1	
9543 G	37 30 54.0	77 56 26.5	12	160	14.4	17.0	20	110	50	<1	
9544 S	37 30 54.0	77 56 29.6	20	300	9.3	11.0	30	90	80	2	
9545 S	37 30 53.5	77 56 22.7	30	320	4.2	5.0	< 10	75	30	2	
9546 S	37 30 47.6	77 56 28.0	12	240	4.2	5.0	20	90	40	<1	
9547 S	37 30 48.1	77 56 32.2	14	230	5.4	7.0	10	100	50	1	
9548 S	37 30 48.7	77 56 36.2	16	190	8.0	9.5	< 10	95	30	<1	
9549 S	37 30 49.1	77 56 40.1	15	190	4.7	5.5	10	105	50	<1	
9550 S	37 30 39.0	77 56 46.7	10	160	3.8	4.5	10	80	50	<1	
9551 S	37 30 37.4	77 56 51.1	15	325	2.1	2.5	20	75	80	<1	
9552 S	37 30 39.5	77 56 55.0	18	410	1.3	1.5	< 10	80	30	1	
9553 R	37 30 29.4	77 55 43.3	25	265	1.3	1.5	10	100	60	1	
9554 S	37 30 29.4	77 55 52.5	17	440	1.7	2.0	< 10	80	20	<1	
9555 S	37 30 29.8	77 55 34.8	14	120	1.7	2.0	< 10	65	10	<1	
9556 S	37 30 32.7	77 55 35.7	14	410	1.3	1.5	< 10	80	20	1	
9557 S	37 30 26.7	77 55 54.7	30	250	3.0	3.5	< 10	75	20	1	
9558 R	37 30 26.5	77 55 56.1	35	410	1.3	1.5	< 10	95	30	2	
9559 S	37 30 26.0	77 55 58.6	35	400	2.1	2.5	10	85	10	2	
9560 S	37 30 25.5	77 56 03.7	20	325	2.1	2.5	< 10	85	20	1	
9561 S	37 30 26.5	77 56 06.6	20	290	2.1	2.5		95		1	
9562 S	37 30 27.0	77 56 10.7	12	385	2.1	2.5		70		4	
9563 S	37 30 27.7	77 56 14.6	15	260	1.7	2.0		80		2	
9564 S	37 30 29.0	77 56 18.4	12	140	2.1	2.5		90		<1	
9565 S	37 30 30.0	77 56 22.1	9	185	4.2	5.0		85		<1	

Sample Number	Location Latitude ° ' "	Longitude ° ' "	Co	V_2O_5	U	U_3O_8	eU	Th	eTh	Mo	Au
9566 S	37 30 29.8	77 56 26.2	11	145	4.7	5.5		65		1	
9567 S	37 30 31.5	77 56 30.2	9	265	5.0	6.0		70		<1	
9568 S	37 30 31.2	77 56 34.6	10	145	6.4	7.5		85		1	
9569 S	37 30 33.0	77 56 38.3	8	105	5.5	6.5		80		<1	
9570 S	37 30 33.6	77 56 42.3	15	300	5.4	7.0		85		<1	
9571 S	37 31 23.2	77 56 44.4	18	145	3.8	4.5		70		<1	
9572 S	37 31 23.9	77 56 48.2	11	130	5.0	6.0		70		<1	
9573 S	37 31 24.3	77 56 52.1	20	225	2.5	3.0		70		<1	
9574 S	37 31 25.0	77 56 56.1	15	125	3.0	3.5		70		<1	
9575 S	37 31 26.0	77 56 00.1	13	140	1.7	2.0		60		<1	
9576 S	37 31 26.5	77 57 04.1	10	130	3.0	3.5		60		<1	
9577 S	37 31 27.2	77 56 07.7	30	160	1.7	2.0		75		<1	
9578 S	37 31 28.0	77 57 11.9	20	185	2.1	2.5		85		<1	
9579 S	37 31 28.5	77 57 16.0	19	160	2.1	2.5		85		1	
9580 S	37 31 22.0	77 57 17.6	19	120	1.7	2.0		85		<1	
9581 G	37 31 15.7	77 57 19.0	12	250	2.1	2.5		85		<1	
9582 S	37 31 15.2	77 57 19.2	9	165	2.1	2.5		85		<1	
9583 S	37 31 15.0	77 57 15.0	5	95	1.7	2.0		75		<1	
9584 S	37 31 14.5	77 57 11.1	5	160	1.3	1.5		80		<1	
9585 S	37 31 14.0	77 57 07.2	20	200	2.1	2.5		75		<1	
9586 S	37 31 13.4	77 57 03.0	20	200	1.3	1.5		70		<1	
9587 S	37 31 12.1	77 56 55.2	18	180	2.1	2.5		75		<1	
9588 S	37 31 13.3	77 56 50.7	18	175	2.1	2.5		80		<1	
9589 S	37 31 14.0	77 56 46.7	20	220	2.5	3.0		70		<	
9590 S	37 31 13.5	77 56 38.5	12	140	3.8	4.5		60		<1	
9591 S	37 31 14.2	77 56 42.5	17	155	3.8	4.5		55		<1	
9592 S	37 31 15.5	77 56 46.0	10	125	4.2	5.0		60		<1	

S Soil (B horizon only)
G Stream sediment
R Rock chip
All units are ppm
* Selected coarse gravel with black coating

Analyses by CMS, Inc., Salt Lake City, Utah

measurements, were obtained in September, 1986. An additional 19 samples of soil, gravel, and pebbles were collected and analyzed for as many as 49 elements (Table 8). Sixteen water samples were collected and analyzed for uranium and thorium (Table 9).

GEOLOGY

Regional Geology

The Powhatan study area is underlain by a variety of metamorphic rocks. Farrar (1984) included the Powhatan study area in the "Goochland terrane" or "Goochland granulite terrane" which comprises characteristic lithologies and structural elements (Figure 3). The Goochland terrane consists of the State Farm Gneiss, the Sabot amphibolite (Sabot gneiss of Marr, 1985), the Maidens gneiss, and the Montpelier meta-anorthosite, which intruded both the Sabot amphibolite and Maidens gneiss (Farrar, 1984; Marr, 1985). Goochland terrane rocks are probably correlative with the Po River Metamorphic Suite of Pavlides (1980). The State Farm Gneiss has been dated as Grenvillian (1031±94 m.y.) by Rb-Sr whole rock analyses (Glover and others, 1978; Glover and others, 1982). The entire lithostratigraphic sequence of rocks in the Goochland terrane was metamorphosed to granulite facies. Although only the State Farm Gneiss has been dated, the entire Goochland terrane is tentatively considered to be Grenvillian (Glover and others, 1978), because the Sabot and Maidens units also show evidence of similar metamorphism.

The State Farm Gneiss is medium to coarse grained, foliated, and massive to layered. It is predominantly a light-gray, biotite-hornblende-quartz-titanite-potassium feldspar-plagioclase gneiss. Quartzo-feldspathic segregations and pegmatite dikes are common (Marr, 1985). The State Farm Gneiss is granodioritic to tonalitic in composition,

Table 2. Geochemical analyses of core samples from Drill Hole P-1.

SAMPLE NUMBER	SAMPLE INTERVAL Feet	ANALYTICAL DETERMINATION[1]																				
		Ag	As	Au (ppb)	B	Ba	Be	Bi	Br	Ca (%)	Cd	Co	Cr	Cs	Cu	Fe (%)	Ge	Hf	K (%)	Li	Mg (%)	Mn
P-1-15	0.0 - 1.0	<0.5	4	< 5	<10	330	2	0.2	2.0	0.08	<0.2	5	80	2.6	32	6.2	<10	9.7	1.6	26	0.16	140
P-1-16	1.0 - 2.0	<0.5	5	< 5	<10	320	2	0.2	1.5	0.16	<0.2	5	70	2.3	24	6.6	<10	8.4	1.8	24	0.19	90
P-1-17	11.2 - 11.7	<0.5	<1	< 5	20	390	2	<0.1	0.8	0.20	<0.2	2	-	0.7	22	0.9	10	11.0	1.6	22	0.05	60
P-1-18	70.0 - 70.3	<0.5	<1	< 5	<10	810	1	<0.1	0.5	1.11	<0.2	5	-	0.9	17	2.1	<10	2.1	6.8	24	0.50	200
P-1-1	10.0 - 17.0	0.5		<10						0.04	<1.0	9	320		9	1.1			0.8		0.06	76
P-1-2	20.0 - 21.0	<0.5		<10						0.04	<1.0	5	420		6	1.2			1.1		0.07	100
P-1-3	21.0 - 27.0	0.5		<10						0.84	<1.0	21	420		28	3.9			2.6		0.74	470
P-1-4	40.0 - 41.6	<0.5		<10						0.53	<1.0	5	330		9	2.8			4.4		0.20	570
P-1-5	45.0 - 46.0	0.5		<10						1.70	<1.0	32	420		16	6.9			1.1		2.00	760
P-1-6	46.0 - 47.0	0.5		<10						0.32	<1.0	27	320		36	4.4			4.3		0.74	220
P-1-7	50.0 - 52.0	<0.5		<10						0.89	<1.0	9	220		11	1.3			3.4		0.26	82
P-1-8	60.0 - 74.5	0.5		<10						0.94	<1.0	29	270		45	4.4			2.8		0.67	270
P-1-9	84.0 - 86.0	<0.5		<10						0.93	<1.0	10	200		11	3.2			3.7		0.22	190
P-1-10	90.0 -105.3	0.5		<10						1.10	<1.0	24	240		34	4.4			3.5		0.64	660
P-1-11	105.3 -120.0	<0.5		<10						0.78	<1.0	23	270		32	4.7			4.0		0.68	740
P-1-12	120.0 -128.4	0.5		<10						1.90	16.0	25	280		30	5.6			3.4		0.78	550
P-1-13	128.4 -132.0	0.5		<10						2.70	<1.0	20	280		34	3.7			3.2		0.70	490
P-1-14	132.0 -140.0	0.5		<10						1.10	<1.0	24	290		51	5.1			3.9		0.73	700

All values are ppm except as noted.

[1] See Table 3 for detection limit and method of analyses for samples P-1-15 through P-1-18 and Table 4 for samples P-1-1 through P-1-14.

based on modal analyses (Reilly, 1980).

The Sabot amphibolite overlies the State Farm Gneiss. The Sabot is a medium- to coarse-grained amphibolite with minor interlayers of quartz-biotite-plagioclase and quartz-feldspar leucogneiss (Poland, 1976; Reilly, 1980). Marr (1985) believes that the Sabot amphibolite (of Poland and Reilly) also includes interlayered biotite gneiss and schist and informally referred to the unit as the Sabot gneiss. He describes the amphibolite as an equigranular, faintly-banded, weakly-foliated gneiss. Layers of quartz and plagioclase in a black hornblende matrix are common and characteristic. The biotite gneiss is mainly a biotite-plagioclase garnetiferous gneiss, and includes augen gneiss and migmatitic gneiss. Goodwin (1970) and Poland (1976) interpret the Sabot amphibolite as former mafic lava flows or layers of pyroclastics interlayered with sediments.

The Maidens gneiss overlies the Sabot amphibolite and is the lithologic unit that contains the radioactivity anomalies. The Maidens gneiss is a heterogeneous unit, both in lithology and fabric. The dominant rock types, according to Farrar (1984), are garnet-biotite-quartz-plagioclase gneiss and biotite-quartz-plagioclase-potassium feldspar augen gneiss, locally containing lenses of intermediate to mafic gneiss with relict granulite-facies assemblages. Thin, discontinuous mica schists, hornblende-biotite-rich lenses and quartzo-feldspathic lenses are locally common (Marr, 1985). Thin, calc-silicate layers that are also present were derived from marbles (Farrar, 1984). The gneisses in the Maidens lack the abundant titanite found in the State Farm Gneiss.

The Montpelier meta-anorthosite (Bice and Clement, 1982; Clement and Bice, 1982) intrudes the Sabot amphibolite and lower Maidens gneiss. The Montpelier is a gray, coarse-grained, generally non-foliated, meta-anorthosite containing plagioclase megacrysts that constitute about 85 to 90 percent of the total rock. The unit also exhibits a granulated, medium- to coarse-grained, foliated phase (recrystallized). The recrystallized phase of the Montpelier meta-anorthosite is mainly plagioclase with minor interstitial microcline and quartz. The meta-anorthosite also contains large xenoliths of uralitized pyroxenite and garnetiferous amphibolite.

The Goochland terrane has undergone two high-grade metamorphic events (Farrar, 1984). The first event was of granulite grade. This was followed by an amphibolite-grade event that remobilized at least 90 percent of the granulite terrane. The amphibolite-grade event introduced water, partially recrystallizing the existing granulite gneisses, and was accompanied by intense deformation.

Pegmatites in the general area (mainly in Powhatan and Amelia counties) have been described in detail (Brown, 1962; Glass, 1935; Pegau, 1932). The pegmatites in the Amelia district are probably Permian in age (Deuser and Herzog, 1962). The pegmatites in Powhatan County contain the radioactive minerals betafite, columbite-tantalite, euxenite, microlite, monazite, pyrochlore, samarskite, and xenotime (Grauch and Zarinski, 1976; Dietrich, 1970). In addition to the radioactive minerals found in Powhatan, occurrences of the radioactive minerals zircon, fergusonite, bastnaesite, uranpyrochlore, and phosphuranylite have been noted in the pegmatites located in Amelia County (Grauch and Zarinski,

Mo	Na	Nb	Ni	P	Pb	Rb	Sb	Sc	Se	Sr	Ta	Th	Ti [%]	U	V	W	Y	Zn	Zr	La	Ce	Nd	Sm	Eu	Tb	Yb	Lu
<2	0.08	30	22	660	34	80	0.2	10.5	<0.5	40	1.3	58.0	1.06	5.2	94	1	10	40	490	142	241	88	12.0	1.00	0.7	1.19	0.23
<2	0.12	30	24	400	36	110	0.3	12.4	<0.5	40	1.0	18.0	1.00	3.5	98	1	<10	40	300	34	61	22	3.2	0.57	0.5	1.00	0.19
<2	0.15	30	16	460	32	70	0.1	5.1	0.5	50	1.5	88.0	1.05	5.6	56	2	40	18	560	180	319	124	17.5	1.12	1.3	1.38	0.27
<2	0.14	10	12	860	44	200	<0.1	4.9	<0.5	290	0.6	5.7	0.40	1.0	44	<1	10	42	50	31	54	20	3.6	1.91	0.5	0.96	0.15
4	0.15		17	340	16							3.3	0.48	0.2	50			19									
4	0.17		9	490	30							73.0	1.30	2.7	20			23									
6	0.23		20	460	20							9.3	0.85	1.3	150			120									
4	0.52		10	610	54							23.0	0.10	1.3	26			20									
5	0.33		100	140	8							6.1	1.20	1.9	230			170									
6	0.86		50	240	38							8.9	0.60	1.9	150			99									
4	2.30		16	230	44							8.9	0.19	1.2	46			33									
6	0.73		51	360	24							12.0	0.51	2.6	110			82									
3	2.10		14	200	34							3.2	0.14	1.6	36			22									
6	1.10		37	340	44							11.0	0.48	1.8	110			73									
4	0.76		37	290	40							13.0	0.51	1.8	130			86									
6	1.20		47	290	34							6.9	0.61	1.4	170			110									
6	1.80		38	230	30							4.3	0.44	1.3	120			88									
11	1.10		48	380	40							12.0	0.44	2.3	150			87									

1976; Dietrich, 1970; Gabelman, 1968). Locally, monazite occurrences (thorium content 11 to 14 percent) have been reported in the Amelia district (Overstreet, 1967). Within the study area, coarse crystalline pegmatite with large muscovite plates was found in a few locations.

Mertie (1953) lists a locality of monazite-bearing saprolite from "white granite gneiss" about 0.3 mile west of Macon; this site is about 1.4 miles due west of the central Powhatan study area. The Macon locality is contained within the "western monazite belt," which extends northeasterly for 170 miles in Virginia (Mertie, 1953). He also describes an "eastern monazite belt." The two "belts" join in the vicinity of Manakin, Goochland County, about 14 miles northeast of Powhatan.

Petrography

The study area is underlain entirely by the Maidens gneiss. Analysis of 39 thin sections prepared from selected core samples from P-1 and P-2 (Appendix III) indicates that the Maidens gneiss is a heterogenous unit consisting predominantly of a migmatitic, biotite-quartz-two feldspar gneiss. Locally, it contains thin discontinuous muscovite schist layers, hornblende-biotite-rich lenses, quartzofeldspathic segregations, and granitic pegmatite dikes and stringers. The dominant mineral assemblage of the Maidens is biotite-quartz-plagioclase-orthoclase-garnet-muscovite-kyanite. Other mineral assemblages present include orthoclase-quartz-biotite-muscovite; biotite-quartz-plagioclase-orthoclase-garnet; and quartz-feldspar (Tables 5 and 7). These mineral assemblages indicate amphibolite-grade metamorphism.

Quartz is the most abundant mineral and occurs as both ubiquitous crystals displaying undulatory extinction and as recrystallized anhedral polygons. Plagioclase (An_{29} to An_{32}, Michel-Levy method) is the most abundant feldspar. The plagioclase is twinned (Carlsbad, albite, and/or pericline) and exhibits considerable sericitization along cleavage planes. Untwinned orthoclase is subordinate to plagioclase, occurring as relict augen surrounded by foliated biotite. Titanium-rich biotite occurs as raggedly-terminated laths that form a lepidoblastic foliation. Garnet is present as fractured poikiloblasts with inclusions of biotite, quartz, feldspar, and epidote. Muscovite is present as clear laths. Kyanite occurs as scattered laths associated with K-feldspar-rich assemblages. Minerals that occur in minor amounts include graphite, as finely disseminated flakes and as elongate grains; pyrite as both disseminated grains and vein fillings; chlorite as an alteration product of biotite; and apatite, sphene, epidote, monazite, calcite, and zircon. Modal analyses of samples selected from the drill holes are presented in Tables 10 and 11.

The mineralogy observed in the drill holes is suggestive of graywacke-type sediments that have been subjected to amphibolite-grade metamorphism and late retrograde hydrothermal alteration. Evidence for regional granulite-grade metamorphism reported by Farrar (1984) is not strong at this site, but masses of chlorite, sericite, and biotite may represent original pyroxene. Hydration reactions involving the formation of biotite and muscovite may have obliterated other evidence of possible granulite-grade metamorphism. Hydration of the original sediments is indicated by the breakdown of potassium feldspar to form rims of biotite and microcline around feldspar augen. Any sillimanite present would have been converted to kyanite through the reaction sillimanite + potassium feldspar + water = muscovite + quartz + kyanite. Amphibolite-grade

Table 3. Detection limit and method of analyses [samples P-1-15 through P-1-18 and P-2-15 through P-2-21].

Elements	Detection Limit	Method	Elements	Detection Limit	Method
Ag	0.5000	DCP	Rb	10.0000	XRF
As	1.0000	INAA	Sb	0.1000	INAA
Au	5.0000	INAA	Sc	0.0100	INAA
B	10.0000	DCP	Se	0.5000	INAA
Ba	10.0000	XRF	Sr	10.0000	XRF
Be	1.0000	DCP	Ta	0.5000	INAA
Bi	0.1000	DCP	Th	0.2000	INAA
Br	0.5000	INAA	U	0.1000	INAA
Cd	0.2000	DCP	V	2.0000	DCP
Co	0.1000	INAA	W	1.0000	INAA
Cr	0.5000	INAA	Y	10.0000	XRF
Cs	0.2000	INAA	Zn	0.5000	DCP
Cu	0.5000	DCP	Zr	10.0000	XRF
Ge	10.0000	DCP	La	0.1000	INAA
Hf	0.2000	INAA	Ce	1.0000	INAA
Li	1.0000	AA	Nd	3.0000	INAA
Mn	2.0000	DCP	Sm	0.0100	INAA
Mo	2.0000	INAA	Eu	0.0500	INAA
Nb	10.0000	XRF	Tb	0.1000	INAA
Ni	1.0000	DCP	Yb	0.0500	INAA
Pb	2.0000	DCP	Lu	0.0100	INAA

AA Atomic Absorption
XRF X-ray Fluorescence
DCP D. C. Plasma Spectrometry
INAA Instrumental neutron activation analysis
Analyses are research accuracy.
Analyses by Nuclear Activation Service, Inc. [NAS], Ann Arbor, Michigan.

Table 4. Detection limit and method of analyses (samples P-1-1 through P-1-14 and P-2-1 through P-2-14).

Elements	Detection Limit	Method
Ag	0.5000	DCP
Au	10.0000	INAA
Ce	10.0000	DCP
Cd	0.2000	DCP
Co	1.0000	DCP
Cr	2.0000	DCP
Cu	0.0500	DCP
Fe	10.0000	DCP
K	10.0000	DCP
Mg	10.0000	DCP
Mn	2.0000	DCP
Mo	1.0000	DCP
Na	10.0000	DCP
Ni	0.1000	DCP
P	10.0000	DCP
Pb	0.2000	DCP
Th	0.2000	INAA
Ti	10.0000	DCP
U	0.1000	INAA
V	2.0000	DCP
Zn	0.0500	DCP

DCP D. C. Plasma Spectrometry
INAA Instrumental neutron activation analysis
Samples milled in a chrome steel mill.
Analyses are research accuracy.

Analyses by Nuclear Activation Service, Inc. (NAS), Ann Arbor, Michigan.

Table 5. Mineralogy of selected samples from Drill Hole P-1.

Sample Number	Interval (feet)	Thin Section	X-ray Diffraction	Powder Diffraction
P-1-6	21.9 - 22.3		Gp	
P-1-5	40.0 - 42.0		Mg; Qz	
P-1-4	129.5 - 129.9		Bt; Py; Ca; Ka	
P-1-3	125.1 - 125.4		Ca; Qz	
P-1-2	138.6		Bt; Ka; Qz	
P-1-1	138.5 - 138.8		Ka; Kf	
P-1-61	61.0	Qz; Pf; Bt; Py; Mu; Gp; Kf; Ap		
P-1-65	65.0	Bt; Qz; Pf; Kf; Mu; Ky; Ep; Py; Gp		
P-1-75	75.0	Pk; Bt; Mu; Qz; Zr; Cl; Mz; Pf	Mz; Qz; Gp; Py	Mz; Py
P-1-88	88.0	Bt; Qz; Pf; Kf; Gt; Ky; Mg; Py		
P-1-103	103.0	Qz; Pf; Mu; Bt; Py; Ep; Ky; Pf; Sp		
P-1-105	105.0	Pf; Qz; Bt; Gt; Mu; Ap; Mz; Py; Mg; Sp		
P-1-115	115.0	Qz; Pf; Mu; Py; Tc		
P-1-129	129.0	Qz; Pf; Mu; Ca; Ap; Mz; Py		

Index of mineral abbreviations used: Qz-quartz; Ka-kaolin; Tc-talc; Ppy-pyrophylite; Gp-graphite; Gt-garnet; Bt-biotite; Zr-zircon; Py-pyrite; Mu-muscovite; Kf-potassium feldspar; Pf-plagioclase feldspar; Ap-apatite; Ep-epidote; Mt-montmorillonite; Cl-chlorite; Ky-kyanite; Hb-hornblende; Il-ilmenite; Ca-calcite; Mg-magnetite; Mz-monazite; Sp-sphene.

Table 6. Geochemical analyses of core samples from Drill Hole P-2.

SAMPLE NUMBER	SAMPLE INTERVAL Feet	ANALYTICAL DETERMINATION[1]																			
		Ag	As	Au (ppb)	B	Ba	Be	Bi	Br	Ca (%)	Cd	Co	Cr	Cs	Cu	Fe (%)	Ge	Hf	K (%)	Li	Mg (%)	Mn
P-2-15	0.0 - 0.5	<0.5	5	7	<10	360	5	0.2	1.3	0.11	<0.2	25	110	2.3	52	8.9	<10	14.0	1.5	34	0.43	400
P-2-16	0.5 - 1.5	<0.5	5	11	<10	340	4	0.2	2.0	0.07	<0.2	12	110	1.9	44	13.3	<10	2.6	0.1	46	0.58	340
P-2-17	7.0 - 7.2	<0.5	4	< 5	<10	520	5	<0.1	0.9	0.13	<0.2	29	80	1.5	8	13.7	<10	6.6	1.4	52	1.75	1100
P-2-18	15.0 - 15.1	<0.5	<1	< 5	<10	1500	4	<0.1	0.5	0.08	<0.2	4	-	1.2	16	2.3	<10	2.4	10.5	14	0.20	240
P-2-19	31.0 - 31.1	<0.5	1	6	<10	640	4	0.2	1.1	1.89	<0.2	10	-	0.8	36	5.1	<10	5.5	3.7	40	1.25	340
P-2-20	61.8 - 62.0	<0.5	<1	< 5	<10	1300	3	<0.1	0.9	2.38	<0.2	8	-	1.1	14	5.0	<10	4.3	5.8	40	1.44	680
P-2-21	96.0 - 96.2	<0.5	1	13	<10	590	2	0.2	0.7	2.15	<0.2	28	-	0.8	92	9.8	<10	3.0	2.6	34	1.56	960
P-2-1	2.0 - 12.0	0.5		<10						0.07	<1.0	58	290		41	8.2			1.3		0.92	1600
P-2-2	15.0 - 20.0	<0.5		<10						0.04	<1.0	6	270		4	1.5			7.0		0.15	240
P-2-3	20.0 - 20.5	<0.5		<10						0.15	<1.0	22	290		58	13.0			2.7		0.50	910
P-2-4	25.0 - 26.0	0.5		<10						3.10	<1.0	59	360		32	8.4			1.5		2.30	1500
P-2-5	30.0 - 32.0	0.5		<10						1.90	<1.0	18	260		27	5.3			2.9		0.59	680
P-2-6	43.4 - 61.0	<0.5		<10						0.18	<1.0	21	270		42	4.3			3.5		0.65	610
P-2-7	61.7 - 71.0	<0.5		<10						0.78	<1.0	28	270		76	4.2			2.5		0.55	370
P-2-8	71.0 - 82.0	<0.5		<10						1.50	<1.0	21	280		48	3.5			2.3		0.58	340
P-2-9	82.0 -100.0	<0.5		<10						1.40	<1.0	24	260		37	4.1			1.5		1.10	710
P-2-10	100.0 -110.0	0.5		<10						1.30	<1.0	23	210		39	3.8			3.3		0.87	420
P-2-11	110.0 -118.8	0.5		120						1.40	<1.0	32	280		55	6.2			3.6		0.81	730
P-2-12	118.6 -130.0	<0.5		10						0.91	<1.0	15	270		18	3.6			4.0		0.57	500
P-2-13	130.0 -150.0	<0.5		<10						1.40	<1.0	19	280		26	6.7			2.6		0.84	280
P-2-14	150.0 -160.0	<0.5		<10						1.40	<1.0	26	350		37	5.3			3.3		0.75	1000

All values are ppm except as noted.

[1] See Table 3 for detection limit and method of analyses for samples P-2-15 through P-2-21 and Table 4 for samples P-2-1 through P-2-14.

metamorphism is indicated by the coexistence of biotite and garnet, and by the muscovite-quartz-kyanite assemblage. Hydrothermal alteration that occurred after the amphibolite event is indicated by discordant pyrite veins, by the alteration of biotite to chlorite, and by reaction rims consisting of biotite-chlorite-white mica-pyrite. Cataclasis, in the form of polygonized and recrystallized grains, provided pathways for hydrothermal fluids.

Surficial Geology

Almost the entire study area is covered with mature residual soil and saprolite as much as 60 feet thick. The soil map of Powhatan County (Reber and others, in press) indicates that Wedowee soil is present at P-1 and Cecil soil at P-2. The Wedowee and Cecil soils are very deep, well drained, and moderately permeable (Reber and others, in press). These soils have a dominantly clayey subsoil and are very strongly to strongly acid (Nicholson and others, 1980).

The A soil horizon (top soil) is typically light yellowish brown, dark gray, or gray. The organic matter content ranges from insignificant to more than 30 percent, and the mineral composition also varies. In the study area, the A horizon is mostly composed of clayey minerals but is locally silty and/or sandy. The thickness of the A horizon ranges from about 2 inches to 3 feet, and averages about 6 inches. The B horizon is commonly dark red, yellow-red, or yellow-brown, and its upper part is almost exclusively composed of clayey, iron-rich minerals. Locally, it is mixed with various amounts of regolith material. The boundary between the A and B horizons is not sharp but is recognizable mainly by a decrease in the amount of organic matter. The B horizon shows evidence of accumulation of clay and iron and grades downward into decomposed blocky bedrock or partly weathered parent material of the C horizon or saprolite. Some of the lithological and structural features of the bedrock are characteristically preserved in saprolite, except for density and consistency. Prevailing red, yellow-brown, and brown colors indicate that chemical depletion of the more soluble elements including silica, calcium, manganese, potassium, sodium, uranium, and trace and base metals has been extensive.

Because of the intensity of weathering processes, the saprolite in the Powhatan area is thick, averaging about 40 to 60 feet. The differences between the original bedrock character and saprolite are due particularly to chemical weathering processes. The oxidation and hydration of iron and aluminum during saprolite formation is intense above the water table. The water table occurs here at a depth of about 40 feet. The saprolitic material is characteristically non-plastic and loosely unconsolidated; consequently, the upper part of the saprolite is loose and porous, which facilitates the easy access of water, and the resulting leaching processes. The saprolite forms the transition from soil to bedrock. The litho-

Mo	Na	Nb	Ni	P	Pb	Rb	Sb	Sc	Se	Sr	Ta	Th	Ti (%)	U	V	W	Y	Zn	Zr	La	Ce	Nd	Sm	Eu	Tb	Yb	Lu
< 2	0.09	30	38	660	28	90	0.2	19.8	<0.5	10	1.3	57.0	1.23	5.4	130	1	30	58	690	144	274	101	16.8	1.47	1.5	2.38	0.42
< 2	0.06	30	44	1170	20	110	0.1	22.0	<0.5	< 10	1.5	140.0	1.99	9.0	180	2	20	66	410	387	669	278	43.9	2.04	2.4	1.80	0.32
< 2	0.07	20	56	1730	8	130	<0.1	32.9	<0.5	< 10	1.2	2.0	2.42	2.8	170	<1	40	92	400	31	42	21	5.2	2.20	1.2	3.83	0.55
< 2	1.17	10	12	990	44	330	<0.1	4.5	<0.5	300	0.6	14.0	0.48	2.2	42	<1	20	22	70	43	75	29	5.3	2.97	0.4	0.84	0.16
< 2	3.10	10	30	670	36	140	0.1	12.2	<0.5	400	0.7	11.0	0.80	2.0	94	1	40	74	260	42	76	29	5.3	1.71	0.8	1.82	0.30
< 2	3.84	20	20	1260	36	200	<0.1	11.7	<0.5	530	<0.5	14.0	0.84	2.5	88	<1	10	92	140	49	90	38	7.4	2.02	0.9	1.80	0.28
11	2.23	10	96	1460	16	120	<0.1	10.1	1.2	180	<0.5	22.0	0.73	4.3	20	1	30	85	110	65	131	60	11.1	1.77	1.1	1.95	0.32
7	0.22		63	1500	24							8.0	0.73	3.1	160			130									
2	0.80		11	800	68							5.8	0.24	1.5	38			27									
3	0.35		38	3200	22							17.0	0.53	3.5	220			110									
3	0.57		130	4400	16							13.0	1.00	2.8	180			130									
6	2.20		21	520	28							14.0	0.52	2.6	130			110									
5	1.00		38	370	40							11.0	0.57	2.5	110			78									
28	1.40		110	260	20							6.8	0.28	4.4	150			55									
24	1.80		85	410	20							15.0	0.28	3.8	150			69									
17	1.70		78	750	24							7.1	3.80	2.6	140			110									
17	1.90		62	350	30							16.0	0.50	2.5	170			92									
15	1.40		70	350	32							15.0	0.56	2.2	190			110									
5	1.30		24	490	32							27.0	0.47	2.2	110			84									
4	0.74		33	350	20							10.0	0.64	1.5	120			95									
5	0.68		46	300	22							14.0	0.57	1.9	160			83									

Table 7. Mineralogy of selected samples from Drill Hole P-2.

Sample Number	Interval [feet]	Thin Section	X-ray Diffraction	Powder Diffraction
P-2-1	5.0 - 5.3		Qz	
P-2-2	5.0 - 5.3		Ka; Qz; Tc; Ppy	
P-2-3	15.0 - 20.0		Gp; Ru	
P-2-4	15.0 - 20.0		Gt; Bt; Ka	
P-2-5	35.0 - 35.2		Gp; Zr	
P-2-6	37.9 - 38.1		Gt; Bt; Qz; Ka	
P-2-7	39.0 - 39.2		Mt	
P-2-8	45.0 - 45.2		Gt	
P-2-9	44.8 - 44.9		Gt; Qz; Cl	
P-2-10	120.5 - 120.8		Mt; Ka; Il; Qz	
P-2-11	129.8 - 129.9		Hb; Qz; Py	
P-2-12	157.9 - 158.1		Py; Qz; Ka	
P-2-44	44.0	Bt; Qz; Kf; Pf; Sp; Ky; Gt		
P-2-49	49.0	Qz; Kf; Pf; Mu; Py; Gp		
P-2-53	53.0	Qz; Bt; Pf; Ap; Sp; Kf; Py; Cpy		
P-2-54	54.0	Pf; Qz; Bt; Kf; Gt; Py; Ap; Zr; Mz	Qz	
P-2-61.5	61.5	Qz; Pf; Kf; Bt; Gt; Mu; Cl		
P-2-75	75.0	Qz; Bt; Pf; Zr; Ep; Mz; Py; Mt	Mz; Qz; Gp; Py	Mz; Py; Gp
P-2-82	82.0	Qz; Pf; Kf; Bt; Gp		Gp
P-2-87	87.0	Qz; Pf; Bt; Mu; Py; Mz; Sp; Zr; Ep; Kf; Gt		
P-2-93	93.0	Qz; Pf; Kf; Py; Cl; Mu; Ep		
P-2-96.5	96.5	Pf; Qz; Mu; Bt; Ca; Py; Gp; Si; Mz; Sp		
P-2-98	98.0	Qz; Pf; Bt; Kf; Py; Gp; Gt; Ca; Mu		
P-2-120	120.0	Qz; Pf; Bt; Kf; Mu; Py; Ca; Gt; Ep; Ky; Mz; Mt		
P-2-134	134.0	Qz; Gt; Bt; Pf; Kf; Ky; Ap; Mu; Py; Gp		

Index of mineral abbreviations used: Qz-quartz; Ka-kaolin; Tc-talc; Ppy-pyrophylite; Gp-graphite; Gt-garnet; Bt-biotite; Zr-zircon; Py-pyrite; Mu-muscovite; Kf-potassium feldspar; Pf-plagioclase feldspar; Ap-apatite; Ep-epidote; Mt-montmorillonite; Cl-chlorite; Ky-kyanite; Hb-hornblende; Il-ilmenite; Ca-calcite; Mg-magnetite; Mz-monazite; Sp-sphene.

logic logs of drill holes and water wells indicate that the saprolite boundary with the bedrock is sharp. All 282 soil samples collected in 1977 and 1978 were collected from the B horizon at a depth of about 1 foot (Plates 1, 4, 5, 6, 7, 8, and 9; Table 1).

The lateral changes in soil characteristics depend upon changes in the lithology of the underlying rock. The few bedrock outcrops in the Powhatan area are deeply weathered. Generally, in the northern half of the study area, red, clayey soil with minor amounts of the regolithic material prevails. In the southern part of the area, the clayey part of the B horizon appears to be thinner, and quartz and other mineral and rock fragments which are not yet entirely decomposed, are more common.

Alluvial sediments are confined to stream valleys. Most of the streams are intermittent and have low gradients. These streams occur in wide valleys that, in many cases, contain locally developed swamps because of the numerous beaver dams. Poorly sorted fluvial sediments form a veneer in local flood plains and in the valleys.

Numerous springs, which yield from 0.25 to 2.0 gallons per minute, are situated in the headwaters of Fighting Creek and its tributaries. Anomalously high radioactivity has been measured over many of these springs. In Fighting Creek and some of its tributaries, black- and rusty-coated sand, gravel, pebbles, and boulders are common. Most of the stream gravel is composed of quartz, biotite gneiss, and biotite-quartz-chlorite schist. Black heavy minerals are abundant in the sand-size fraction.

GROUND RADIOACTIVITY

Survey Grid

A grid was established over the aeroradiometric anomalies and adjacent areas (Plates 1 and 2). A

central NNE-SSW grid line was located over the length of the main anomalies. This line was approximately parallel to the strike of the regional foliation (N10°-15°E) and to anticipated lithologic boundaries. Additional NNE-SSW lines were established about 330 feet apart. Parallel cross lines oriented WNW-ESE were spaced about 660 feet apart. Data for five of the WNW-ESE grid lines are presented in profile form to show total-count radioactivity, uranium, thorium, cobalt, and vanadium values (Figures 4, 5, 6, 7, and 8).

At each grid intersection a soil sample was collected from the B horizon for geochemical analysis and a radioactivity reading was taken. Where the collection of samples and readings was not feasible, nearby alternate sites were chosen.

Radioactivity Survey

Ground radioactivity values range from less than 30 counts-per-second (cps) just outside the grid area to over 4000 counts-per-second as measured with a small-crystal-volume (2.65 cubic inches), hand-held scintillometer. Background surface radioactivity in the grid area away from the anomalies averages 50 cps. The contour map of ground radioactivity (Plate 3) shows anomalously high radioactivity values with a general NNE trend.

Ground radioactivity values measured at three areas within the survey grid are over 20 times background (Plate 3). Two of these anomalies define a larger linear anomaly near the NNE base line and on either side of grid line B-B'. The third anomaly is located about a mile due south on grid line E-E'. Four other areas with radioactivity values over 10 times background, generally aligned along the same N to NNE trend, are contoured on Plate 3. The major anomalies are discontinuous over the 1.5-mile-long trend, and all are enclosed within the four-times background contour.

Several isolated ground radioactivity values as large as 40 times background were measured in the northeastern part of the survey area. This may indicate a "broadening" to the east of the NNE-trending anomalously radioactive area. The radioactivity is particularly high over almost all streams in this area. This northeastern area was not surveyed systematically or sufficiently sampled to be contoured in detail.

Fifty-two radioactivity measurements were taken over streams, in addition to those taken over areas covered with soil. Most of the high radioactivity readings detected over the intermittent and perennial streams coincide with areas of anomalous soil radioactivity. Higher radioactivity values occur near spring areas and associated black- and brown-coated boulders and gravel in stream beds. Average background radioactivity occurs over stream valleys that are filled with silt and clay. In the coarse sandy alluvium, opaque minerals (mainly magnetite and black, metallic, nonmagnetic minerals), garnet, zircon, ilmenite, and rutile are common.

Because of the radioactivity over the streams, which is thought to be caused by the black- and brown-coated sediments, reconnaissance water sampling and analysis were done to determine if uranium and thorium were being taken from the ground water and deposited on the surfaces of the sediment. The analyses of the water samples (Table 9) do not reflect the high radioactivity of the stream beds. All of the radionuclides are probably rapidly extracted from the water by absorption, by coprecipitation on mineral surfaces, or by organic matter. In the Swanson uranium deposit and vicinity (Pittsylvania County, Virginia), the uranium content in surface water is below detection limit, and in the ground water, maximum values did not exceed 0.9 ppm (Marline Uranium Corporatio and Carbide Corporation, 1983).

Within the Powhatan study area, loose blocks of coarse pegmatite as much as a foot in diameter, with large plates of muscovite and biotite, occur on the upland surface and in stream bottoms. However, gamma-ray spectrometer readings (airborne and ground surveys) do not indicate any significant radioactivity from ^{40}K, which suggests that pegmatites are either absent or leached of K-feldspar. Because of deep leaching and destruction of feldspar in the A horizon, ^{40}K signatures may be artificially low.

GEOCHEMISTRY

A total of 394 samples from outcrops, drill cores, stream sediments, gravels, and soils collected from the study area in 1977-1978 and 1986 were analyzed for a variety of elements. All samples were analyzed for uranium and thorium (Tables 1, 2, 3, 4, 6 and 8).

Of the 336 samples collected in 1977 and 1978, 282 were soil, taken with a hand-sample auger from the B horizon soil zone at an average depth of one foot. The remaining 54 samples consisted of stream sediment (49) and chips taken from bedrock outcrops (5) (Plate 2).

Thirty-nine additional samples from cores from P-1 and P-2 were collected for analyses in 1986 (Tables 2, 3, 4, and 6). Eleven samples were selected on the basis of a slight increase in radioactivity as compared to core above and below, and these specific anomalous intervals of core were analyzed. These 11 samples were analyzed for 49 elements, including rare-earth elements. The remaining 28 samples were rock chips taken as the core was geologically logged and were selected to comprise a

Table 8. Geochemical analyses of supplementary samples.

SAMPLE NUMBER	LOCATION LATITUDE ° ' "	LONGITUDE ° ' "	ANALYTICAL DETERMINATIONS[1] Ag	Au (ppb)	Ca (%)	Cd	Co	Cr	Cu	Fe	K (%)	Mg (%)	Mn	Mo	Na (%)	Ni	P	Pb	Th	Ti (%)	U
SS-1	37 31 49	77 56 29	1.0	-	0.09	<1	17	220	18.0	5.00	0.67	0.12	150	14	0.19	29	2600	32	600.0	0.69	17.6
SS-2	37 32 11	77 56 12	<0.5	<10	0.02	<1	2	230	2.0	0.34	0.86	0.01	160	< 1	0.12	5	70	14	3.6	0.01	0.5
SS-3	37 32 29	77 56 16	<0.5	10	0.05	<1	5	310	1.5	0.34	0.01	0.01	290	1	<0.01	7	< 10	<2	0.3	0.01	<0.1
SS-4	37 32 33	77 56 14	<0.5	10	0.02	<1	3	290	1.0	0.34	1.40	0.01	180	1	0.27	5	120	16	7.8	0.01	0.6
SS-5	37 32 47	77 56 19	<0.5	<10	0.04	<1	3	280	1.0	0.31	2.90	0.02	150	1	0.50	5	150	<2	2.4	0.01	0.4
SS-6	37 32 46	77 56 13	<0.5	<10	0.45	<1	5	350	1.0	0.58	0.01	0.10	260	1	0.03	8	150	<2	1.4	0.04	0.4
SS-7	37 32 54	77 56 09	<0.5	<10	0.03	<1	2	380	1.5	0.62	<0.01	0.01	80	1	0.02	7	180	<2	1.8	0.01	0.1
SS-8	37 33 01	77 56 07	<0.5	<10	0.09	<1	31	310	13.0	5.20	1.20	0.12	920	3	0.29	13	870	28	9.8	0.20	2.2
SS-9	37 32 57	77 55 51	<0.5	<10	<0.01	<1	2	420	3.5	0.78	0.01	<0.01	40	1	0.02	7	90	4	5.6	0.01	0.5
SS-10	37 32 52	77 55 50	0.5	10	0.01	<1	3	330	1.5	0.85	0.03	0.01	80	2	0.02	9	100	<2	0.8	0.01	0.3
SS-11	37 32 41	77 55 38	<0.5	<10	0.11	<1	2	330	1.0	0.52	0.03	0.07	60	2	0.05	7	160	2	27.0	0.02	1.8
SS-12	37 32 36	77 55 40	0.5	<10	0.08	<1	17	420	5.5	2.00	0.82	0.07	1000	13	0.19	23	2200	20	410.0	0.30	14.7
SS-13	37 32 35	77 55 31	<0.5	<10	0.03	<1	3	270	1.0	0.37	0.01	<0.01	180	< 1	0.01	6	50	4	6.6	0.01	0.2
SS-14	37 32 31	77 55 43	<0.5	<10	1.40	<1	15	410	16.0	2.30	0.14	0.76	540	2	0.43	26	220	2	3.7	0.15	0.2
SS-15	37 32 30	77 55 47	<0.5	<10	0.02	<1	4	320	1.0	0.51	0.69	0.02	250	1	0.11	6	70	10	1.3	0.01	0.1
SS-16	37 32 29	77 55 45	<0.5	<10	2.40	<1	22	420	26.0	3.30	0.20	1.80	600	2	0.38	63	420	<2	3.3	0.16	0.5
SS-17	37 32 17	77 55 47	<0.5	<10	0.47	<1	5	480	2.0	1.20	0.26	0.29	180	1	0.12	18	310	8	2.2	0.06	0.6
SS-18	37 32 10	77 55 47	0.5	<10	1.40	<1	62	500	28.0	8.30	3.00	0.72	4700	6	0.51	35	1600	20	26.0	0.46	2.6
SS-19	37 32 04	77 55 56	<0.5	<10	0.34	<1	4	340	0.5	0.70	1.40	0.11	340	2	0.31	10	150	14	3.7	0.10	0.6

All values are ppm except as noted.

[1] See Table 4 for detection limit and method of analyses.

composite representative sample for a specific cored interval. These 28 samples were analyzed for 20 elements. A group of 19 other samples, including one bulk soil sample (taken at P-1) and 18 selected black-coated gravel and pebble samples, were analyzed for 21 elements (Table 8).

Analytical Methods

The analytical methods used on the samples collected in 1977 and 1978 were different from those used on the samples collected in 1986. Samples collected in 1977 and 1978, consisting of soil, stream sediments, and rock chips (Table 1) were analyzed by traditional wet-chemical procedures and by radiometric assay using a radiometric gross gamma counter (U and Th). Following standard sample preparation, splits of the 1977 and 1978 samples were dissolved in acid. Analyses for cobalt, gold, and vanadium were by atomic absorption; molybdenum by colorimetric thiocyanate; uranium by florimetric methods; and thorium by colorimetric methods. Radiometric uranium (eU) and radiometric thorium (eTh) were determined by duplicate counts of 30 minutes duration separated by four days.

The samples collected in 1986 were analyzed by several methods (Tables 2, 3, 4, 6 and 8). Following standard sample preparation and splitting, the samples were analyzed by atomic absorption (AA), X-ray fluorescence (XRF), direct current plasma spectrometry (DCP), and instrumental neutron activation analysis (INAA).

Reliability of Data

The results of the geochemical analyses from the 1977-1978 and 1986 surveys are not directly comparable because of the differences in sample type, elements selected for analysis, and analytical methods. The only elements common to both data sets, uranium and thorium, had values that would chemically reflect the radioactivity noted on the

V	Zn	REMARKS
100	42.0	Bulk soil sample from drill hole P-1 site; radioactivity up to 5000 cps; 50 cps background.
6	4.0	Quartz and gneiss pebbles coated with Mn oxide.
4	4.0	Quartz gravel coated with Mn oxide.
6	4.5	Quartz and gneiss pebbles coated with Mn oxide, radioactivity up to 4000 cps; 100 cps background.
6	4.0	Quartz and biotite gneiss gravel coated with Mn oxide, radioactivity up to 2000 cps; 100 cps background.
10	9.5	Gravel coated with Mn oxide, radioactivity up to 500 cps; 70 cps background.
8	6.5	Gravel partly coated with Mn oxide, radioactivity 500 cps; 70 cps background.
50	59.0	Fine-grained gravel, black coated; radioactivity 400 cps; 70 cps background.
12	4.0	Quartz pebbles coated with Mn oxide, radioactivity up to 2000 cps; 50 cps background.
8	6.5	Quartz pebbles partly coated with Mn oxide, radioactivity up to 500 cps; 70 cps background.
10	4.5	Quartz pebbles with muscovite, coated with Mn oxide, radioactivity 1700 cps; 50 cps background.
36	13.0	Pebbles partly coated with Mn oxide, radioactivity 1500-1700 cps; 50 cps background.
4	2.5	Pebbles coated with Mn oxide, radioactivity 1000-1500 cps; <100 cps background.
78	28.0	Gravel coated with Mn oxide with pegmatite blocks; radioactivity up to 1000 cps; 100 cps background.
12	4.5	Pebbles coated with Mn oxide, radioactivity up to 250 cps; 100 cps background.
84	45.0	Pebbles coated with Mn oxide, radioactivity up to 1000 cps; 100 cps background.
22	13.0	Gravel poorly coated with Mn oxide, rusty; radioactivity up to 1000 cps; 100 cps background.
140	99.0	Quartz gravel with Fe oxide coating; radioactivity 300-500 cps; 50 cps background.
14	9.0	Gravel coated with Mn oxide, radioactivity 400-500 cps; 50 cps background.

ground and in the aeroradiometric surveys. The amounts (in ppm) of these elements can be directly compared in a few places. In these places, the quantities determined by the different methods show a considerable difference; therefore, differences in the methods (and possible accuracy of the methods) used for analyses in the 1977-1978 and 1986 surveys could lead to incorrect conclusions if the two data sets were combined. A comparison of the laboratory techniques (and accuracy) used in 1977-1978 and 1986 is not possible because splits from the earlier survey are not available.

Distribution of Elements

Uranium

The combined histogram of uranium distribution for the 1977-1978 and 1986 data sets (Figure 9) suggests a lognormal distribution of uranium. Figure 10 shows the distribution of uranium values among core, stream sediment, and soil samples. All core samples have uranium values of less than 10 ppm (most are less than 2.5 ppm). Values in stream-sediment samples are more highly variable, and have a higher mean value than the core samples. Some very high uranium values were recorded for a few stream-sediment samples. Soil samples are intermediate between core and stream sediment samples in uranium content. The rock samples (not illustrated) are similar to the core samples in uranium content.

A cumulative probability plot of uranium content in all samples (Figure 11) confirms the lognormal distribution suggested in the histograms by the distinct linear alignment of samples. On this graph, the intersection of the line defined by the sample points and the 50 percent probability axis indicate the median value of the logarithm of uranium concentration in ppm. The slope of the line defined by the sample values is inversely proportional to the standard deviation of the samples. Thus, the stream sediment samples have a higher median value and a greater variability as indicated by the histogram. The plot also demonstrates the close correspondence of cor ' and rock-chip samples.

Table 8. Analysis of water samples.

SAMPLE NUMBER	LOCATION LATITUDE	LOCATION LONGITUDE	ANALYTICAL DETERMINATIONS U	Th	HCO_3	SO_4	PO_4	pH	REMARKS
	° ' "	° ' "	ppb	mg/l	mg/l	mg/l	mg/l		
W-1	37 32 01	77 55 58	<2	<1	24	<2	<0.1	6.0	Small spring discharged to Fighting Creek.
W-2	37 32 01	77 56 04	<2	<1	16	2	<0.1	5.2	Seepage from saprolite, 0.5 gal./min.
W-3	37 32 11	77 56 12	<2	<1	20	<2	<0.1	6.0	Water below water pond, 3 gal./min.
W-4	37 32 29	77 56 16	<2	<1	18	<2	<0.1	6.1	Small creek cut in saprolite, 3 gal./min. radioactivity 600 cps; 100 cps background.
W-5	37 32 32	77 56 30	<2	<1	24	<2	<0.1	6.2	Small creek, 1 gal./min., close to outcrop of biotite gneiss; radioactivity 500-600 cps; 100 cps background.
W-6	37 32 33	77 56 14	<2	<1	20	2	<0.1	6.0	Small creek with outcrops of biotite gneiss; radioactivity up to 4000 cps; 100 cps background.
W-7	37 32 47	77 56 19	<2	<1	22	<2	<0.1	6.1	Creek cut in saprolite soil (2-3 m) with outcrops of biotite gneiss; radioactivity up to 2000 cps; 100 cps background.
W-8	37 32 46	77 56 13	<2	<1	64	20	2.3	6.8	Creek, approx. 5 gal./min.; radioactivity 500-700 cps; 100 cps background.
W-9	37 32 54	77 56 09	<2	<1	82	28	4.8	6.6	Creek, approx. 3 gal./min.; radioactivity up to 500 cps; 100 cps background.
W-10	37 32 01	77 56 07	<2	<1	86	26	4.9	6.7	Seepage from saprolite, radioactivity up to 400 cps; 70 cps background.
W-11	37 32 52	77 55 50	<2	<1	18	<2	<0.1	5.8	Spring area of Fighting Creek; 0.25 gal./min.; radioactivity up to 500 cps; 70 cps background.
W-12	37 32 35	77 55 31	<2	<1	20	<2	<0.1	6.6	Spring area of Fighting Creek; 2 gal./min., radioactivity 1000-1500 cps; 100 cps background.
W-13	37 32 31	77 55 43	<2	<1	22	<2	<0.1	6.4	Small creek, 2 gal./min.; radioactivity 100 cps; 100 cps background.
W-14	37 32 30	77 55 47	<2	<1	18	<2	<0.1	6.3	Fighting Creek 2 gal./min.; radioactivity up to 250 cps; 100 cps background.
W-15	37 32 29	77 55 45	<2	<1	22	<2	<0.1	6.3	Fighting Creek, 2 gal./min.; radioactivity up to 250 cps; 100 cps background.
W-16	37 32 17	77 55 47	<2	<1	14	<2	<0.1	6.7	Fighting Creek, 10 gal./min., radioactivity up to 1000 cps; 100 cps background.

Analyses by Skyline Labs, Inc., Wheat Ridge, Colorado.
Samples were not acidified.

The validity of the higher content of uranium in stream-sediment samples can be tested by the statistical technique of multiple comparisons. The uranium content of stream-sediment samples is significantly higher than that of the soil, core, or rock samples at a 95 percent confidence level. However, uranium content of the soil, core, and rock samples is not sufficiently different to distinguish them from one another at a 95 percent confidence level.

Uranium (U_3O_8) content of the 282 soil samples is contoured on Plate 4. Elevated uranium concentrations above the mean of 4.0 ppm can be noted in the

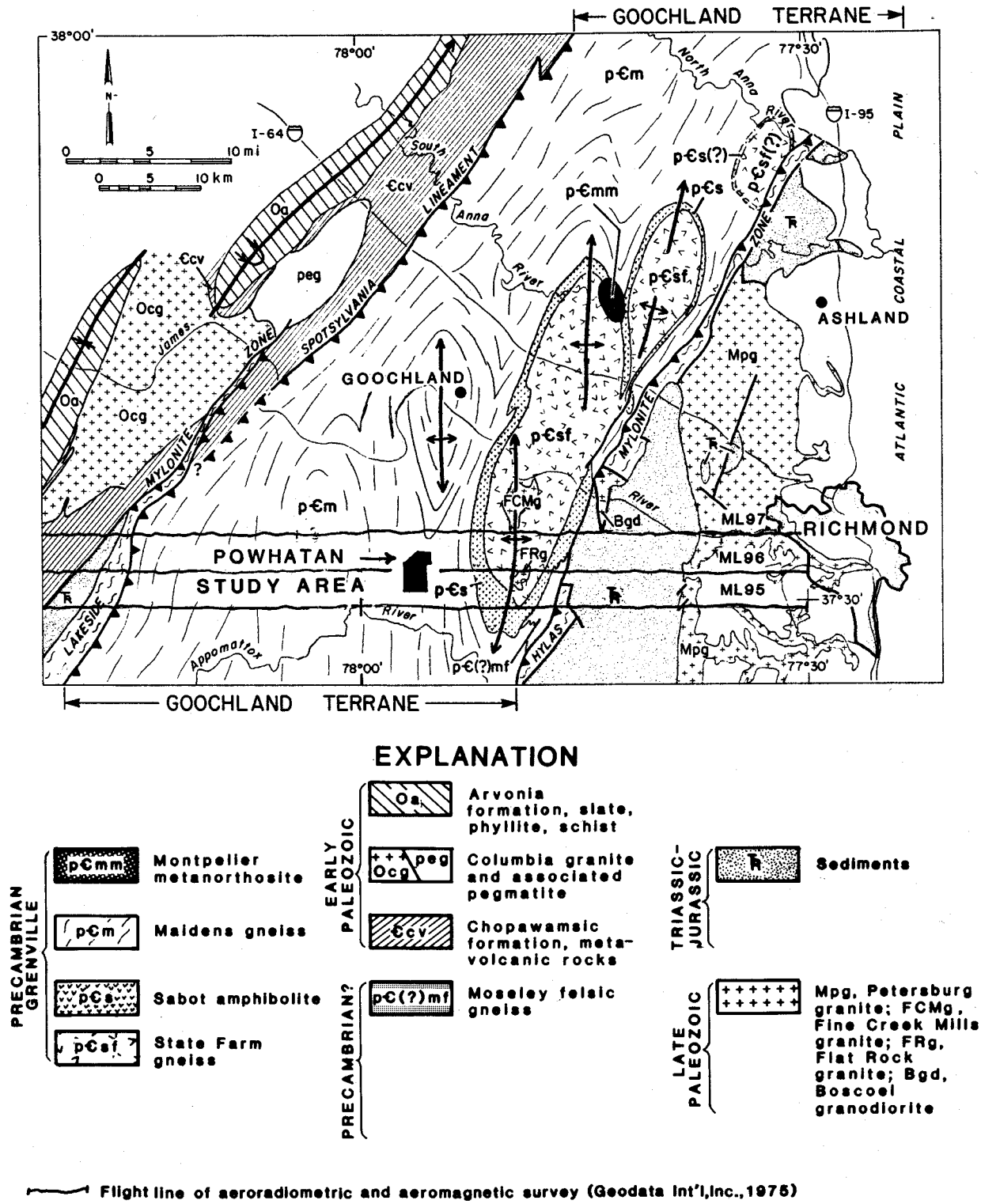

Figure 3. Regional geologic map of the Powhatan study area, Virginia (without Tertiary and Quaternary sediments; modified from Farrar, 1984).

Table 10. Modal analyses of samples from Drill Hole P-1 (1,000 points counted).

Mineral	Sample Number				
	P-1-61	P-1-75	P-1-103	P-1-105	P-1-129
Quartz	50.9	34.0	68.0	19.0	52.8
Plagioclase	20.8	20.8	6.6	29.5	38.0
Biotite	11.2	15.8	3.5	24.9	1.7
Orthoclase	14.0	18.9	16.0	x	x
Muscovite	0.5	7.8	3.5	1.6	3.0
Pyrite	2.4	x	0.7	tr	0.8
Graphite	tr	tr	x	tr	tr
Apatite	tr	x	tr	1.9	0.4
Chlorite	x	0.8	x	x	x
Monazite	x	1.0	0.5	0.6	0.4
Epidote	tr	x	tr	x	tr
Kyanite	x	x	0.6	x	x
Sphene	tr	tr	0.4	x	tr
Garnet*	x	x	x	17.7	x
Magnetite	x	x	x	4.5	x
Calcite	x	tr	x	x	tr
Rutile	tr	tr	tr	x	tr

* Pyralspite series
tr trace
x not present

Table 11. Modal analyses of samples from Drill Hole P-2 (1,000 points counted).

Mineral	Sample Number						
	P-2-49	P-2-54	P-2-75	P-2-87	P-2-96.5	P-2-120	P-2-134
Quartz	72.1	34.2	65.3	46.4	32.4	44.5	46.2
Plagioclase	1.3	39.5	7.3	18.6	42.1	29.7	8.8
Orthoclase	25.7	15.1	x	x	10.9	8.2	1.1
Biotite	x	3.3	15.7	16.7	1.1	10.0	17.6
Muscovite	1.0	x	x	3.2	7.9	4.1	0.9
Pyrite	0.3	0.7	4.4	0.8	0.6	0.4	0.3
Apatite	x	0.2	x	x	tr	x	0.2
Sphene	x	x	x	0.4	0.6	tr	tr
Garnet*	x	4.7	4.9	2.4	x	0.4	23.1
Zircon	tr	0.2	0.3	0.4	tr	tr	tr
Monazite	tr	0.5	0.5	10.3	0.6	0.2	tr
Epidote	x	x	x	0.8	tr	0.4	x
Sillimanite	x	x	x	x	0.9	x	x
Calcite	tr	x	tr	tr	2.7	0.4	tr
Kyanite	x	x	x	x	x	0.9	1.5
Montmorillonite		x	x	x	x	0.4	x
Graphite	tr	tr	tr	0.1	0.2	tr	0.4

* Pyralspite series
tr trace
x not present

northeastern and southern part of the study area. Areas with less than two ppm of uranium are limited to the peripheral areas of the map.

A comparison of the uranium contour map (Plate 4) and the ground radioactivity contour map (Plate 3) indicates a good correspondence between the southern uranium anomaly and a radioactivity anomaly in the same area. The highest soil uranium values occur near the site of P-2. The radiometric values are 10 to 20 times background in this area. The radiometric anomalies (Plate 3) on grid lines B-B′ and C-C′ do not have a uranium counterpart.

The distribution of radiometric uranium is similar to that of chemical uranium values, with a mean of 2.5 ppm and a standard deviation of 0.6 (Figure 12). The similarity holds in the distribution among different sample types (Figure 13) with all rock samples and 96 percent of the soil samples having values of less than 10 ppm. Only 57 percent of the stream-sediment samples have radiometric uranium values of 5 ppm or less, with 31 percent between 5 and 10 ppm. The remaining 12 percent of the stream-sediment samples have values ranging from 17 ppm to 83 ppm.

Uranium content was also measured by gamma-ray spectrometry at 11 locations (Table 12). These sites were near areas where the highest ground radioactivity values had previously been measured. Radiometric uranium values obtained on site range from 1.2 to 14 ppm with a mean value of 5.9 ppm. If the sample of fresh gneiss bedrock (GR-9) is typical for the study area, the mean of the uranium values recorded near the radioactivity anomalies is 70 percent greater than that of the bedrock (3.6 ppm).

Thorium

The distribution of thorium concentrations of the combined sample suite, including all of the 1977-1978 and 1986 samples, is bimodal (Figure 14). Although most of the samples contain from 50 to 100 ppm thorium, a small peak in the histogram occurs between 0 and 25 ppm. The histogram of thorium content in core, stream sediment, and soil samples (Figure 15) demonstrates that 84 percent of the core samples and 23 percent of the stream sediment samples have thorium values in the 0 to 25 ppm range. All of the core and gravel samples in the 0 to 25 ppm range were collected in 1986 (Tables 2, 6, and 8). As previously discussed, the thorium values for the samples collected in 1977 and 1978 may not accurately reflect thorium content at low concentrations. The bimodality of the thorium distribution may reflect the sensitivity of the analytical methods used for thorium determination in 1977 and 1978.

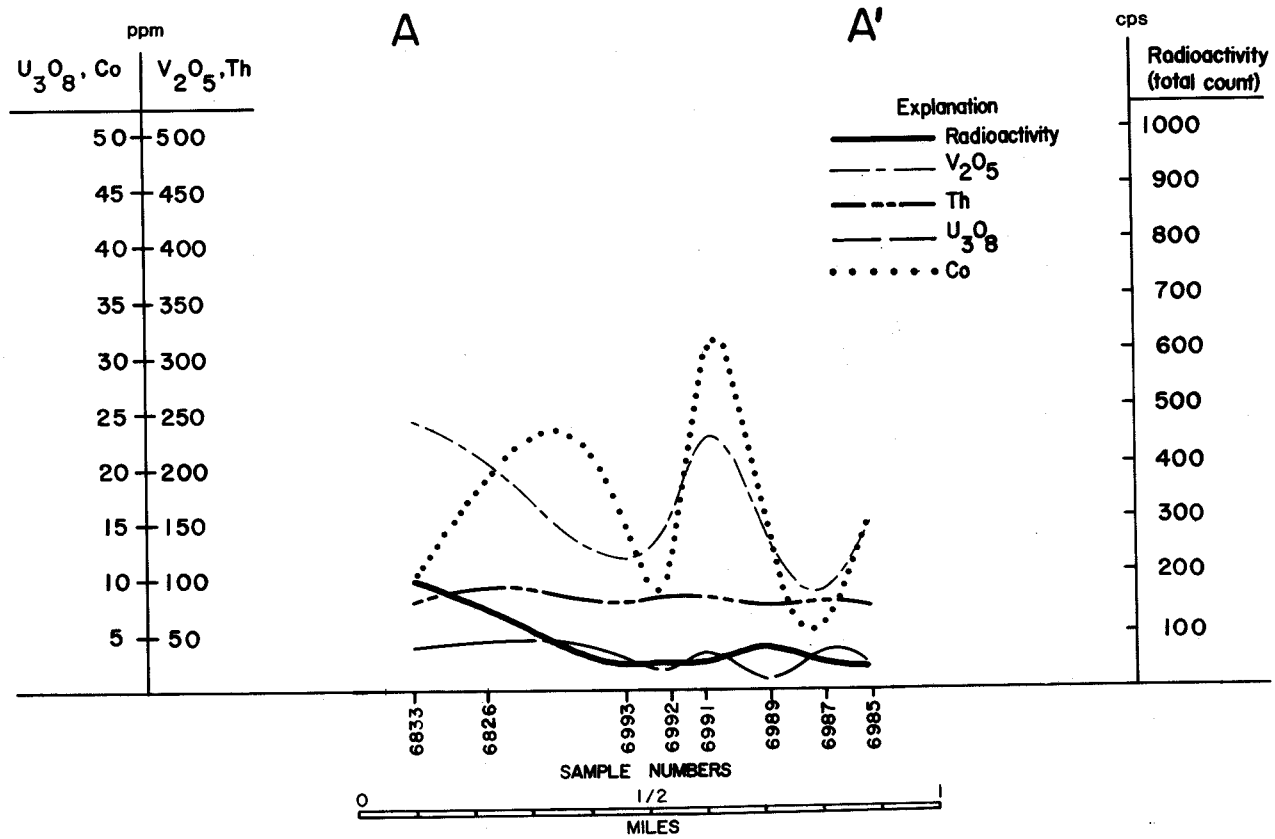

Figure 4. Radioactivity and geochemical profile A-A′.

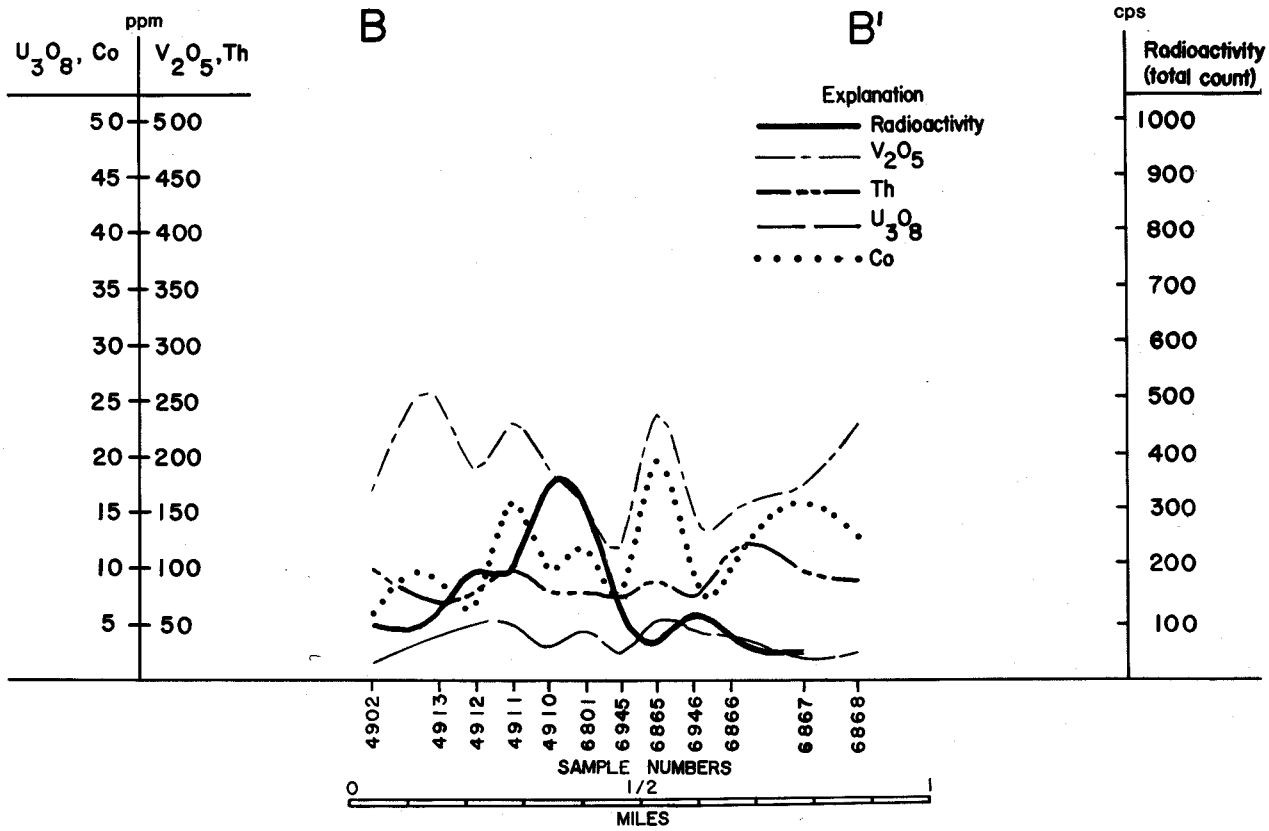

Figure 5. Radioactivity and geochemical profile B-B′.

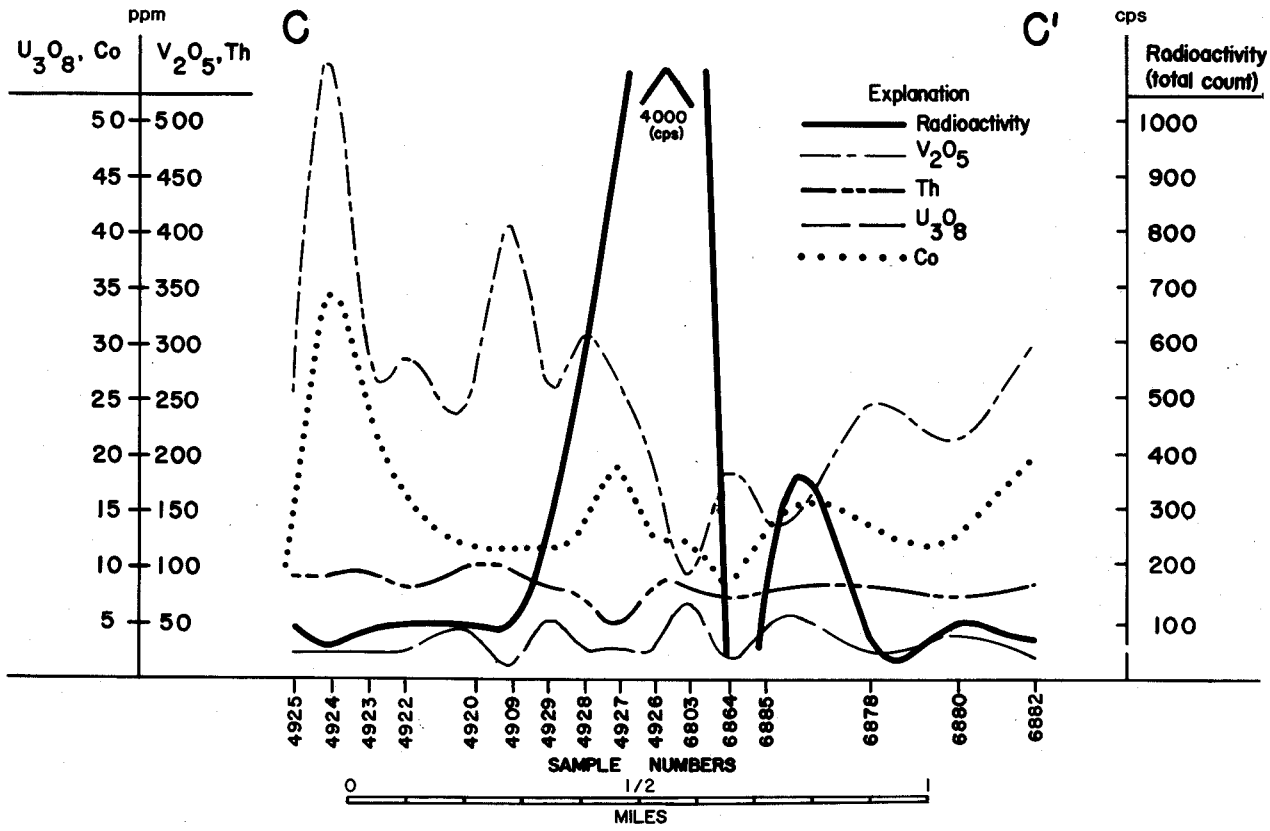

Figure 6. Radioactivity and geochemical profile C-C′.

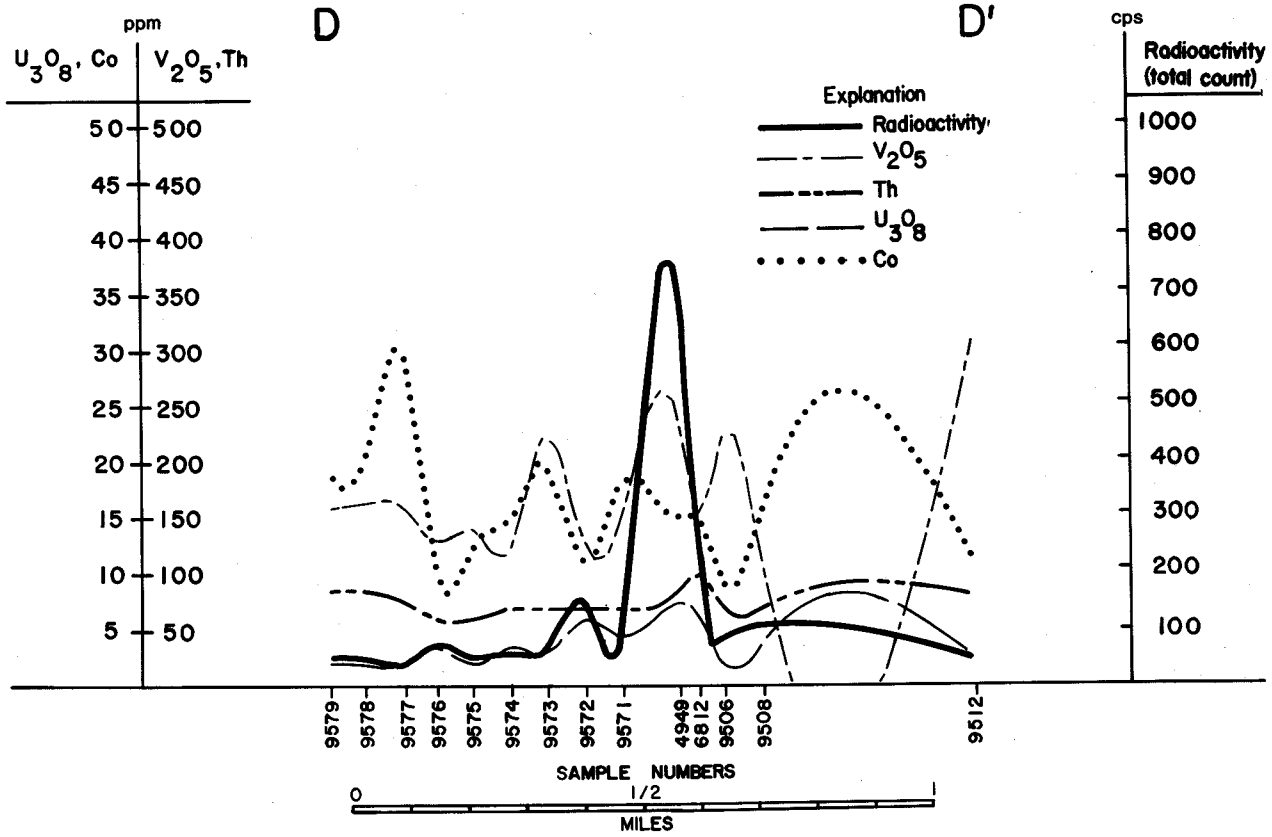

Figure 7. Radioactivity and geochemical profile D-D′.

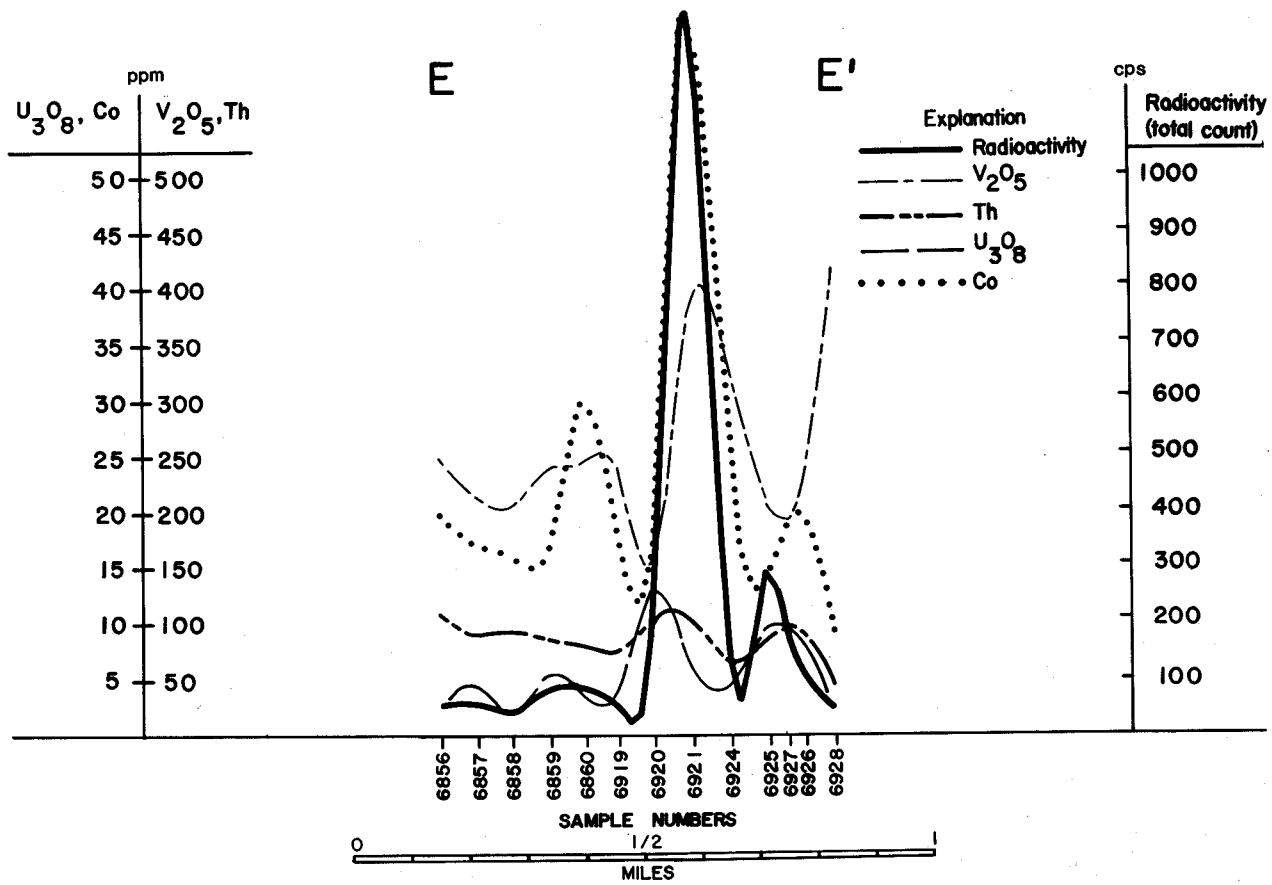

Figure 8. Radioactivity and geochemical profile E-E′.

The cumulative probability plot for thorium (Figure 16) shows consistently lower thorium values for the core samples. The narrow range of thorium values in the soil samples is indicated by the steep slope of its plot. Multiple comparison analysis of the different groups of thorium values indicates that only the cores are significantly different from the other sample types.

Thorium content of soil samples from the 1977 and 1978 data set is contoured on Plate 5. Several thorium highs are located along the western edge of the study area, in the east along Fighting Creek, in the south-central area, and near the intersection of the powerline and grid line D-D'.

Drill hole P-2 was drilled in a high-thorium area. This is apparent when the map is compared with the ground radioactivity map (Plate 3). The thorium highs in the western survey area correspond with ground radiometric values that are four times background. The anomalies in the northeastern part of the study area correspond with ground radioactivity values near background. The site where P-1 was drilled (radioactivity 80 times background) contains thorium values that are lower than typical.

Radiometrically determined thorium content of the 1977 and 1978 samples averages 11.7 ppm. Stream-sediment samples average 30 ppm, rock samples average 11 ppm, and soils average 7 ppm. The high standard deviation in the data set (36 ppm) suggests that these differences may be due to random scatter rather than to consistent differences in thorium content (Figures 17 and 18). Multiple comparison analysis shows no significant difference in the mean radiometric thorium samples at a 95 percent confidence level (Figure 16).

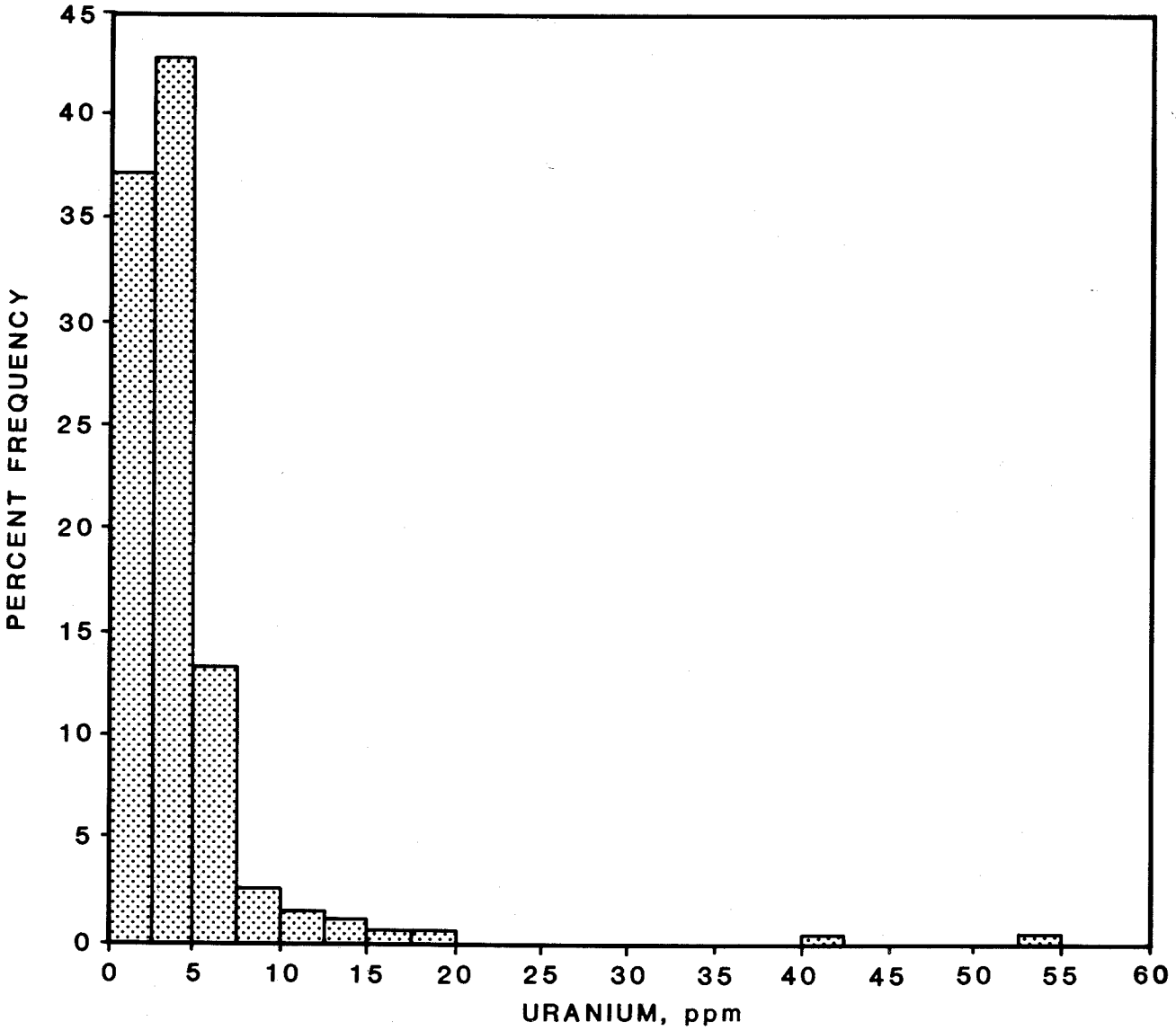

Figure 9. Histogram of uranium content in all samples.

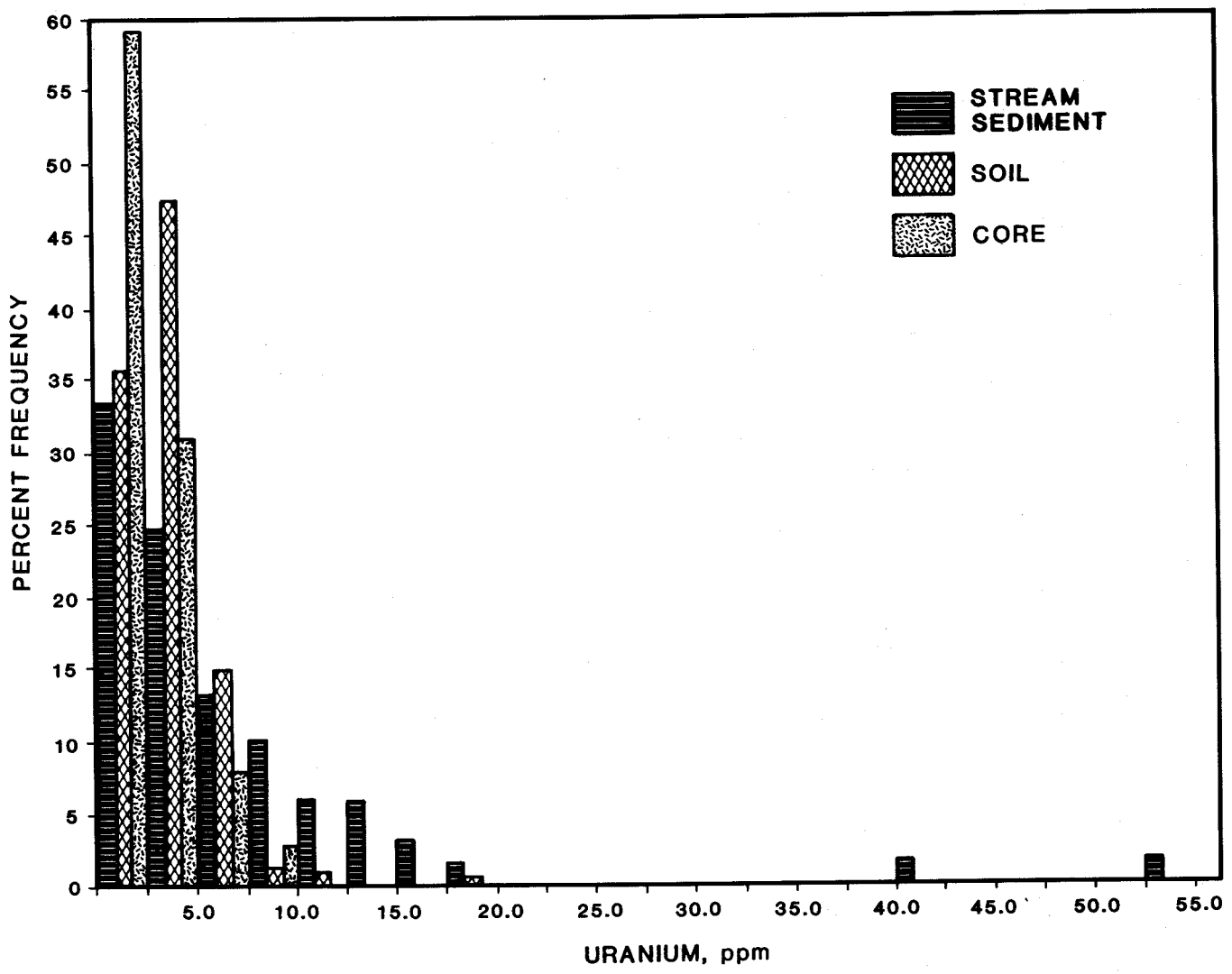

Figure 10. Histogram of uranium content in core, stream sediment, and soil.

On-site measurements for radiometric thorium by gamma-ray spectrometry show high values near the ground radioactivity anomalies (Table 12). The mean radiometric thorium content near the radioactivity anomalies is 186 ppm. This value is over seven times the amount of thorium found in bedrock (location GR-9, Table 12). These data suggest that the ground radioactivity anomalies are due to increased abundance of thorium-bearing minerals. The ratio of radiometric thorium to radiometric uranium from the gamma-ray spectrometer survey ranges from 7 to 93. The lowest thorium to uranium ratio corresponds to unaltered gneiss (location GR-9, Table 12). The mean value of 43 for the thorium to uranium ratio is over six times the ratio in the bedrock. This suggests that the anomalous ground radioactivity may be due to enrichment in thorium-bearing minerals, and minor enrichment in uranium-bearing minerals, in the soil and stream sediment compared to bedrock.

Cobalt and Vanadium

Cobalt and vanadium content show approximately normal distribution. In contrast with the chemical and radiometric uranium and thorium data, no anomalously high values were detected. The mean values of cobalt and vanadium for stream-sediment, rock-chip, and soil samples vary only slightly from each other. Contour maps of cobalt (Plate 9) and vanadium (Plate 8) content in soil lack the north-south trend observed in the contour maps of uranium and thorium. This suggests that the pronounced north-south alignment of contours on the uranium, thorium, ratio, and ground radioactivity maps reflects a mutual geological correlation and is not merely a result of the distribution of sample sites.

Elemental Relationships

Only with uranium values is any one sample type consistently different from the others. Stream-sediment samples have significantly more uranium

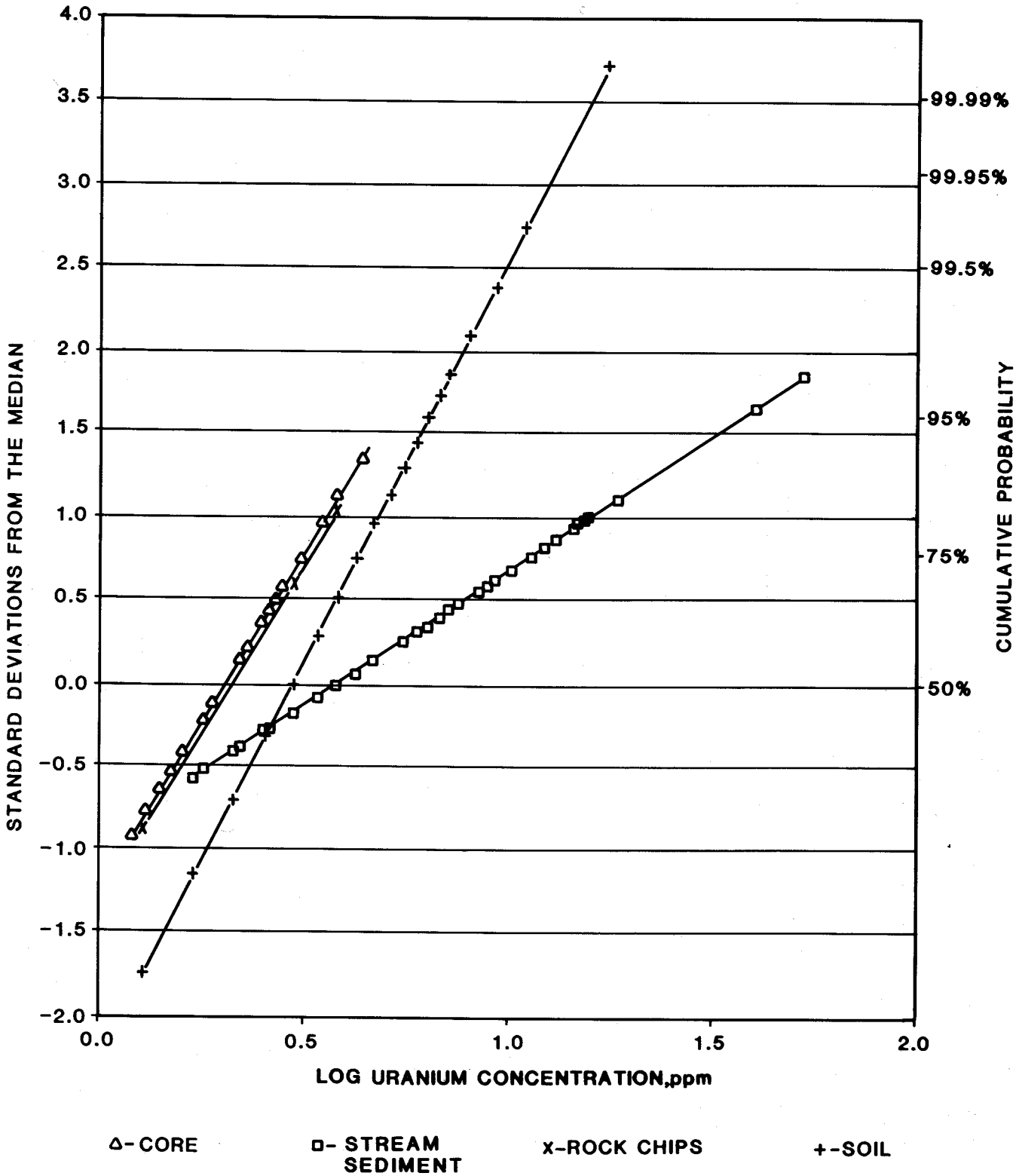

Figure 11. Cumulative probability plot for uranium.

than soil, core, or rock-chip samples. Some samples exhibit anomalously high concentrations of uranium and thorium. The stream-sediment samples with high levels of radioactive elements include 6962, 6900, 6899, and SS-12, all of which were collected from the bed of Fighting Creek. The soil samples with the highest contents of uranium and thorium include SS-1, 6920, 6921, 6922, 6925, and 9544 (Tables 1 and 6). Correspondence of ground radiometric anomalies and soil uranium or thorium on

the geochemical maps is not consistent (Plates 3 and 4 through 7). The soil samples with the very highest values occur on or near the ground radioactivity anomalies.

The bimodality of the thorium distribution supports the possibility that the analytical methods used on samples collected in 1977 and 1978 may overestimate thorium content where near-background levels are recorded. If so, the lack of thorium enrichment and low thorium to uranium ratios over radioactivity anomalies may not be accurate (Plate 7).

Correlation Analysis

Correlation analysis of the geochemical data indicates that the uranium and thorium components of stream-sediment and core samples are directly related. In these samples, high uranium values generally correspond with high thorium values. However, in soil samples, no correlation of radioactive components can be demonstrated. This suggests that in the process of soil formation, one or both of the mobilized radioactive elements is depleted and/or enriched to some degree.

Core Samples

Least-square correlation of thorium and uranium content of the 39 samples from P-1 and P-2 shows a correlation coefficient (r) of 0.81. These samples were not tested for thorium or uranium by radiometric assay methods.

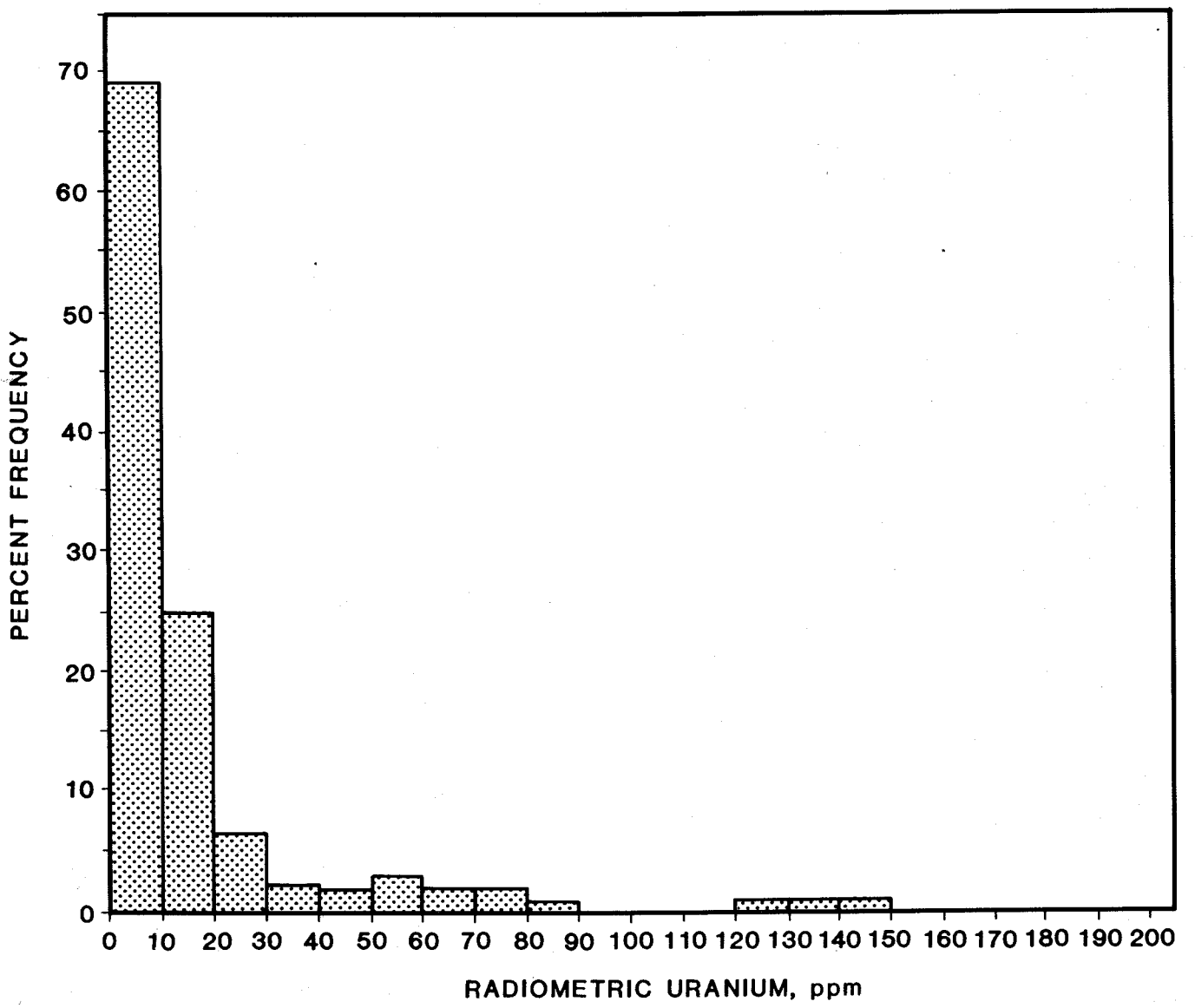

Figure 12. Histogram of radiometric uranium content in all samples analyzed.

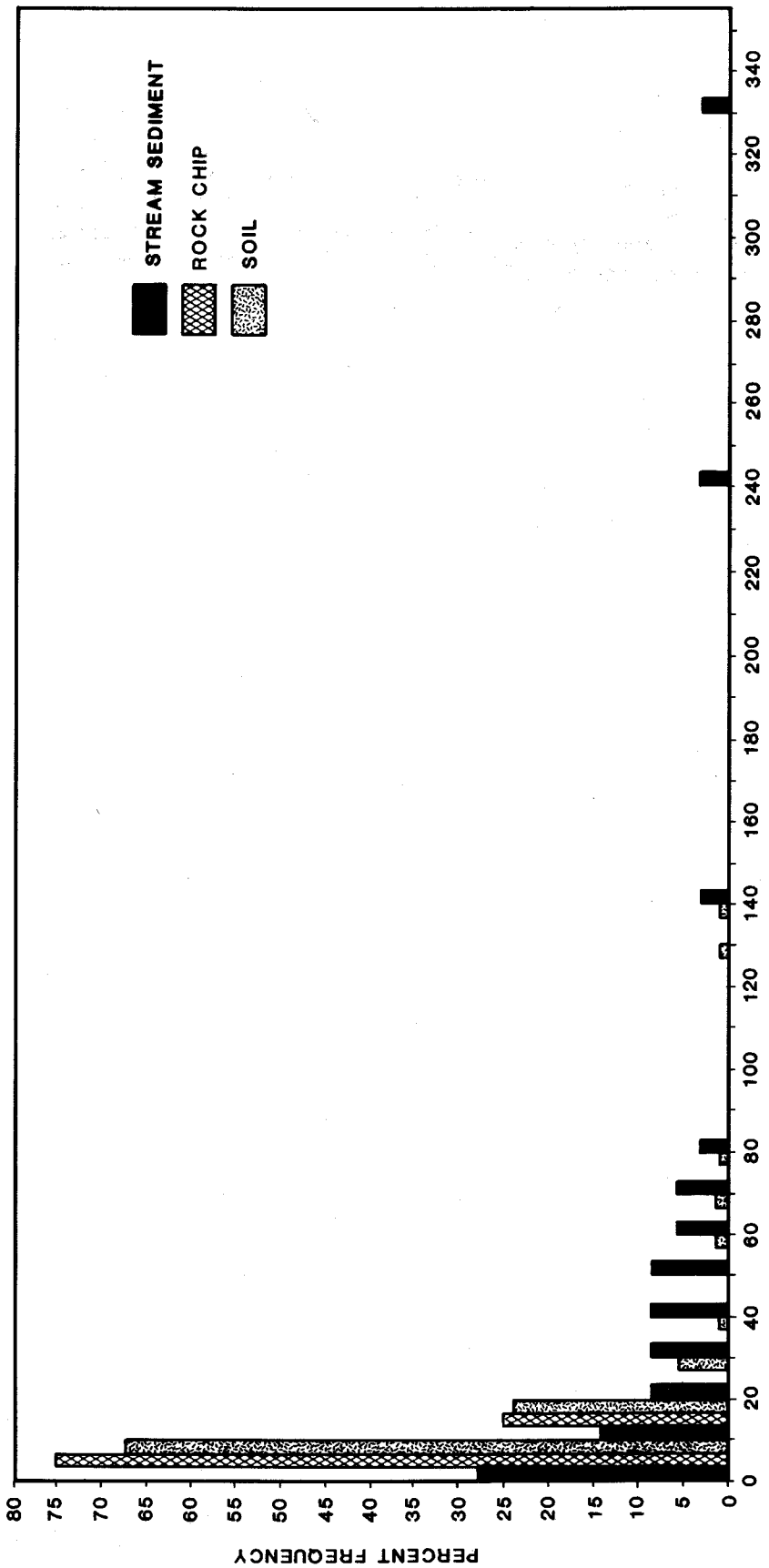

Figure 13. Histogram of radiometric uranium content in stream sediment, rock chips, and soil.

Stream Sediment

The correlation matrix of stream-sediment samples is shown in Table 13. Neither cobalt nor vanadium shows any correlation with the radioactive elements. Uranium and thorium are correlated to a similar extent as in the cores with r = 0.77, which is similar to the correlation of uranium and radiometrically measured thorium. Chemically determined thorium is correlated with both radiometric uranium (r = 0.90) and radiometric thorium (r = 0.92). Radiometric thorium and radiometric uranium show almost perfect correlation (r = 0.99). Uranium measured chemically and radiometrically shows moderate correlation with r=0.71. It is possible that the preponderance of thorium over uranium may diminish the accuracy of the radiometric uranium assays.

Soil

The correlation matrix for the 283 soil samples (Table 14) shows a correlation among uranium, radiometric uranium, and radiometric thorium values in soil. The radiometric assays (eU and eTh) are well correlated (r=0.732). Chemically determined uranium is marginally correlated with both radiometric uranium (r=0.400) and radiometric thorium (r=0.450). However, no correlation exists between chemically determined thorium and either radiometric uranium (r=0.011) or radiometric thorium (r=0.090). A very slight correlation at best exists between chemically determined uranium and thorium (r=0.162). The notable lack of distinct correlation of chemical thorium values in soil samples with the other three measures of radioactive element abundance suggests a possible lack of accuracy in chemical thorium values.

Core Data Analysis

In soil and saprolite, both thorium and uranium are present at levels greater than typical for unaltered bedrock. This suggests that thorium and uranium are contained in minerals which are resistant to weathering processes. The uranium- and thorium-bearing minerals are concentrated in regolith and soil by removal of the bulk of easily weathered minerals. The thorium to uranium ratio in the soil and saprolite at P-1 is significantly higher than in the unaltered bedrock, suggesting that while both uranium and thorium are enriched near the surface, thorium is enriched to a greater degree. Thus, some uranium may have been mobilized into ground water and extracted from the rock during weathering and was deposited in the saprolite and soils. The observed abundant monazite and the high content of rare-earth elements in core samples indicate that monazite is the principal thorium-bearing mineral. Although some uranium may be incorporated in the monazite, geochemical data suggest that uranium and possibly thorium are also present in another form.

Drill Hole P-1

Cores were recovered to a depth of 140 feet at P-1. Samples from 18 depth intervals were analyzed for geochemical composition (Tables 2, 3, and 4). A soil sample collected near P-1 (SS-1, Table 8) contains the highest uranium (14.7 ppm) and thorium (600 ppm) values found in all soil samples from the area.

Thorium concentrations in the cores decrease with depth. Thorium values of samples from less than 45 feet deep are both higher and more variable than samples deeper in the hole. Core descriptions (Appendix I) indicate that the transition from saprolite to bedrock occurs at about 46 feet. The mean thorium value of the saprolite and soil section (0-45 ft) is 33.4 ppm and the mean for bedrock is 8.6 ppm. This suggests that the weathering process tends to concentrate thorium-bearing minerals.

The uranium log of P-1 (Figure 19) resembles the thorium log, with higher values at shallow depths. The principal difference in the two logs is a less-marked enrichment in shallow cores, especially evident in core sample P-1-2 (21.0-ft depth), which has moderate uranium but high thorium. The mean uranium content of the saprolite cores (2.6 ppm) is greater than that for the bedrock cores (1.6 ppm). Uranium and thorium content are moderately correlated in the P-1 samples (r=0.778). Saprolite shows a slightly better uranium to thorium correlation than bedrock (0.75 vs 0.68).

The thorium to uranium ratio of samples from P-1 decreases with depth (Figure 19). The mean thorium to uranium ratio of soil and saprolite (11.7 ppm) is greater than that of the gneiss (5.1 ppm). The difference was determined to be significant at a 95 percent confidence level by multiple comparison analysis.

Drill Hole P-2

Drill hole P-2 penetrated soil and saprolite to a depth of about 32 feet, then gneissic bedrock to a total depth of 160 feet (Appendix II). The uranium and thorium contents of soil samples collected near this drill site (6920, 6921, 6922) are among the highest of the 1977 and 1978 survey. The mean thorium content of the 21 core samples from P-2 (21 ppm) is nearly the same as at P-1 (Table 6). The saprolite and soil section has a higher mean thorium content

Table 12. Gamma-ray spectrometer survey.

	Location		Ground					
	Latitude ° ' "	Longitude ° ' "	Total Count (cps)	eU ppm	eTh ppm	K %	Th/U	Comments
GR-1	37 32 10	77 56 42	405	6.0	321.4	1.1	53.6	Western part of northern radioactivity anomaly
GR-2	37 32 07	77 56 29	400	7.1	51.8	1.1	7.7	North-central part of northern radioactivity anomaly
GR-3	37 31 54	77 56 28	3000	14.0	641.0	2.2	45.8	Central part of northern radioactivity anomaly
GR-4	37 31 48	77 56 17	100	10.0	70.3	1.2	7.0	Southwest part of northern radioactivity anomaly
GR-5	37 31 48	77 56 17	400	6.2	179.0	0.3	28.9	Southwest part of northern radioactivity anomaly
GR-6	37 31 40	77 56 21	400	4.5	53.3	1.3	11.8	South-central part of northern radioactivity anomaly
GR-7	37 31 40	77 56 18	700	4.0	193.4	1.2	48.2	Stream sediment, tributary to Fighting Creek
GR-8	37 31 03	77 56 32	400	1.2	93.2	0.7	77.5	Southern radioactivity anomaly
GR-9	37 30 55	77 56 37	-	3.6	25.2	4.8	7.0	Maidens gneiss, fresh exposure in creek
GR-10	37 30 56	77 56 35	700	5.8	291.0	0.6	50.2	Stream sediment, Fighting Creek tributary south of southern anomaly
GR-11	37 30 54	77 56 30	900	2.0	186.0	0.1	93.0	Ground water seep

(28.2 ppm) than the gneiss (14.3 ppm). The thorium log shows, however, that only the uppermost few feet of core have elevated thorium content (98 ppm). The remainder of the saprolite has thorium values similar to bedrock.

The mean uranium content of samples from P-2 cores (3.1 ppm) is higher than the mean of samples from P-1 cores (2.1 ppm). The difference between core samples is expressed in both the soil/saprolite (3.5 ppm vs 2.6 ppm) and the gneiss (2.6 ppm vs 1.6 ppm). As with thorium, elevated uranium levels in P-2 are limited to the two uppermost core samples. There is no distinct change in the uranium content at the saprolite-bedrock boundary at the 32-foot depth (Figure 20). The thorium to uranium ratio at P-2 is high in the near-surface core samples (Figure 20). No relationship of the ratio to core depth is seen except in the soil zone.

Uranium and thorium are correlated at P-2 with an overall correlation coefficient of 0.87. The uranium and thorium content correlate in the saprolite ($r = 0.97$) but fluctuate randomly in the gneiss ($r = 0.003$), suggesting that the weathering and transport processes deplete the rock of uranium, leaving fewer minerals with relatively fixed uranium and thorium proportions in the residuum.

Rare-Earth Elements

Four core samples from P-1 and seven core samples from P-2 were analyzed for a wide range of elements including eight rare-earth elements of the lanthanum series (Tables 2, 3, 4, and 6). Correlation analysis on the results of the rare-earth analyses indicates that the amount of thorium in the core samples is directly related to the concentration of lanthanum, cerium, neodymium, and samarium. All of these elements show high correlation coefficients of 0.96 to 0.99 among the 24 possible pairs (Table 15). Other rare-earth elements show little or no correlation with the exception of terbium, which shows correlation coefficients 0.85 to 0.90 with

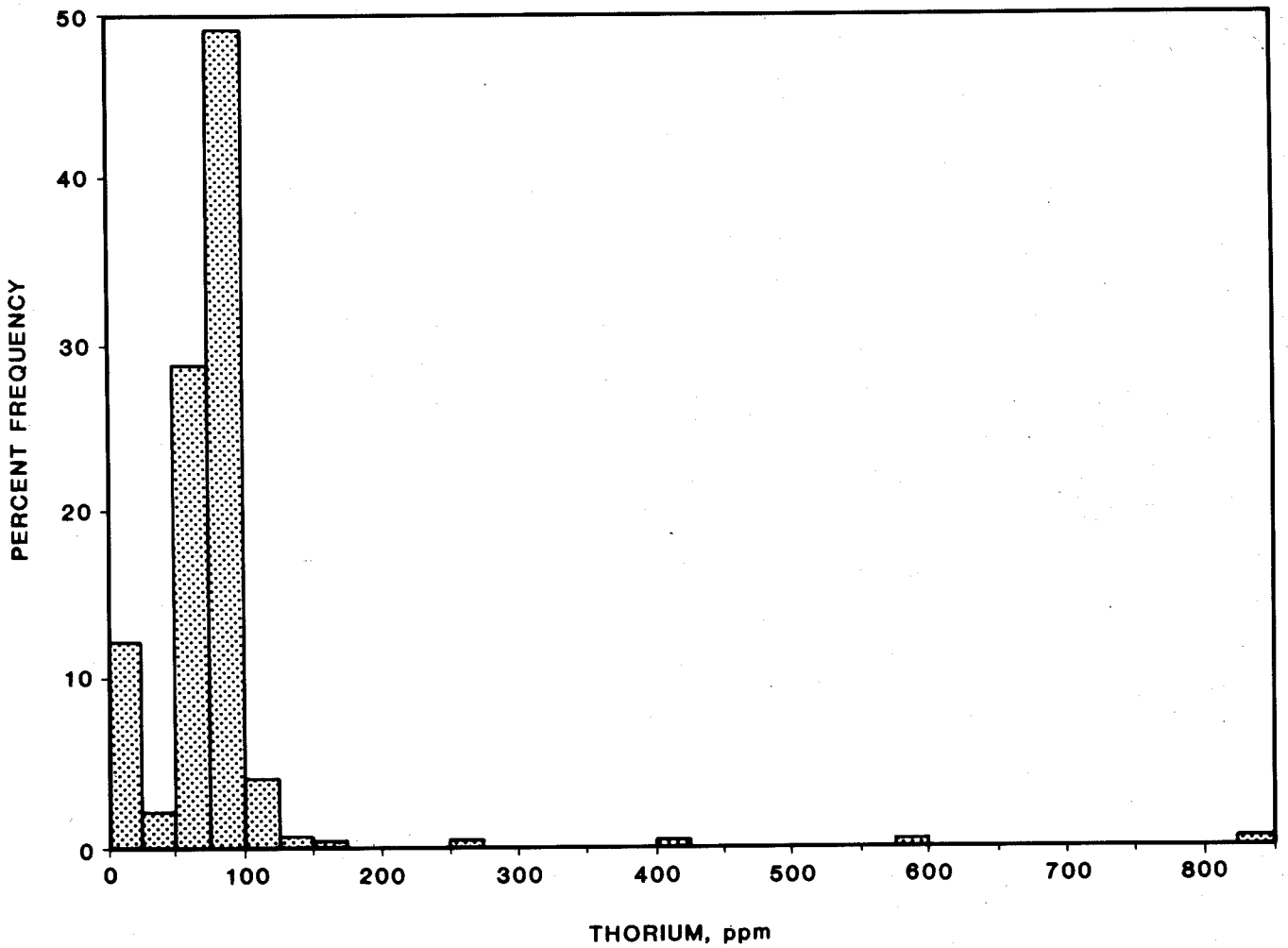

Figure 14. Histogram of thorium content in all samples.

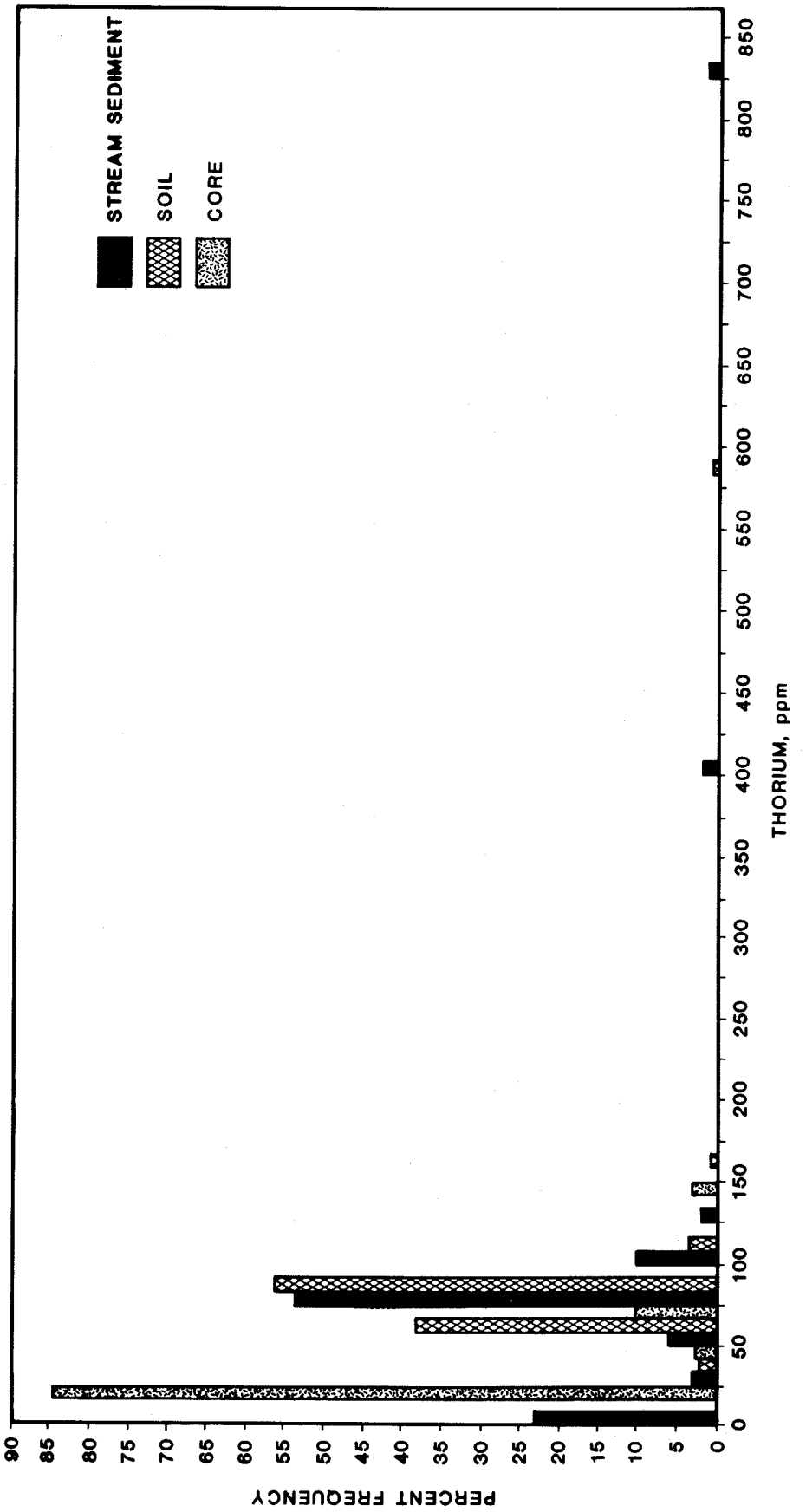

Figure 15. Histogram of thorium content in core, stream sediment, and soil.

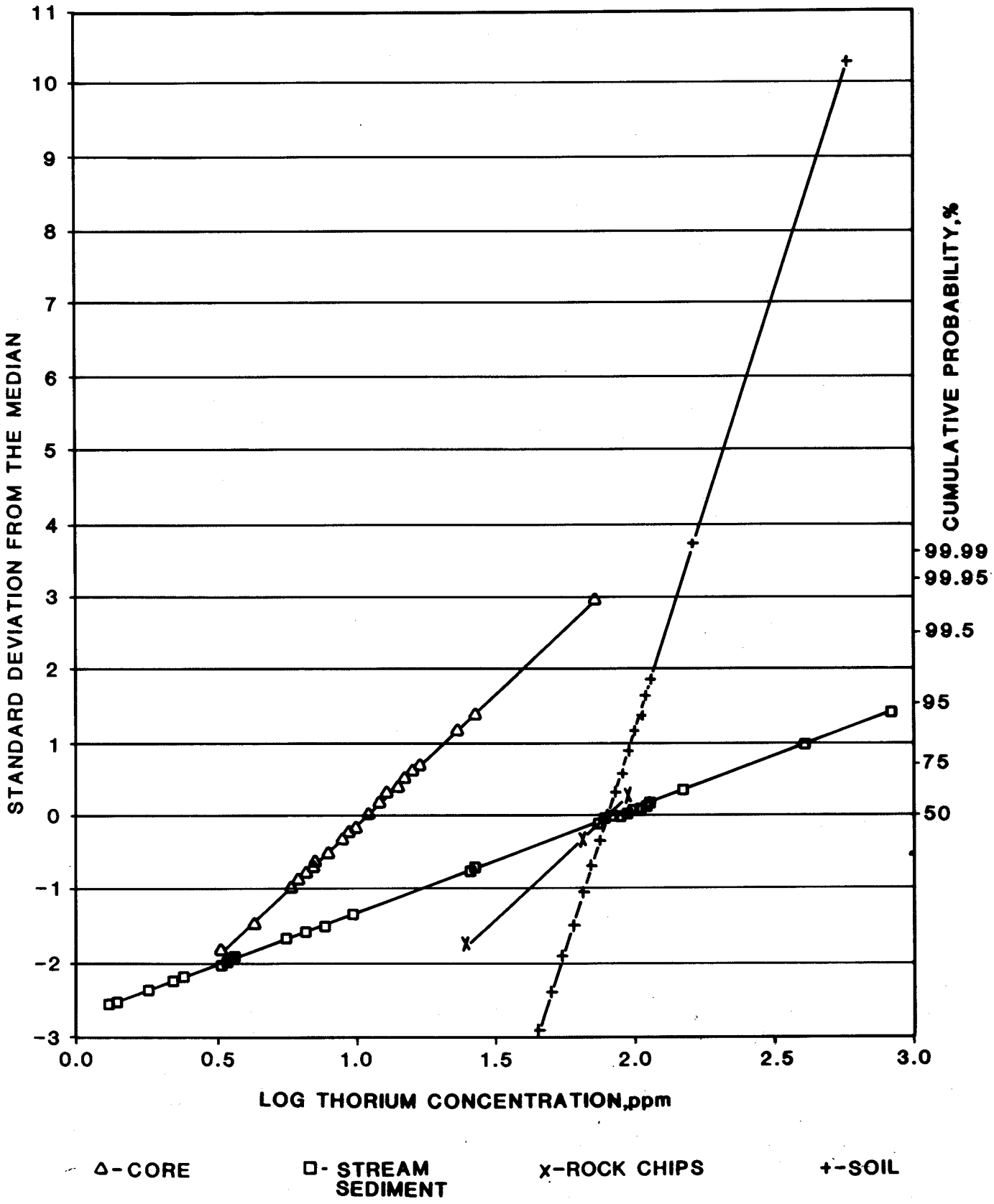

Figure 16. Cumulative probability plot for thorium.

lanthanum, cerium, neodymium, and samarium and 0.96 with thorium. Uranium correlates well with lanthanum, cerium, neodymium, and samarium with coefficients of 0.93 to 0.95. Uranium content varies with thorium content (r=0.95), but the correlation is not as close as that between thorium and lanthanum, cerium, neodymium, and samarium.

The strong correlation of thorium and the four rare earths indicates that thorium is present principally as monazite, which is a phosphate of lanthanum, cerium, and thorium, often with significant amounts of other lanthanum series elements. Analyses of monazite from pegmatite in Amelia County (Overstreet, 1967) show that in addition to lanthanum, cerium, neodymium, samarium, and thorium, the monazite contains minor amounts of praseodymium, yttrium, and gadolinium. Praseodymium and gadolinium were not determined in the analyses of the Powhatan cores. Yttrium was measured in the core samples but was not well correlated with the other reported rare-earth constituents of monazite or thorium. The relative abundance of yttrium in the core samples is higher than that reported for Amelia monazite (Overstreet, 1967). Yttrium is probably present in zircon where relatively heavy rare earths are characteristic.

Comparison of the analytical data from the Amelia monazite sample and the Powhatan cores normalized to a constant lanthanum content indicates that the core has more cerium and less neodymium, samarium, and thorium assuming that all of these elements in the core are present principally as monazite (Table 16). With a constant lanthanum or cerium content the thorium content of the presumed monazite in the Powhatan cores is 24 to 30 percent of that in the most thoroughly analyzed sample from Amelia (2.4 percent). This implies that 0.6 percent of core sample P-2-16 with a thorium content of 140 ppm is composed of monazite. Similarly, 2.4 percent

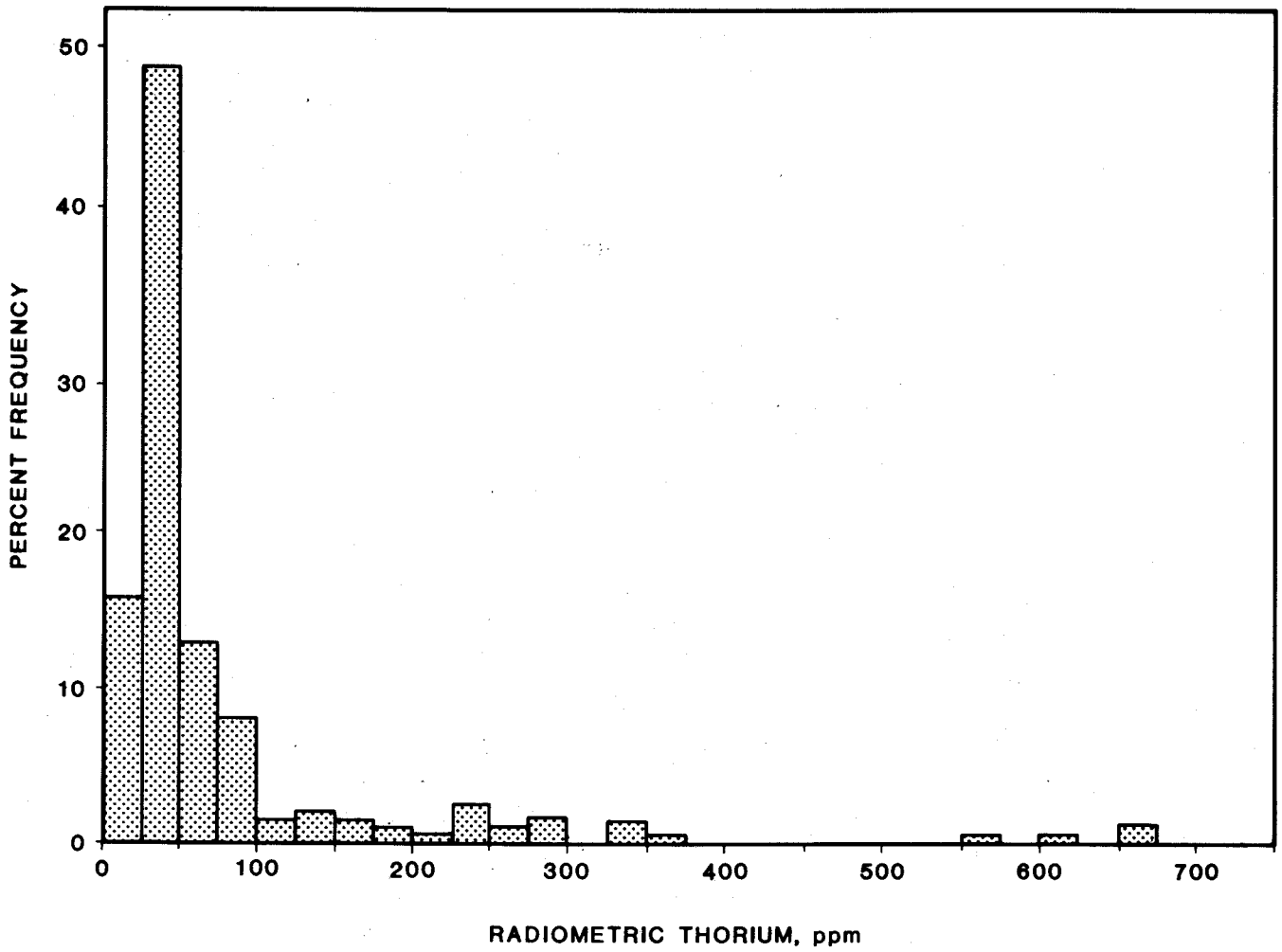

Figure 17. Histogram of radiometric thorium content in all samples analyzed.

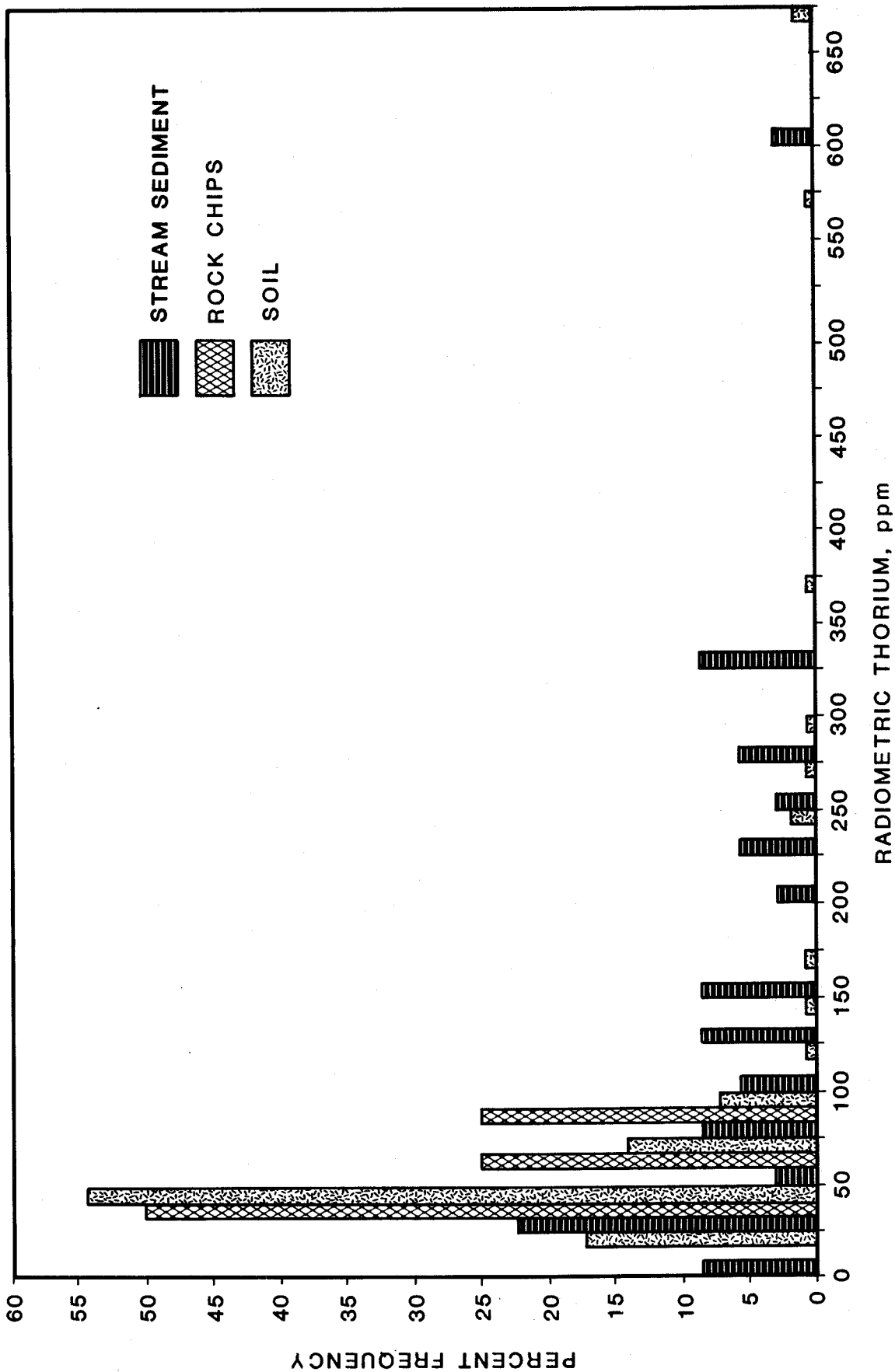

Figure 18. Histogram of radiometric thorium content in stream sediment, rock chips, and soil.

Table 13. Correlation matrix of selected geochemical values of stream sediment samples.

	Co	V_2O_5	U	eU	Th	eTh
Co	1.000	0.488	-0.173	-0.048	-0.207	-0.067
V_2O_5	0.488	1.000	-0.340	-0.281	-0.293	-0.272
U	-0.173	-0.340	1.000	0.380	0.470	0.400
eU	-0.048	-0.281	0.380	1.000	0.594	0.959
Th	-0.207	-0.293	0.470	0.594	1.000	0.552
eTh	-0.067	-0.277	0.400	0.959	0.552	1.000

Table 14. Correlation matrix of selected geochemical values of soil samples.

	Co	V_2O_5	U	eU	Th	eTh
Co	1.000	0.386	-0.057	0.040	0.140	0.219
V_2O_5	0.386	1.000	-0.175	-0.215	-0.089	-0.136
U	-0.057	-0.175	1.000	0.400	0.162	0.450
eU	0.040	-0.215	0.400	1.000	0.011	0.732
Th	0.140	-0.089	0.162	0.011	1.000	0.090
eTh	0.219	-0.136	0.450	0.732	0.090	1.000

of the soil sample near P-1 (SS-1) would have to be monazite to account for the thorium content of 600 ppm.

Uranium in the cores is correlated with the rare-earth and thorium components with correlation coefficients of 0.93 and 0.95. This indicates that at least some of the uranium also occurs in monazite. There is a good possibility that some of the uranium may also occur in zircon. Overstreet (1967) reported analyses of two Amelia monazite samples with U_3O_8 content of 0.1 percent and 0.2 percent, and thorium to uranium ratios of 24 and 37. This compares with a mean thorium to uranium ratio of 9.42 for the 11 core samples analyzed for rare-earth elements.

The lower correlation of uranium to thorium and rare earths (r = 0.93 and 0.95) compared with thorium to rare earth correlations (r = 0.97 and 0.99) may indicate that uranium varies in abundance within the monazite crystal structure, with relatively fixed thorium and rare-earth proportions, or that uranium is also present in another mineral. The presence of uranium in a form other than monazite, or variation in the uranium content of monazite, is also suggested by comparison of the radioactive-element and rare-earth enrichment in saprolite relative to gneiss. The mean values of thorium and uranium are higher in saprolite (45 ppm and 4.4 ppm) than in gneiss (14 ppm and 2.6 ppm). The enrichment is also apparent in mean values of lanthanum (125 ppm and 48 ppm), cerium (219 ppm and 92 ppm), neodymium (88 ppm and 40 ppm), and samarium (13.6 ppm and 7.4 ppm). Thus, the relative enrichment in the saprolite cores expressed as ratios of mean values is 3.3 times for thorium, 2.2 times for the four rare earths, and 1.7 times for uranium. This suggests that although uranium is generally enriched during the weathering process, it is not enriched to the extent of thorium or the rare earths.

The presence of radioactive zircon grains in the Maidens gneiss was indicated by pleochroic haloes

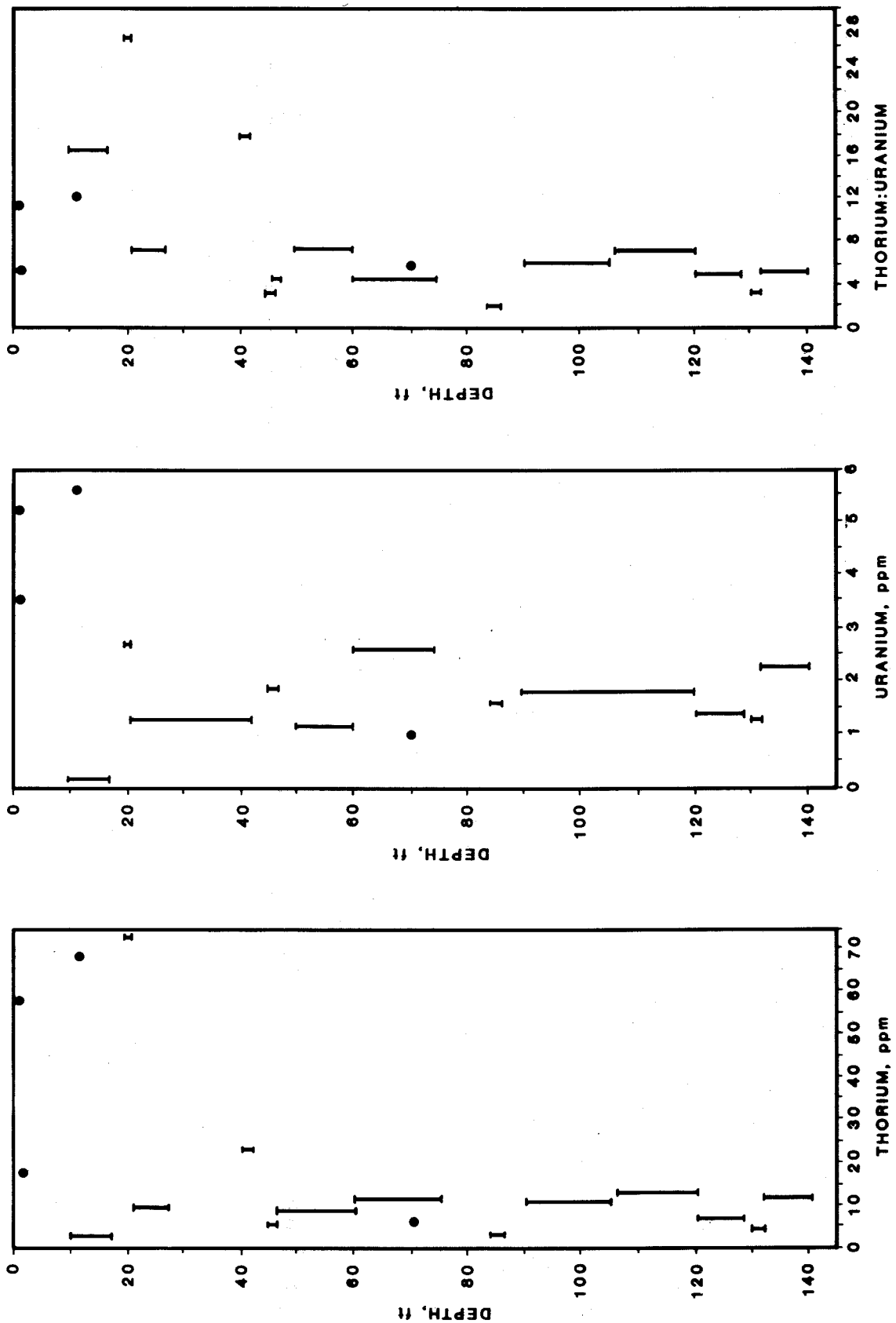

Figure 19. Thorium and uranium content and thorium to uranium ratios of cores from drill hole P-1 (dot represents point sample; bar represents interval sample).

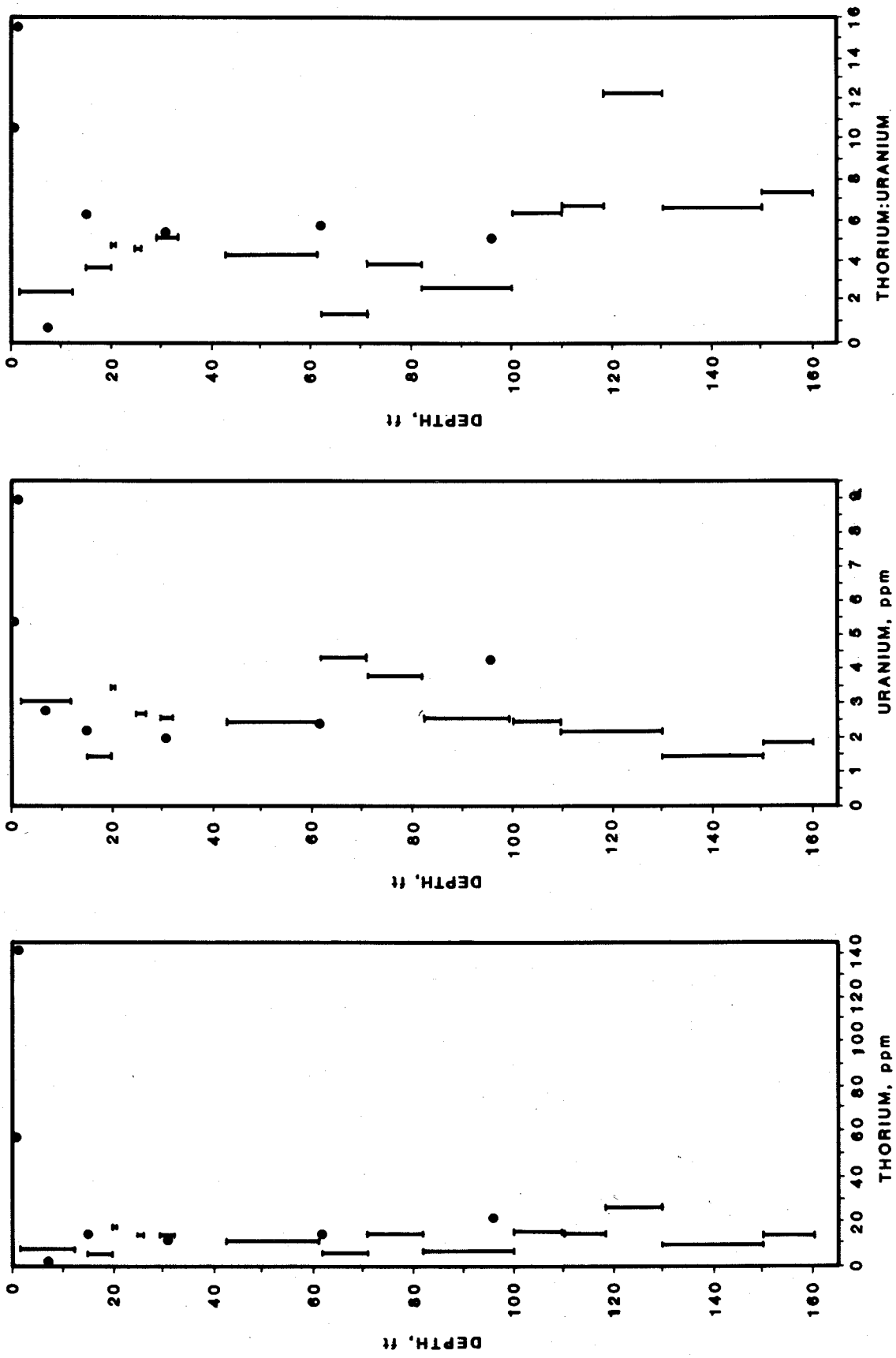

Figure 20. Thorium and uranium content and thorium to uranium ratios of cores from drill hole P-2 (dot represents point sample; bar represents interval sample).

Table 15. Correlation matrix of radioactive and selected rare earth elements in 11 core samples.

	U	Th	La	Ce	Nd	Sm	Eu	Tb	Yb	Lu	Ta	Nb	Y	Zr
U	1.000	0.952	0.935	0.941	0.937	0.921	-0.258	0.841	0.099	0.236	0.665	0.714	0.085	0.634
Th	0.952	1.000	0.993	0.994	0.987	0.966	-0.159	0.820	-0.054	0.072	0.665	0.646	-0.007	0.551
La	0.935	0.993	1.000	0.998	0.996	0.985	-0.076	0.857	0.004	0.118	0.644	0.590	0.031	0.510
Ce	0.941	0.994	0.998	1.000	0.997	0.986	-0.087	0.863	0.001	0.119	0.631	0.589	0.039	0.518
Nd	0.937	0.987	0.996	0.997	1.000	0.992	-0.060	0.878	0.020	0.131	0.607	0.561	0.063	0.484
Sm	0.921	0.966	0.985	0.986	0.992	1.000	0.017	0.910	0.087	0.188	0.549	0.506	0.066	0.438
Eu	-0.258	-0.159	-0.076	-0.087	-0.060	0.017	1.000	0.044	0.188	0.106	-0.379	-0.626	0.115	-0.500
Tb	0.841	0.820	0.857	0.863	0.878	0.910	0.044	1.000	0.483	0.548	0.528	0.472	0.335	0.530
Yb	0.099	-0.054	0.004	0.001	0.020	0.087	0.188	0.483	1.000	0.984	0.168	0.061	0.604	0.350
Lu	0.236	0.072	0.118	0.119	0.131	0.188	0.106	0.548	0.984	1.000	0.295	0.190	0.644	0.497
Ta	0.665	0.665	0.644	0.631	0.607	0.549	-0.379	0.528	0.168	0.295	1.000	0.785	0.246	0.853
Nb	0.714	0.646	0.590	0.589	0.561	0.506	-0.626	0.472	0.061	0.190	0.785	1.000	-0.112	0.818
Y	0.085	-0.007	0.031	0.039	0.063	0.066	0.115	0.335	0.604	0.644	0.246	-0.112	1.000	0.363
Zr	0.634	0.551	0.510	0.518	0.484	0.438	-0.500	0.530	0.350	0.497	0.853	0.818	0.363	1.000

Table 16. Relative distribution of selected rare earth elements in core samples and Amelia County monazite.

Element	Core Samples (Powhatan County)		Monazite (Amelia County)	
	P-2-16	Mean of 11 samples	(Overstreet, 1967)	Konig (1882)
La	1.00	1.00	1.00	1.00
Ce	1.73	1.77	2.21	1.58
Nd	0.72	0.72	1.14	
Sm	0.11	0.12	0.31	
Th	0.36	0.35	1.14	1.80

in biotite (Appendix III). Because zircon is heavy and very resistant to weathering, it tends to concentrate in soil and stream sediment with monazite. In most cases, the amount of uranium in zircon is higher than the amount of thorium in zircon (Peterman and others, 1986; Zartman and others, 1986; Stern and others, 1981) but the reverse has been reported in some cases where zircon contains up to 13.1 percent thorium and 2.7 percent uranium (Hounflow, 1976). The composition of zircon in the Maidens gneiss is unknown. Some of the fluctuation of uranium and thorium content in cores relative to lanthanum, cerium, and neodymium may be caused by the presence of zircon. The correlation matrix for selected core samples (Table 15) indicates that zirconium is slightly more correlated with uranium (r = 0.634) than with thorium (r = 0.551). However, the stronger correlation of uranium and thorium to the rare-earth elements which characterize monazite (r = 0.92 and 0.99) indicates that the contribution of zircon to the observed radioactivity is probably much less than that of monazite.

A nonquantitative analysis of the soil portions using a germanium-lithium gamma-ray spectrometer of the P-1 and P-2 cores was done by Paul E. Benneche at the Department of Nuclear Engineering, University of Virginia. Based on a gross 30-minute count (measured at top of detector), most of the "counts" are attributed to the thorium-232 series. The daughters detected were lead-212, actinium-228, radium-224, and thallium-208. For the uranium-238 series, polonium-214, lead-214, minor bismuth-214, and very minor radium-226 were measured. The overall counts from the uranium daughters are small when compared with the thorium daughters.

Summary of Geochemistry

Analysis of data collected in 1977-1978 and 1986 indicates that the different analytical methods employed give comparable results with samples of similar type. The principal source of the lower thorium and uranium values in the two data sets is a difference in sample type. Most of the 1986 samples were gravel or core samples in which the radioactive heavy minerals would not have been concentrated. It is possible that the colorimetric and radiometric methods used to determine thorium in the 1977-1978 survey may have overestimated the quantities present at low absolute concentrations.

Contour maps of element distribution in soil samples show a north-south lineation in radioactive elements but a random pattern of cobalt and vanadium. Elevated levels of uranium and thorium coincide with the ground radioactivity anomaly where P-2 was drilled. Although both elements are enriched near the anomaly, uranium is more enriched. Thus, a high in the uranium to thorium ratio corresponds with the anomaly. Local highs in uranium and thorium do not correspond with the ground radioactivity anomaly located at P-1. Local chemical highs were found in soil east (downslope) of the P-1 ground radioactivity anomaly.

Uranium content of the stream sediment is significantly higher than that of soil samples, with the very highest uranium values limited to stream sediment. Similarly, the highest thorium values are from selected stream sediment. A few soil samples collected near P-1 and P-2, however, show very high uranium and thorium levels that are nearly as enriched as the anomalous stream-sediment samples.

Uranium and thorium content are well correlated in core samples, moderately correlated in stream-sediment samples, and not related in soil samples. Uranium values measured chemically and by radiometric assay are not always correlated.

Samples from both drill sites indicate higher uranium and thorium levels at shallow depths. The elevated values appear to extend throughout the 30-foot saprolite zone at P-1 but to be limited to the soil zone at P-2. Thorium appears to be more enriched in shallow cores than uranium, implying that the two radioactive elements may be present in different minerals with most of the thorium in more resistant minerals. Both uranium and thorium are present in the bedrock at higher levels at P-2 than at P-1.

Thorium content of the core samples which were more extensively analyzed shows a very strong correlation with lanthanum, cerium, neodymium, and samarium and a much lower correlation with other rare earths. These four rare-earth elements are principal components of monazite, a thorium-bearing mineral. Lower, but strong, correlations of the monazite constituents with uranium suggest that some uranium occurs with thorium in the monazite. Thorium and uranium are enriched in near-surface core samples as expected for a resistant mineral like monazite. Comparison of the degree of weathering enrichment of the monazite constituent elements suggests that other uranium and thorium-bearing minerals may also be present in small amounts and indicates that the monazite is unevenly distributed through the rock.

DISCUSSION

The petrographic study of 39 thin sections, supplemented with X-ray diffraction analysis, did not confirm any granulite-grade mineral assemblages suggested for the Goochland terrane by Farrar (1984). This may be due to the sample selection procedure. Some alteration products suggest the former presence of pyroxene from an earlier metamorphic event, possibly of granulite grade. The petrographic study confirmed that the Maidens gneiss exhibits evidence of amphibolite-grade metamorphism and later hydrothermal alteration. Sericitization occurs along cleavage planes. Chlorite commonly replaces biotite. The only radioactive minerals identified are monazite and zircon. Monazite content averages about 0.5 percent in the gneiss but in one thin section totals 10.3 percent.

A layer of saprolite that ranges from 0 to 60 feet in thickness overlies the Maidens gneiss in the Powhatan study area. Chemical analyses of this saprolite indicate considerable depletion of soluble elements. They also indicate relative concentration of resistant heavy minerals, locally highly radioactive, in the upper part of the saprolite.

In some of the streams, where the ground water is discharged from saprolite as springs, radioactivity is much higher than away from the immediate vicinity of the spring. The source of the radioactivity is uncertain but may be due to radioactive precipitates on rocks or degassing of ^{220}Rn and ^{222}Rn.

The ground radioactivity survey confirms the anomalous radioactivity mapped from the air and shows that the intensity of the anomalies relative to the background is much higher than indicated by airborne measurements. The results of the geochemical analyses indicate that the highly anomalous radioactive zone coincides with the axial trace of the Goochland anticline. The results of the Geodata International, Inc. (1975) aeroradiometric survey indicate that the radioactive zone is at least 20 miles long and as much as 5 miles wide (Figures 21, 22, and 23) and appears to follow the Goochland anticline.

Geochemical analyses of soil near the radioactivity anomalies indicate enhanced values of uranium but near-background levels of thorium. Analyses of soil and very shallow cores using a different method of determination (INAA) and gamma-ray spectrometry show that the increase in uranium near radioactive anomalies is accompanied by a proportionately larger increase in thorium. Thus, the correspondence of low thorium to uranium ratios over radioactivity anomalies may be due to analytical differences in determining thorium.

Uranium and thorium values define anomalies which parallel the trends in aeroradiometric anomalies, ground radioactivity, metamorphic foliation, and regional structures. Increased levels of thorium and uranium are present in the soil sampled near P-2. However, local maxima of both uranium and thorium in soil are displaced to the east and downslope from the major radioactivity anomaly at P-1. Uranium and thorium values are not correlated in soils, indicating redistribution of these elements during soil formation.

Gamma-ray spectrometry of the anomalies shows that both thorium and uranium are enriched in the near-surface compared to bedrock. Thorium is enriched to a greater degree, however, implying that the two radioactive elements may occur in different minerals.

Uranium and thorium are enriched in some sediment samples from Fighting Creek and its tributaries. The radioactive stream sediments are not systematically concentrated in any particular stream. The high-value sample locations are at times separated by a number of sample locations with only background values. The sporadic distribution of these samples with high uranium and thorium values may indicate that the radioactive material is

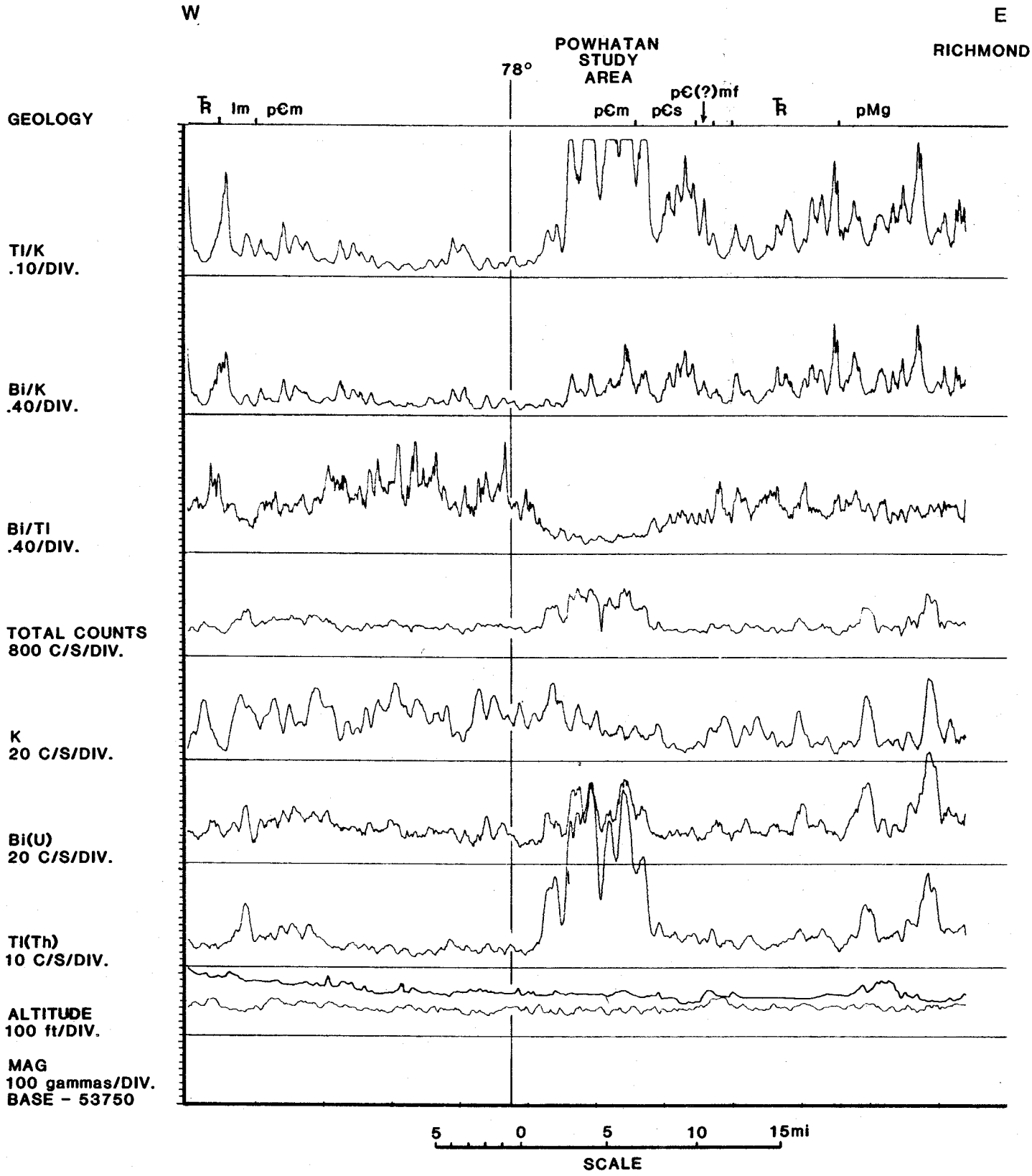

Figure 21. Aeroradiometric profile ML-95 (for geologic symbols see Figure 3) (modified after Geodata International, Inc., 1975).

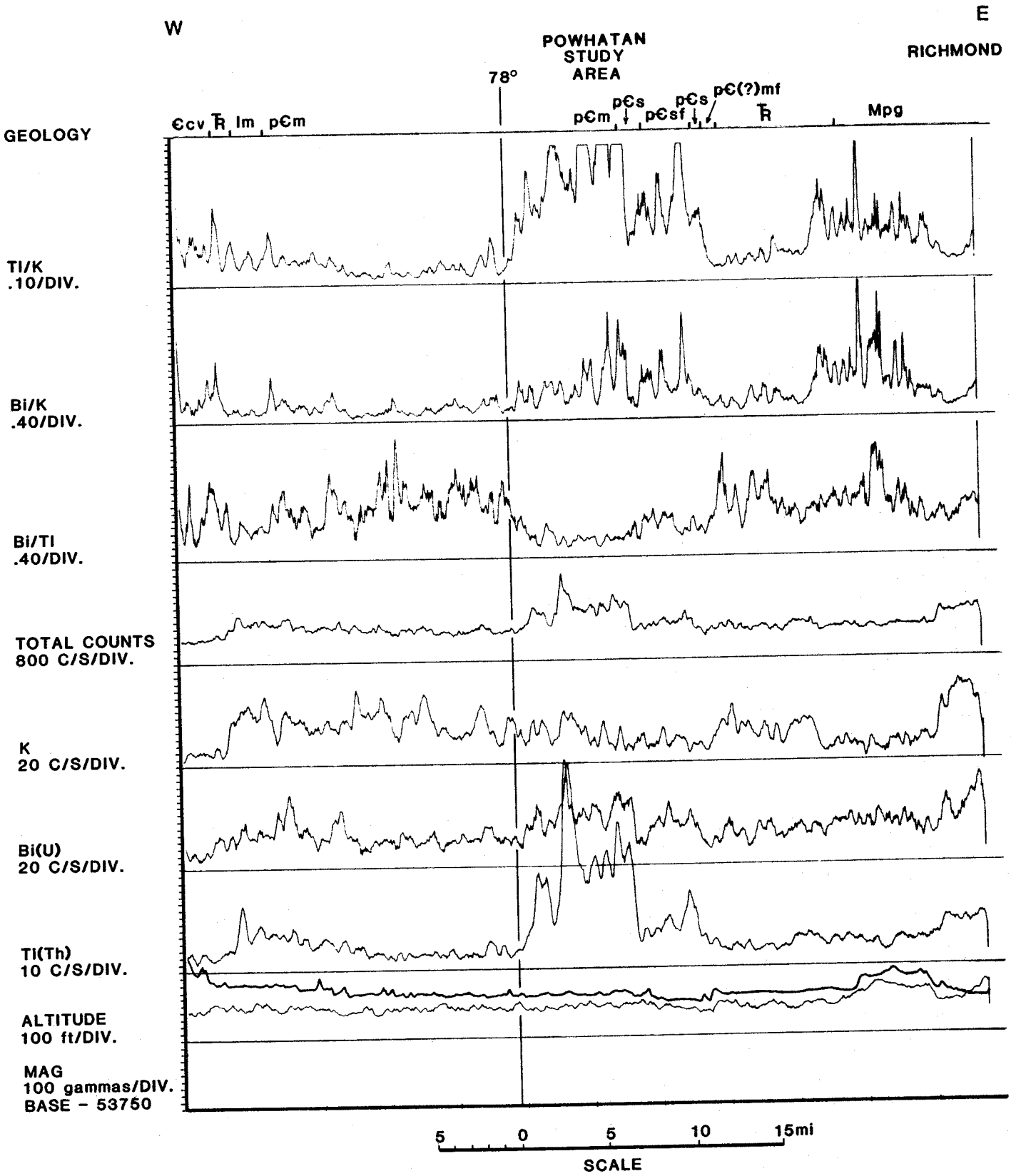

Figure 22. Aeroradiometric profile ML-96 (for geologic symbols see Figure 3) (modified after Geodata International, Inc., 1975).

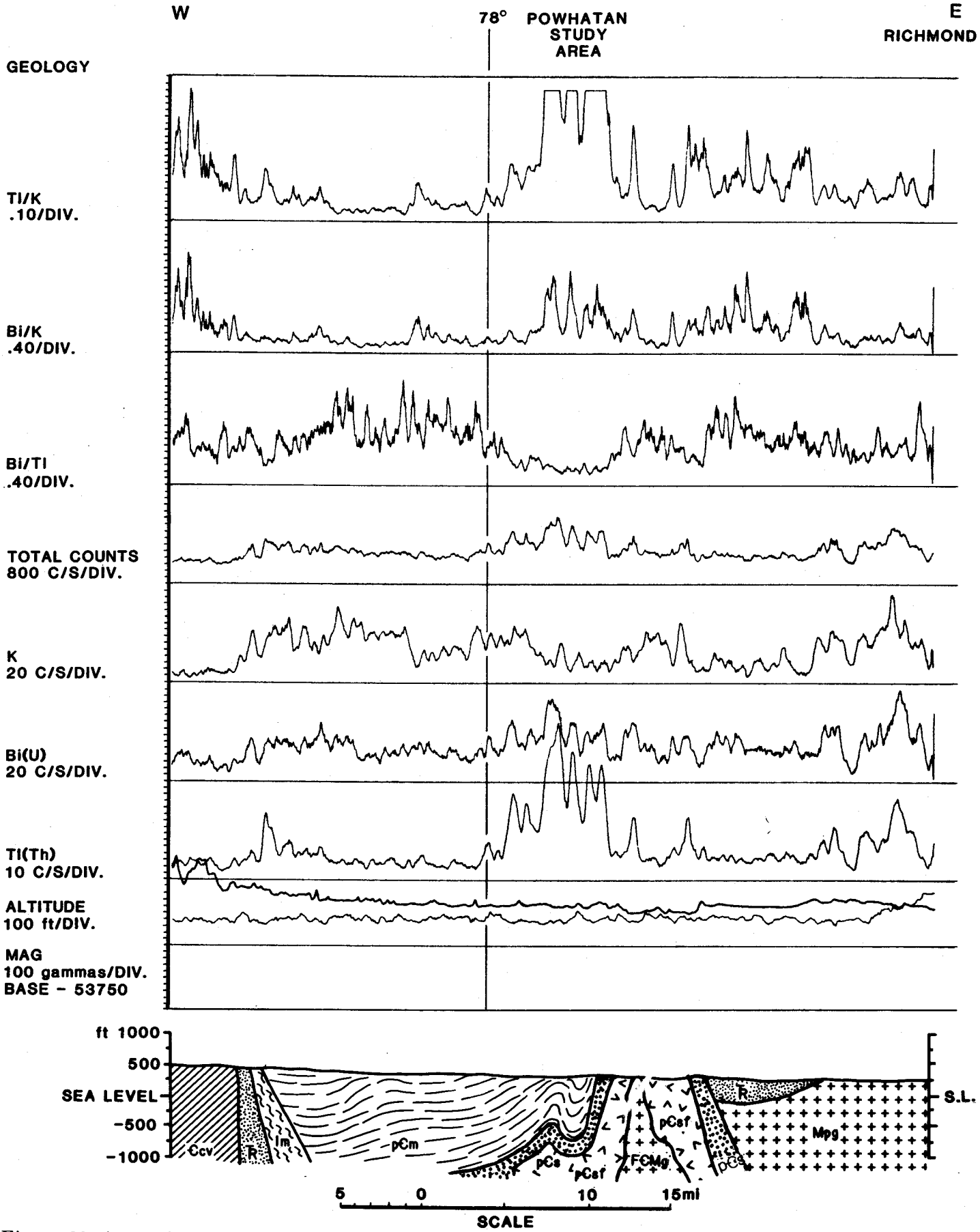

Figure 23. Aeroradiometric profile ML-97 and geologic cross section (for geologic symbols see Figure 3) (modified after Geodata International, Inc., 1975).

unevenly distributed in the sediment or that it was not consistently sampled. The distribution of highly radioactive samples of stream sediment is consistent with gravity segregation of heavy minerals. Uranium and thorium are moderately correlated in gravel samples, indicating that the minerals concentrated in the stream beds contain both uranium and thorium, although not necessarily in the same mineral.

Agreement of geochemically determined elemental abundance and measured radioactivity is imperfect. Although near-surface cores and some soil samples have a high content of thorium and uranium, the soil samples collected do not have consistently anomalous concentrations at the radioactivity maxima. The very high radioactivity measured on the ground (up to 80 times background) does not have a correspondingly large geochemical value in any sample. The A soil horizon, which was not sampled due to possible interaction of organic matter and mobile uranium, could potentially host higher quantities of radioactive minerals than the B horizon, which was sampled. The increase in both thorium and uranium at shallow depths in both cores limits the most radioactive zone to the soil and shallow saprolite zones.

The geochemical evidence points to concentration of resistant radioactive minerals during weathering and stream transport as the dominant factor in locally increasing surface radioactivity. Monazite was identified petrographically in the bedrock and can be inferred geochemically from characteristic rare-earth values in core samples.

Previous calculations based on abundance of monazite-specific rare-earth elements suggest that the monazite in the Maidens gneiss cored at P-1 and P-2 probably contains 2 to 5 percent thorium. An 80-times enrichment of thorium levels over a probable bedrock background of 15 ppm would yield 1200 ppm thorium. This thorium concentration could be achieved in a sample of 3 to 6 percent monazite. The core logs indicate an enrichment of thorium of five to 10 times in the soil relative to bedrock. It is not known whether very efficient weathering concentration could increase the monazite to the requisite 3 to 6 percent to produce the observed ground radioactivity anomalies.

Weathering or alluvial concentration of monazite could achieve the high levels suggested by the radioactivity anomalies if the rock from which the soil, saprolite, or stream sediment was derived was anomalously rich in monazite prior to decomposition. Petrographic analysis of cores from the two drill sites demonstrates that the Maidens gneiss contains intervals with high monazite concentrations. The median monazite content of the 12 samples submitted for petrographic analysis is 0.5 percent. One gneiss sample (P-2-87), however, has a monazite content of 10.3 percent. Such a concentration of monazite with thorium content of 2 to 5 percent results in a thorium concentration of 2000 to 5000 ppm in the rock, and is clearly sufficient to produce a radiometric anomaly of 80 times background even without concentration of residual heavy minerals by weathering.

A discrepancy in the petrographic and geochemical data suggests that the monazite in the Maidens gneiss may not have the thorium content indicated from geochemistry alone. The median monazite content of the 12 petrographic samples is 0.5 percent. However, the median thorium content of the Maidens gneiss cores is 10 to 20 ppm. The thorium content of monazite in the cores would appear to be at most 0.2 to 0.4 percent rather than the 2 to 5 percent calculated from geochemical parameters alone. The monazite-rich core sample (P-2-87) may therefore contain only 200 to 400 ppm thorium. If the monazite contains so little thorium, then another thorium-bearing mineral is necessary to achieve the same thorium to rare-earth ratios measured in the core samples. Even if the monazite grains in the Maidens gneiss are of unusually low thorium content, a zone with a monazite content of 20 times background could produce a strong radioactivity anomaly if concentrated by in-place weathering or stream transport.

Monazite abundance is often related to the presence of pegmatites. The well-documented monazite-bearing pegmatites in Amelia County are an example. Petrographic analysis of a pegmatite sample (P-2-96.5) indicates 0.6 percent monazite, very close to the typical monazite content of Maidens gneiss (0.5 percent). Monazite appears to be about as abundant in Maidens gneiss as in pegmatite in the cores examined and in one instance 17 times as abundant in Maidens gneiss as in pegmatite. Mertie (1953) estimated the typical monazite in monazite-bearing crystalline rocks of the southern Piedmont, including Virginia, to range from 0.00005 to 0.02 percent, with rare pegmatites ranging up to 0.1 percent monazite. Thus, the baseline monazite content of the bedrock of the study area appears to be richer in monazite by a factor of at least 10 compared with regional trends in monazite-rich rocks.

The occurrence of Maidens gneiss with extremely high monazite content (as much as 10.3 percent in one sample) in the subsurface of the study area suggests a possible mechanism to explain the correspondence of the radioactivity anomaly in the study area with the axial zone of the Goochland anticline. Although migration of radioactive elements through tension fractures along the crest of the anticline could produce a radioactivity trend conformable with the trend of the anticlinal axis (Walthier,

1955), only dissolved uranium would have the necessary mobility to migrate, because thorium is practically insoluble. Because the Powhatan anomaly is principally due to thorium, mobilization and migration is not the principal mechanism. If another interval of Maidens gneiss with high monazite content and lateral continuity had been present above the monazite zone found in sample P-2-87, progressive weathering and erosion may have removed all but the most resistant minerals. Thus, the radioactivity anomaly coincident with the crest of the Goochland anticline could result from a monazite-rich interval of Maidens gneiss, which was exposed by erosion and weathering due to its location on the anticlinal crest.

CONCLUSIONS

The results of the 1976-1978 and 1986 surveys and analyses indicate that the radioactive anomalies in the Powhatan area can be mainly attributed to thorium. In addition to thorium, elevated quantities of uranium are also present. Monazite, the main radioactive mineral, has been observed in thin sections and can be inferred to be present in soil and stream sediment based on geochemistry. The primary lithologic zone causing the anomalous radioactivity was not found, either in the surface outcrops or in the cores of two exploratory drill holes. The presence of significant pegmatite within the study area is doubtful because of the absence of anomalous amounts of ^{40}K.

Highly anomalous radioactivity of the Powhatan area extends south and north from the study area to form a significant radioactive zone. The entire zone coincides with the axis of the Goochland anticline. Both features trend parallel with the regional foliation, especially of the Maidens gneiss. Thus, it is concluded that the highly anomalous radioactive zone, at least in the Powhatan area, may be structurally controlled. A radioactive source containing sufficient monazite to produce the ground radioactivity anomalies was not detected in the P-1 and P-2 cores. It is suggested that the radiometric anomalies could be due to a zone in the Maidens gneiss with high concentrations of radioactive minerals which has been exposed by erosion in the Fighting Creek watershed, intrusion of a radioactive rock body along metamorphic foliations or regional fractures, or migration of radioactive elements in hydrothermal solutions along an existing fracture system. Alternatively, it may be confined to a lithostratigraphic unit exposed to the present geomorphologic surface along the axial part of the Goochland anticline.

ACKNOWLEDGMENTS

The writers would like to thank the management personnel of Wyoming Mineral Corporation (a former subsidiary of Westinghouse Electric Corporation no longer in business) for permission to utilize and publish company data. Special thanks are given to the management of Continental Forest Investments, Inc. for permission to drill on their property. We thank S. Leland Spradlin, Jr., Area Manager for Continental, for his time and efforts that resulted in a prompt and smooth drilling operation. Mr. E.W. Decker, Old Dominion University, prepared the computer-derived maps that were used as the basis for final contouring and some of the figures. The U.S. Geological Survey provided partial funding for the drilling and for geochemical analyses under the COGEOMAP project (Cooperative agreement No. 14-08-0001-A387). Special thanks are given to James K. Otton, David Gottfried, and Albert J. Froelich, U.S. Geological Survey, for their review of this paper. Many of their suggestions have been incorporated into this report; however, the writers are solely responsible for the data and interpretations.

REFERENCES CITED

Bice, K.L., and Clement, S.C., 1982, A study of the feldspars of the Montpelier andesine anorthosite, Hanover County, Virginia: Geological Society of America Abstracts with Programs, v. 14, p.5.

Brown, W.R., 1962, Mica and feldspar deposits of Virginia: Virginia Division of Mineral Resources Mineral Resources Report 3, 195 p.

Clement, S.C., and Bice, K.L., 1982, Andesine anorthosite in the eastern Piedmont of Virginia: Geological Society of America Abstracts with Programs, v. 14, p. 10.

Deuser, W.G., and Herzog, L.F., 1962, Rubidium-strontium age determinations of muscovites and biotites from pegmatites of the Blue Ridge and Piedmont: Journal Geophysical Research, v. 67, n. 5, p. 1997-2004.

Dietrich, R.V., 1970, Minerals in Virginia: Virginia Polytechnic Institute Research Divison Bulletin 47, 325 p.

Farrar, S.S., 1984, The Goochland granulite terrane: Remobilized Grenville basement in the eastern Virginia Piedmont, *in* M.J. Bartholomew, editor, The Grenville event in the Appalachians and related topics: Geological Society of America Special Paper 194, p. 215-227.

Gabelman, J.W., 1968, Uranium in Appalachian Mobil Belt: U.S. Atomic Energy Commission RME-4107, 41 p.

Geodata International, Inc., 1975, Aerial radiometric and magnetic survey of central Appalachian Triassic basin—parts of Virginia and the Carolinas: U.S. Energy Research and Development Administration Contract no. AT(05-2)-1644, v. 1, 63 p., v. 2, 111 p.

Glass, J.J., 1935, The pegmatite minerals from near Amelia, Virginia: American Mineralogist, v. 20, p. 741-768.

Glover, Lynn, III, Mose, D.G., Costain, J.K., Poland, F.B., and Reilly, J.M., 1982, Grenville basement in the eastern Piedmont of Virginia: a progress report: Geological Society of America Abstracts with Programs, v. 14, p. 20.

Glover, Lynn, III, Mose, D.G., Poland, F.G., Bobyarchick, A.R., and Bourland, W.C., 1978, Grenville basement in the eastern Piedmont of Virginia: implications for orogenic models: Geological Society of America Abstracts with Programs, v. 10, p. 169.

Goodwin, B.K., 1970, Geology of the Hylas and Midlothian quadrangles, Virginia: Virginia Division of Mineral Resources Report of Investigations 23, 51 p.

Grauch, R.I., and Zarinski, Katrin, 1976, Generalized descriptions of uranium-bearing veins, pegmatites, and disseminations in non-sedimentary rocks, eastern United States: U.S. Geological Survey Open-file Report 76-582, 114 p.

Hounflow, A.W., 1976, Mineralogy of uranium and thorium: a tabular summary: Colorado School of Mines Research Institute, chart.

Marline Uranium Corporation and Union Carbide Corporation, 1983, An evaluation of uranium development in Pittsylvania County, Virginia: Report prepared jointly to the Virginia Uranium Administrative Group, v. 1, 304 p.

Marr, J.D., Jr., 1985, Geology of the crystalline portion of the Richmond 1°x2° quadrangle: a progress report, *in* Geology of portions of the Richmond 1°x2° quadrangle: Seventeenth Annual Virginia Geological Field Conference, October 19-20, 1985: Virginia Division of Mineral Resources, 52 p.

Mertie, J.B., Jr., 1953, Monazite deposits of the southeastern Atlantic states: U.S. Geological Survey Circular 237, 31 p.

Nicholson, J.C., Burruss, T.R., and Jones, D.L., 1980, Soil survey of Goochland County, Virginia: U.S. Department of Agriculture, Soil Conservation Service in cooperation with Virginia Polytechnic Institute and State University, 137 p.

Overstreet, W.C., 1967, The geologic occurrence of monazite: U.S. Geological Survey Professional Paper 530, 327 p.

Pavlides, Louis, 1980, Revised nomenclature and stratigraphic relationships of the Fredericksburg Complex and Quantico Formation of the Virginia Piedmont: U.S. Geological Survey Professional Paper 1146, 29 p.

Pegau, A.A., 1932, Pegmatite deposits of Virginia: Virginia Geological Survey Bulletin 33, 123 p.

Peterman, Z.E., Zartman, R.E., and Sims, P.K. 1986, A protracted Archean history in the Watersmeet Gneiss dome, Northern Michigan, *in* Z.E. Peterman and D.C. Schnabel, editors, Shorter contributions to isotope research: U.S. Geological Survey Bulletin 1622, 221 p.

Poland, F.B., 1976, Geology of the rocks along the James River between Sabot and Cedar Point, Virginia [M.S. thesis]: Blacksburg, Virginia Polytechnic Institute and State University, 98 p.

Reber, E.J., Owens, V.M., and Swanson, C.B., in press, Soil survey of Powhatan County, Virginia: U.S. Department of Agriculture, Soil Conservation Service in cooperation with Virginia Polytechnic Institute and State University.

Reilly, J.M., 1980, A geologic and potential field investigation of the central Virginia Piedmont [M.S. thesis]: Blacksburg, Virginia Polytechnic Institute and State University, 111 p.

Stern, T.W., Bateman, P.C., Morgan, B.A., Newell, M.F., and Peck, D.C., 1981, Isotopic U-Pb ages of zircon from the granitoids of the Central Sierra Nevada, California: U.S. Geological Survey Professional Paper 1185, 17 p.

Virginia Division of Mineral Resources, 1975, Aeroradiometric contour map of the Powhatan 15-minute quadrangle: Virginia Division of Mineral Resources Open-file map, 1:62,500 scale.

Walthier, T.N., 1955, Uranium occurrences of the eastern United States: Mining Engineering, v. 37, p. 64-65.

Zartman, R.E., Kwak, L.M., and Christian, R.P., 1986, Uranium-lead systematics of a mixed zircon population-the granite at Yale Farm, Berkshire Massif, Connecticut, *in* Z.E. Peterman and D.C. Schnabel, editors, Shorter contributions to isotope research: U.S. Geological Survey Bulletin 1622, 221 p.

APPENDIX I
GEOLOGIC LOG: CORE HOLE P-1

Drilled by: Joy Manufacturing Co.
Spudding date: June 11, 1986
Completion date: June 12, 1986
Drilling method: diamond coring
Diameter of hole: NX(76.2 mm)
Inclination: vertical
Total depth: 140 feet

Topographic map: Powhatan 7.5-minute Quadrangle
Latitude: 37°31'49"
Longitude: 77°56'29"
Elevation: 325 feet (approx.)
Land owner: Continental Forest Investments, Inc.
Core description: Jan Krason

Depth interval (feet)	Thickness (feet)	Sample type	Sample No. and interval, (feet)	Type of analysis	Lithological characteristics
0.0 - 1.5	1.5	Bulk	P-1-15 (0.0-1.0)	Geochemical	Soil, light-gray and brown, with approx. 10% quartz, muscovite, and organic debris.
1.5 - 10.0	8.5	Bulk	P-1-16 (1.0-2.0)	Geochemical	Soil and saprolite (laterite), in lower part mixed with "sandy"-quartzose material (as much as 30% quartz; maximum to 5 mm) light-gray, yellowish, irregularly brown; includes pink garnet, muscovite flakes, and kaolinized feldspar, rare smoky quartz.
10.0 - 11.0	1.0				Sludge of quartz fragments, kaolinized feldspar, and muscovite.
11.0 - 17.0	6.0	Composite	P-1-1 (10.0-17.0)	Geochemical	Sludge of clayey "sand" mixed with kaolinitic clay, light gray, yellowish, including (as much as 90%) translucent quartz, muscovite and biotite plates, fragments of pink garnet, and kaolinized feldspar (as much as 15%).
		Bulk	P-1-17 (11.2-11.7)	Geochemical	
17.0 - 20.0	3.0				No samples.
20.0 - 21.0	1.0	Bulk	P-1-2 (20.0-21.0)	Geochemical	Sludge of 98% quartz fragments (1 to 3 mm), with feldspar, muscovite and biotite.
21.0 - 27.0	6.0	Composite	P-1-3 (21.0-27.0)	Geochemical	Saprolite (laterite) of decomposed (with fresh, harder blocks) biotite gneiss, thinly layered, with coarse grains of quartz and kaolinized feldspar (maximum to 8 mm), includes equiblasts of muscovite brown and black (in lesser amounts) biotite, pink garnet, and oxidized (into limonite) pyrite, gneissic foliation well preserved.
			P-1-6 (21.9-22.3)	X-ray	
27.0 - 40.0	13.0				No samples.

40.0 - 41.8	1.8	Composite	P-1-4 (40.0-41.8)	Geochemical	Sludge of coarse-grained quartz fragments, flakes of muscovite, pink garnet, and kaolinized feldspar with plagioclase.
			P-1-5 (40.0-42.0)	X-ray	
41.8 - 45.0	3.2				No samples.
45.0 - 46.0	1.0	Composite	P-1-5 (45.0-46.0)	Geochemical	Biotite gneiss, strongly weathered (decomposed), with small grains of limonite (oxidized pyrite).
46.0 - 47.0	1.0	Composite	P-1-6 (46.0-47.0)	Geochemical	Biotite gneiss, with kaolinized feldspar and quartz, with layers rich in biotite, with about 1% pyrite, and pink garnet.
47.0 - 50.0	3.0				No samples.
50.0 - 60.0	10.0	Composite	P-1-7 (50.0-52.0)	Geochemical	Biotite gneiss, equigranular, foliated, with layers of coarse-crystalline plagioclase and quartz (espec. 51 to 52 feet), strongly kaolinized and sericitized, with disseminated pyrite (as much as 3%), and aggregates (maximum to 5 mm) of pink garnet--locally as much as 5% of the rock mass, with brown flakes and black plates of biotite (secondary?).
60.0 - 74.5	14.5	Composite	P-1-8 (60.0-74.5)	Geochemical	Biotite gneiss, porphyroblastic, with feldspathic augen (maximum to 3 cm elongated with foliation), with feldspathic-plagioclase kaolinized and sericitized), quartz (mostly translucent) and biotite-rich layers, typical gneissic foliation, includes aggregates (maximum to 2 cm) of pink garnet, with well developed sillimanitic layers and lenses, also with layers almost exclusively of biotite (brown and black), locally strongly silicified, and chloritized, contains disseminated pyrite (about 2%) in veinlets (mostly euhedral).
			P-1-61 (61.0)	Petrographic	
			P-1-65 (65.0)	Petrographic	
		Chips	P-1-18 (70.0-70.3)	Geochemical	
			P-1-74 (74.0)	Petrographic	
74.5 - 86.0	11.5		P-1-75 (75.0)	Petrographic	Biotite gneiss, migmatitic, locally strongly contorted (with ptygmatic folds), with light gray quartzose-feldspathic-plagioclase and dark biotite-rich typical gneissic bands (ratio approx. 50:50, white bands prevail locally), with K-feldspar-microcline augen, locally strongly sillimanitic, sericitized, silicified with microquartz veins, with poikiloblasts and irregular aggregates of pink garnet, with disseminated pyrite in veinlets (av. approx. 2%).
			P-1-83 (83.0)	Petrographic	
		Composite	P-1-9 (84.0-86.0)	Geochemical	
86.0 - 105.3	19.3		P-1-88 (88.0)	Petrographic	Biotite gneiss, migmatic (with vertical zones and ptygmatic folds), with white (as much as 70%)-quartzose-feldspathic-plagioclase and thinner biotite-rich (with brown flakes and black plates) gneissic layers, locally strongly sillimanitic, sericitic, garnitiferous
		Composite	P-1-10	Geochemical	

			[90.0-105.3]		[with pink garnet as much as 5%], with disseminated pyrite [av. approx. 2%] in veinlets—more common in white bands.
			P-1-98 [98.0]	Petrographic	
			P-1-103 [103.0]	Petrographic	
			P-1-105 [105.0]	Petrographic	
105.3 - 120.0	14.7	Composite	P-1-11 [105.3-120.0]	Geochemical	Biotite gneiss, migmatitic, strongly contorted [with augen, maximum to 3 cm, and micro-ptygmatic folds], white quartzose-feldspathic-plagioclase and dark biotite-rich layers [30% in volume], commonly with pink garnet, locally strongly pyritic [approx. 3%]; in the lower part of this interval, rocks are brecciated with slickensides [fault zone?].
			P-1-106 [106.0]	Petrographic	
			P-1-115 [115.0]	Petrographic	
120.0 - 128.4	8.4	Composite	P-1-12 [120.0-128.4]	Geochemical	Biotite gneiss, migmatitic, contorted, with irregular gneissic layers and augen [maximum to 3 cm] of white quartzose-feldspathic-plagioclase and dark biotite-rich bands, fractured and micro-brecciated [without clear foliation], with pyrite [av. 1%].
			P-1-123 [123.0]	Petrographic	
			P-1-3 [125.1-125.4]	X-ray	
			P-1-127 [127.0]	Petrographic	
128.4 - 132.0	3.6	Composite	P-1-13 [128.4-132.0]	Geochemical	Biotite gneiss, with approx. 15% dark biotite layers, quartzose-feldspathic layers prevail, with pink garnet, locally strongly sericitized, with approx. 5% black plates of biotite [secondary?], with disseminated pyrite in veinlets [av. 2%].
			P-1-129 [129.0]	Petrographic	
			P-1-4 [129.5-129.9]	X-ray	
132.0 - 140.0	8.0	Composite	P-1-14 [132.0-140.0]	Geochemical	Biotite gneiss, and biotite schist with various amounts of quartz-ose-feldspathic porphyroblasts and augen, migmatized, with disseminated pyrite [as much as 3%]; occurs also in veinlets.
			P-1-136 [136.0]	Petrographic	
			P-1-1 [138.5-138.8]	X-ray	
			P-1-2 [138.6]	X-ray	

APPENDIX II
GEOLOGIC LOG: CORE HOLE P-2

Drilled by: Joy Manufacturing Co.
Spudding date: June 13, 1986
Completion date: June 15, 1986
Drilling method: diamond coring
Diameter of hole: NX(76.4 mm)
Inclination: vertical
Total depth: 160 feet

Topographic map: Powhatan 7.5-minute Quadrangle
Longitude: 77°56'33"
Latitude: 37°31'02"
Elevation: 295 feet (approx.)
Land owner: Continental Forest Investments, Inc.
Core description: Jan Krason

Depth interval (feet)	Thickness (feet)	Sample type	Sample No. and interval,(feet)	Type of analysis	Lithological characteristics
0.0 - 2.0	2.0	Bulk	P-2-15 (0.0-0.5)	Geochemical	Soil, light-brown, clayey and silty, with angular quartz fragments (maximum to 2 cm), with mica flakes and organic debris.
			P-2-16 (0.5-1.5)	Geochemical	
2.0 - 12.0	10.0	Bulk	P-2-1 (2.0-12.0)	Geochemical	Saprolite of decomposed biotite gneiss with well preserved gneissic texture, rusty yellowish-brown, with quartz fragments, kaolinized plagioclase in white layers (maximum to 3 cm thick), irregularly coated with manganese and oxidized iron, with strongly weathered biotite to light brownish color, with small grains of pink garnets.
			P-2-1 & 2 (5.0-5.3)	X-ray	
		Bulk	P-2-17 (7.0-7.2	Geochemical	
12.0 - 15.0	3.0				No samples.
15.0 - 20.0	5.0	Chips	P-2-18 (15.0-15.1)	Geochemical	Saprolite, white, mostly decomposed pegmatite, with quartz and plagioclase, with rare muscovite flakes, brown and black plates of biotite (appropx. 5%).
		Composite	P-2-2 (15.0-20.0)	Geochemical	
		Composite	P-2-3 & 4 (15.0-20.0)	X-ray	
20.0 - 20.5	0.5	Composite	P-2-3 (20.0-20.5)	Geochemical	Sludge of 98% quartz fragments (2 to 5 mm), with feldspar fragments (maximum to 10 mm), strongly limonitic.
20.5 - 20.7	0.2				Saprolite of fine crystalline biotite gneiss, with muscovite, decomposed.
20.7 - 25.0	4.3				No samples.

25.0 - 26.0	1.0	Composite	P-2-4 (25.0-26.0)	Geochemical	Saprolite of strongly weathered, limonitic, biotite gneiss, with white, kaolinized bands of plagioclase and quartz (2-4 mm), with loose quartzose fragments.
26.0 - 30.0	4.0				No samples.
30.0 - 32.0	2.0	Composite	P-2-5 (30.0-32.0)	Geochemical	Biotite gneiss, migmatized, partly oxidized (limonitic-transition zone from saprolite to fresh rock), with white plagioclase-quartz and dark biotite layers, locally silicified, sericitized, with pink garnet, contains sillimanite, with disseminated pyrite partly oxidized to limonite.
		Chip	P-2-19 (31.0-31.1)	Geochemical	
32.0 - 43.3	11.3	Chips	P-2-5 (35.0-35.2)	X-ray	Quartzite, white, containing fine- to medium-grained quartz and equigranular feldspar layers (maximum to 20 cm thick), with thinner tite and muscovite bands (total about 10%), includes brown flakes and black plates of biotite, with pink garnet and disseminated pyrite (approx. 2%).
			P-2-36 (36.0)	Petrographic	
		Chips	P-2-6 (37.9-38.1)	X-ray	
		Chips	P-2-7 (39.0-39.2)	X-ray	
43.3 - 61.0	17.7	Composite	P-2-8 (43.4-61.0)	Geochemical	Biotite gneiss, migmatized, contorted with ptygmatic microfolds, brecciated, with about 60% biotite-rich layers and about 40% white plagioclase-quartz layers, includes pink garnet porphyroblasts, with sillimanite, locally silicified and sericitic, with disseminated pyrite (approx. 2%) partly oxidized.
			P-2-44 (44.0)	Petrographic	
		Chips	P-2-9 (44.6-44.9)	X-ray	
		Chips	P-2-8 (45.0-45.2)	X-ray	
			P-2-49 (49.0)	Petrographic	
			P-2-53 (53.0)	Petrographic	
			P-2-54 (54.0)	Petrographic	
			P-2-59 (59.0)	Petrographic	
			P-2-61.5 (61.5)	Petrographic	
61.0 - 61.7	0.7	Chips	P-2-20 (61.8-62.0)	Geochemical	Quartz lens, composed of coarse-crystalline, translucent and smoky quartz, feldspar, flakes of brownish biotite, foliated, with disseminated and aggregates of pyrite.
61.7 - 71.0	9.3	Chips	P-2-7 (61.7-71.0)	Geochemical	Biotite gneiss, migmatized, inhomogeneous, with 90% black minerals, mostly biotite, coarse crystalline, with about 10% feldspar and

			P-2-69 (69.0)	Petrographic	plagioclase and quartz; quartz and plagioclase also occur in small lenses and augen (maximum to 3 cm), locally recrystallized, with pyrite (approx. 2%).
71.0 - 82.0	11.0	Composite	P-2-8 (71.0-82.0)	Geochemical	Biotite gneiss, migmatized, with ptygmatic folds, with white feldspathic-quartzose plagioclase and biotite-rich layers (maximum to 2 cm thick), also with microcline quartz augen (maximum to 2 cm), locally silicified, sericitized, with porphyroblasts of pink garnets (as much as 5% rock mass); besides more common brown flakes of biotite; black plates of secondary (?) biotite also occur; includes disseminated (as much as 3%) pyrite in veinlets.
			P-2-75 (75.0)	Petrographic	
82.0 - 83.0	1.0		P-2-82 (82.0)	Petrographic	Quartz and feldspar lens, white, equigranular, with thin discontinuous biotitic layers, clearly foliated, with muscovite plates and small porphyroblasts of garnet.
83.0 - 110.0	27.0	Composite	P-2-9 (83.0-100.0)	Geochemical	Biotite gneiss, with white feldspar and quartz layers (maximum to 5 cm thick), (resembles typical poorly recrystallized quartzite), sericitic (with single disseminated plates of black biotite) and dark biotite-rich, irregular layers, lenses and augen, foliated, contorted, fractured, deformed into ptygmatic folds, with porphyroblasts of pink garnet, locally coarse crystalline, silicified and sericitized, slightly chloritized, with disseminated pyrite in veins (as much as 5%), locally strongly enriched in secondary (?) black biotite.
			P-2-85 (85.0)	Petrographic	
			P-2-87 (87.0)	Petrographic	
			P-2-93 (93.0)	Petrographic	
		Chips	P-2-21 (96.0-96.2)	Geochemical	
			P-2-96.5 (96.5)	Petrographic	
			P-2-97.5 (97.5)	Petrographic	
			P-2-98 (98.0)	Petrographic	
		Composite	P-2-10 (100.0-110.0)	Geochemical	
			P-2-101 (101.0)	Petrographic	
110.0 - 118.8	8.8	Composite	P-2-11 (110.0-118.8)	Geochemical	Biotite gneiss, thin layered, resembles quartzitic and biotite schists, white plagioclase-feldspar and quartzose inhomogeneous porphyroblastic layers (maximum to 2 cm thick), strongly sericitized, with greenish microcline; also form augen and lenses; contains irregularly scattered pink garnet grains and aggregates; white layers are interlayered with dark biotite-rich, thinner but more common layers, locally contorted, ptygmatically folded and foliated; the whole gneissic sequence includes disseminated pyrite (locally as much as 3%), also concentrated (maximum to 2 mm thick stringers)
			P-2-114 (114)	Petrographic	

					along gneissic layers; less common are pyritic veinlets; the gneiss is locally recrystallized and contains much larger (maximum to 5 mm) plates of black, fresh-looking biotite, probably secondary biotite (?); the rock is weakly chloritized.
118.6 - 130.0	11.4	Composite	P-2-12 (118.6-130.0)	Geochemical	Biotite gneiss, thin layered with well preserved sedimentary texture, strongly garnetiferous, quartzitic, with prevailing layers (as much as 90%) white-greenish-gray layers, lenses and augen composed of feldspar-plagioclase and quartz, interlayered with thin, biotite (with brown flakes and about 20% larger black plates), locally migmatized with ptygmatic folds, foliated, with disseminated pyrite irregularly concentrated in veinlets in the entire sequence.
			P-2-120 (120.0)	Petrographic	
		Chips	P-2-10 (120.5- 120.8)	X-ray	
		Chip	P-2-11 (129.8-129.9)	X-ray	
130.0 - 131.0	1.0				Biotite schist, thin layered with quartz-feldspathic-sericitic schist (less than 20% of volume), equigranular, well foliated, with pyrite mostly in fractures.
131.0 - 160.0	29.0	Composite	P-2-13 (130.0-150.7)	Geochemical	Biotite gneiss, with approx. 50/50 white and dark, all almost regularly and weakly migmatized, thin layers, include also lenses, small and large augen (maximum to 3 cm), strongly garnetiferous (mostly with pink poikiloblastic and porphyroblast garnet), feldspathic-plagioclase-quartzose and coarse crystalline microcline (mostly in augen) layers are medium to coarse grained, inhomogeneous, porphyroblastic with sillimanite and kyanite, foliated with biotite-rich layers (with brown flakes and much larger black plates of biotite-secondary?), locally includes muscovite and sericite, partly chloritized and silicified, fractured; the entire interval is pyritic locally as much as 5%), disseminated in stringers and veinlets (maximum to 10 mm thick); original sedimentary features are well preserved, however, locally the gneissic rock is hydrothermally mostly sericitized, chloitized, kaolinized, much more garnetiferous strongly pyritic; in lowest two feet of this interval the gneiss is strongly contorted; white feldspathic-quartzose layers prevail (approx. 65%), with well developed sillimanite and kyanite porphyroblasts; brown biotites prevail over larger plates of black, fresh, secondary (?) biotite by about 95%.
			P-2-134 (134.0)	Petrographic	
			P-2-144 (144.0)	Petrographic	
		Composite	P-2-14 (150.0-160.0)	Geochemical	
			P-2-156 (156.0)	Petrographic	
		Chips	P-2-12 (157.9-158.1)	X-ray	

APPENDIX III

REPRESENTATIVE THIN SECTION DESCRIPTIONS

P-1-61: Biotite-quartz-two feldspar gneiss with a granoblastic foliate texture. Quartz (52 percnet) is the most abundant mineral. It occurs as equant crystals displaying undulatory extinction and polygonization. Cataclasis has produced mortared and ribboned quartz in a dimensionally preferred orientation. Quartz is also present as inclusions in feldspar augen. Plagioclase feldspar (oligoclase, 21 percent) is found as twinned crystals displaying sericite alteration along cleavage planes. Opaque inclusions of graphite within the feldspar and antiperthitic intergrowths along grain margins are common. Potassium feldspar (orthoclase 14 percent) is found as untwinned crystals with quartz and biotite inclusions. Biotite (10 percent), as raggedly terminated laths, defines a lepidoblastic foliation that wraps around feldspar augen. The biotite exhibits chlorite alteration along grain margins. Graphite (2 percent) is found as disseminated grains and as elongate laths intergrown with biotite. Pyrite (1 percent) occurs as disseminated grains. Muscovite is found as unoriented clear laths and as a secondary mineral after feldspar. Epidote, apatite, sphene, and rutile are present in trace amounts.

P-1-75: Biotite-quartz-feldspar gneiss with a pegmatitic texture and a cataclastic overprint. Quartz (34 percent) occurs as undulatory, fractured, recrystallized grains. Twinned oligoclase feldspar (21 percent) is intergrown with quartz. Potassium feldspar (20 percent) occurs as porphyroblasts with biotite and quartz inclusions. It is untwinned and exhibits myrmekitic intergrowths along grain margins. Biotite (16 percent) occurs as raggedly terminated laths that define a lepidoblastic foliation and exhibits pleochroic haloes surrounding inclusions of both zircon and monazite. Chlorite is an alteration product of biotite. Muscovite (8 percent) consists of clear unoriented laths. Trace amounts of calcite, sphene, rutile, zircon, monazite, and graphite are disseminated throughout the matrix.

P-1-103: Migmatitic quartz-feldspar gneiss with a granoblastic texture. Quartz (68 percent) occurs as equant grains exhibiting undulatory extinction, recrystallized aggregate grains, and as inclusions in garnet, biotite, and feldspar. Untwinned potassium feldspar (orthoclase 16 percent) is found as highly sericitized blasts. Oligoclase feldspar (7 percent) is twinned and occurs as relict augen surrounded by perthitic microcline. Biotite (4 percent), as brown laths in lepidoblastic alignment, provides a metamorphic foliation. Muscovite (4 percent) occurs as clear, randomly oriented laths. Pyrite and graphite together comprise approximately 1 percent. Graphite is disseminated throughout as minute grains. Pyrite occurs as discrete disseminated grains and as intrusive vein fillings. Trace minerals include kyanite as slender fractured laths, and epidote, sphene, and apatite as equant scattered grains.

P-1-105: Migmatitic quartz-feldspar-biotite gneiss with a granoblastic foliate texture and a strong cataclastic imprint. Twinned plagioclase feldspar (30 percent) occurs as highly sericitized ovoid grains surrounded by recrystallized micrographic intergrowths of microcline and quartz. Biotite (25 percent) occurs as brown laths in a sublepidoblastic alignment and is partially retrograded to chlorite. Quartz (19 percent) is found as large undulous relict crystals, as granular aggregates, and as inclusions in feldspar and garnet. Some quartz forms mortared rims around feldspar augen. Porphyroblastic garnet (18 percent) occurs as fractured poikiloblasts containing quartz inclusions. Opaque material (5 percent) consists of pyrite, scattered graphite laths, disseminated chalcopyrite, and magnetite with spinel overgrowths. Muscovite (2 percent) occurs as clear laths in random orientation. Muscovite is secondary and appears to have formed at the expense of feldspar. Monazite occurs as highly birefringent clear crystals and as grumous patches. Minerals that occur in trace amounts include kyanite as fractured laths and epidote as discrete scattered grains.

P-1-129: Mylonitic quartz-biotite-feldspar gneiss with a mylonitic ribboned texture and a strong cataclastic overprint. Quartz (53 percent) occurs as resistant crystals displaying undulatory extinction, as recrystallized granular aggregates and as inclusions in feldspar and garnet. Twinned plagioclase feldspar (40 percent) is found as ovoid blasts displaying intense sericitization and saussuritization. Sericite and calcite have filled fractures within the feldspar as replacement veins. Muscovite (4 percent) is present as clear laths in a random orientation. Muscovite is secondary having formed at the expense of feldspar. Biotite (2 percent) occurs as stubby brown laths that have partially retrograded to chlorite. Minerals that occur in trace amounts include clear monazite crystals, disseminated apatite grains, sphene, and graphite as scattered grains.

P-2-49: Equigranular quartz-feldspar gneiss with a granoblastic polygonal texture and a cataclastic overprint. Quartz (72 percent) occurs as elongate grains displaying undulatory extinction, as granular aggregates of recrystallized grains, and as ovoid

inclusions in feldspar. Potassium feldspar (orthoclase 25 percent) occurs as slightly fractured crystals displaying sericitization along cleavage planes. The feldspar blasts contain inclusions of ovoid quartz and biotite laths. Oligoclase (1 percent) is subordinate to potassium feldspar and occurs as equant crystals displaying stress twinning and sericitization along cleavage planes. Muscovite (1 percent), as clear unoriented laths, occurs as a secondary replacement of feldspar. Trace minerals include pyrite and graphite as disseminated grains, monazite as equant crystals, and intergranular calcite.

P-2-54: Coarse-grained migmatitic quartz feldspar gneiss with a granoblastic elongate texture and a mortared and polygonized matrix. Plagioclase feldspar (oligoclase 40 percent) occurs as sericitized, stress-twinned blasts. Quartz (34 percent) is present as both equant crystals displaying undulatory extinction and as recrystallized elongate grains. Quartz also occurs as recrystallized aggregates, mortared fragments, and inclusions in biotite and feldspar. Potassium feldspar (16 percent) occurs as twinned microcline grains surrounded by granular myrmekitic intergrowths of quartz and plagioclase. Porphyroblastic garnet (5 percent) is found as fractured poikiloblasts with biotite and quartz inclusions. Biotite (4 percent), as stubby brown laths, defines a crude foliation with wispy lenses and layers. Biotite contains numerous pleochroic haloes and is partially altered to chlorite and rutile. Trace minerals include disseminated pyrite grains, scattered equant epidote crystals, euhedral zircon crystals, and clear monazite crystals.

P-2-75: Migmatitic quartz-biotite-feldspar gneiss with a granoblastic elongate texture with hydrothermal pyrite veins (Figure 24). Quartz (65 percent) occurs as relict grains displaying undulatory extinction, as polygonized grains and as inclusions in biotite and garnet. Biotite (16 percent) occurs as light-brown laths in lepidoblastic alignment; grain margins are altered to chlorite. Pyrite injection through biotite grains has resulted in a reaction rim consisting of biotite-chlorite-white mica-pyrite. The biotite contains numerous pleochroic haloes with zircon and monazite inclusions. Plagioclase feldspar, oligoclase (8 percent) occurs as stress twinned crystals exhibiting sericitization along cleavage planes. Plagioclase grain margins exhibit myrmekitic intergrowths of microcline and quartz. Garnet (6 percent) occurs as fractured poikiloblastic crystals with biotite and quartz inclusions. Pyrite (4 percent) occurs as discrete scattered grains and as injection veins which cut across all other minerals (Figure 25). Monazite and zircon are found in trace amounts as scattered grains and as inclusions in biotite. Other minerals that occur in trace amounts include epidote and montmorillonite.

Figure 24. Photomicrograph of a quartz-feldspar-biotite-garnet gneiss; biotite exhibits pleochroic haloes (h) due to zircon inclusions (plain light).

P-2-87: Biotite-quartz-feldspar gneiss with a granoblastic elongate texture and cataclastic overprint (Figure 26). Quartz (46 percent) is present as relict crystals displaying undulatory extinction, as recrystallized ribboned lenses, as polygonal aggregates, and as inclusions in biotite, feldspar, and garnet. Plagioclase feldspar, oligoclase (19 percent) occurs as relict grains displaying sericite alteration along cleavage planes. Biotite (17 percent) occurs as brown laths that are partially altered to chlorite. The biotite laths are in lepidoblastic alignment that provides a mica foliation. Monazite (10 percent) is particularly abundant, as clear crystals scattered throughout the groundmass (Figure 27). Muscovite (4 percent) occurs as clear laths in random orientation as a secondary mineral after feldspar. Garnet (3 percent) occurs as poikiloblastic grains with quartz, biotite, and plagioclase inclusions. Minerals that occur in trace amounts include graphite as disseminated grains, pyrite as scattered crystals, and zircon and sphene as scattered equant crystals.

inclusions in feldspar. Potassium feldspar (orthoclase 25 percent) occurs as slightly fractured crystals displaying sericitization along cleavage planes. The feldspar blasts contain inclusions of ovoid quartz and biotite laths. Oligoclase (1 percent) is subordinate to potassium feldspar and occurs as equant crystals displaying stress twinning and sericitization along cleavage planes. Muscovite (1 percent), as clear unoriented laths, occurs as a secondary replacement of feldspar. Trace minerals include pyrite and graphite as disseminated grains, monazite as equant crystals, and intergranular calcite.

P-2-54: Coarse-grained migmatitic quartz feldspar gneiss with a granoblastic elongate texture and a mortared and polygonized matrix. Plagioclase feldspar (oligoclase 40 percent) occurs as sericitized, stress-twinned blasts. Quartz (34 percent) is present as both equant crystals displaying undulatory extinction and as recrystallized elongate grains. Quartz also occurs as recrystallized aggregates, mortared fragments, and inclusions in biotite and feldspar. Potassium feldspar (16 percent) occurs as twinned microcline grains surrounded by granular myrmekitic intergrowths of quartz and plagioclase. Porphyroblastic garnet (5 percent) is found as fractured poikiloblasts with biotite and quartz inclusions. Biotite (4 percent), as stubby brown laths, defines a crude foliation with wispy lenses and layers. Biotite contains numerous pleochroic haloes and is partially altered to chlorite and rutile. Trace minerals include disseminated pyrite grains, scattered equant epidote crystals, euhedral zircon crystals, and clear monazite crystals.

P-2-75: Migmatitic quartz-biotite-feldspar gneiss with a granoblastic elongate texture with hydrothermal pyrite veins (Figure 24). Quartz (65 percent) occurs as relict grains displaying undulatory extinction, as polygonized grains and as inclusions in biotite and garnet. Biotite (16 percent) occurs as light-brown laths in lepidoblastic alignment; grain margins are altered to chlorite. Pyrite injection through biotite grains has resulted in a reaction rim consisting of biotite-chlorite-white mica-pyrite. The biotite contains numerous pleochroic haloes with zircon and monazite inclusions. Plagioclase feldspar, oligoclase (8 percent) occurs as stress twinned crystals exhibiting sericitization along cleavage planes. Plagioclase grain margins exhibit myrmekitic intergrowths of microcline and quartz. Garnet (6 percent) occurs as fractured poikiloblastic crystals with biotite and quartz inclusions. Pyrite (4 percent) occurs as discrete scattered grains and as injection veins which cut across all other minerals (Figure 25). Monazite and zircon are found in trace amounts as scattered grains and as inclusions in biotite. Other minerals that occur in trace amounts include epidote and montmorillonite.

Figure 24. Photomicrograph of a quartz-feldspar-biotite-garnet gneiss; biotite exhibits pleochroic haloes (h) due to zircon inclusions (plain light).

P-2-87: Biotite-quartz-feldspar gneiss with a granoblastic elongate texture and cataclastic overprint (Figure 26). Quartz (46 percent) is present as relict crystals displaying undulatory extinction, as recrystallized ribboned lenses, as polygonal aggregates, and as inclusions in biotite, feldspar, and garnet. Plagioclase feldspar, oligoclase (19 percent) occurs as relict grains displaying sericite alteration along cleavage planes. Biotite (17 percent) occurs as brown laths that are partially altered to chlorite. The biotite laths are in lepidoblastic alignment that provides a mica foliation. Monazite (10 percent) is particularly abundant, as clear crystals scattered throughout the groundmass (Figure 27). Muscovite (4 percent) occurs as clear laths in random orientation as a secondary mineral after feldspar. Garnet (3 percent) occurs as poikiloblastic grains with quartz, biotite, and plagioclase inclusions. Minerals that occur in trace amounts include graphite as disseminated grains, pyrite as scattered crystals, and zircon and sphene as scattered equant crystals.

Figure 25. Photomicrograph of hydrothermal pyrite vein; rock thin section consists of quartz. feldspar, biotite (b), and garnet (g) (plain light).

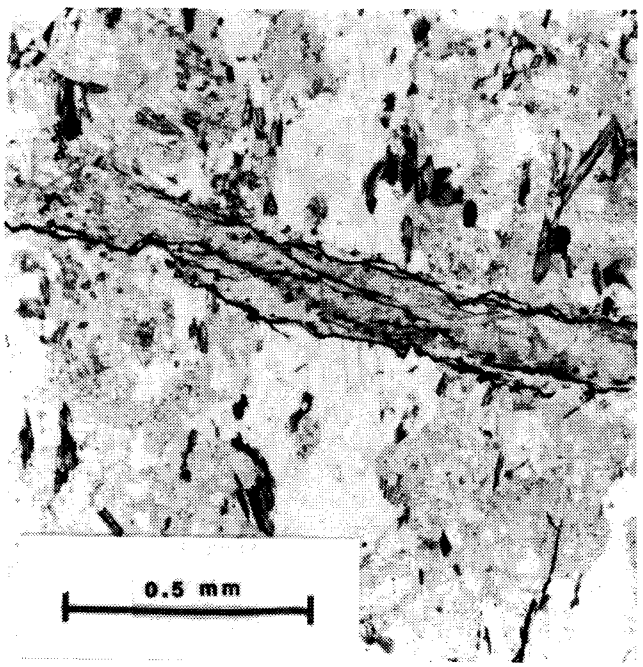

Figure 26. Photomicrograph of microbreccia vein; both the rock and vein are composed of quartz, feldspar, and biotite; brecciation has optically reoriented minerals within the vein (plain light).

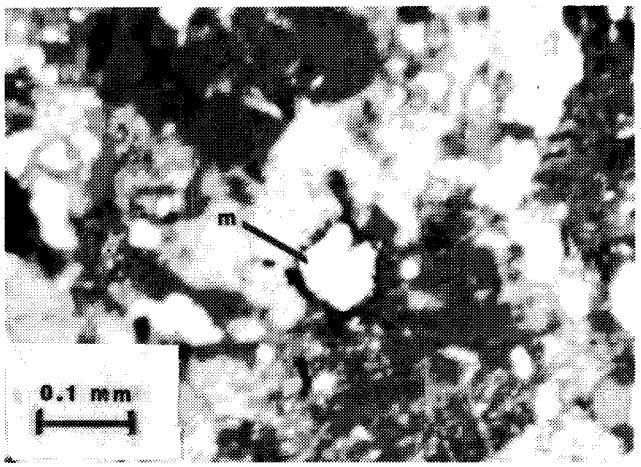

Figure 27. Photomicrograph of monazite crystal in a matrix consisting of sericitized orthoclase and quartz (x-nicols).

P-2-96.5: Quartz-feldspar pegmatite. Plagioclase feldspar (42 percent) occurs as twinned relict grains that are highly sericitized and exhibit antiperthitic intergrowths of orthoclase and quartz along grain margins. Quartz (32 percent) is found as relict and recrystallized grains displaying undulatory extinction, as recrystallized granular aggregates, and as inclusions in feldspar. Potassium feldspar (orthoclase, 11 percent) is found in antiperthitic intergrowths around plagioclase and as untwinned crystals. Muscovite (8 percent) is present as clear laths with mottled coloration. The muscovite is random in orientation and occurs as a secondary mineral after feldspar. Calcite (3 percent) occurs as an intergranular filling. Biotite (1 percent) is found as brown laths in lepidoblastic alignment and is partially altered to chlorite along grain margins. Kyanite (1 percent) occurs as fractured laths. Minerals that occur in trace amounts include graphite and pyrite as disseminated grains, monazite as clear crystals, and sphene.

P-2-120: Quartz-feldspar-biotite migmatite gneiss (Figures 28 and 29). Quartz (45 percent) occurs as large relict undulatory grains, as polygonal aggregates, and as inclusions within biotite, feldspar, and garnet. Some quartz has been recrystallized into elongate shapes (ribboned). Plagioclase feldspar, oligoclase (30 percent) is found as ovoid blasts that are stress-twinned and altered to sericite along cleavage planes. The feldspar blasts are surrounded by myrmekitic intergrowths of quartz and microcline. Biotite (10 percent) occurs as brown laths in lepidoblastic alignment. The biotite has altered to chlorite along grain margins and to amorphous masses of chlorite and rutile. Potassium feldspar

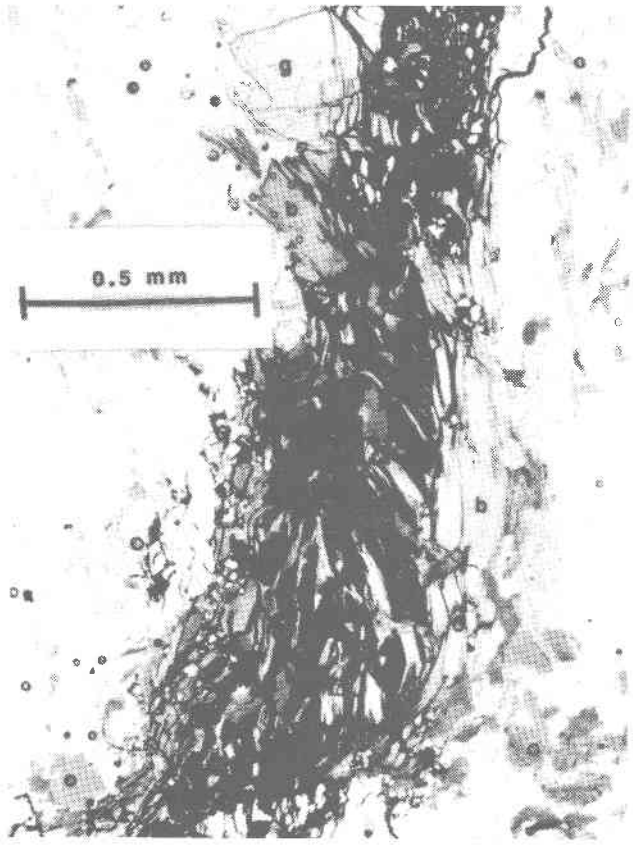

Figure 25. Photomicrograph of hydrothermal pyrite vein; rock thin section consists of quartz. feldspar, biotite (b), and garnet (g) (plain light).

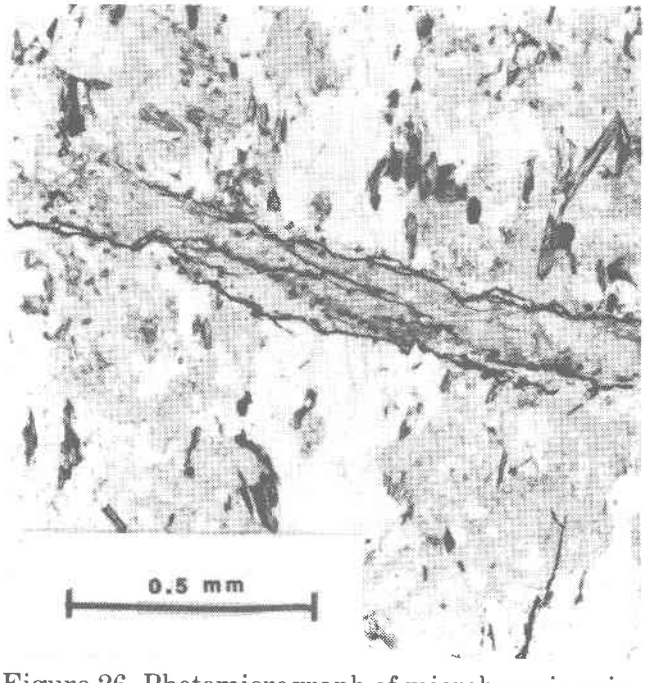

Figure 26. Photomicrograph of microbreccia vein; both the rock and vein are composed of quartz, feldspar, and biotite; brecciation has optically reoriented minerals within the vein (plain light).

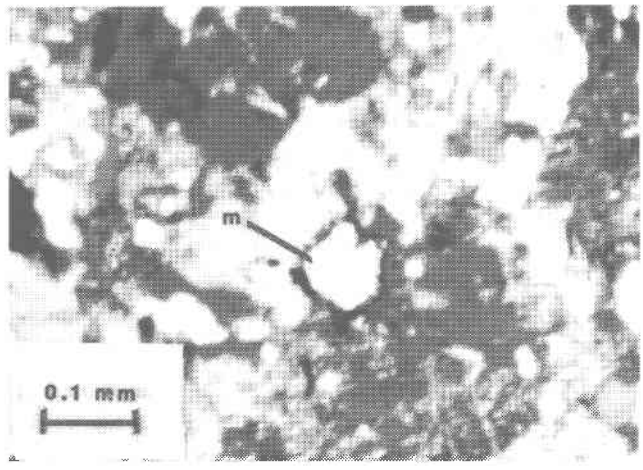

Figure 27. Photomicrograph of monazite crystal in a matrix consisting of sericitized orthoclase and quartz (x-nicols).

P-2-96.5: Quartz-feldspar pegmatite. Plagioclase feldspar (42 percent) occurs as twinned relict grains that are highly sericitized and exhibit antiperthitic intergrowths of orthoclase and quartz along grain margins. Quartz (32 percent) is found as relict and recrystallized grains displaying undulatory extinction, as recrystallized granular aggregates, and as inclusions in feldspar. Potassium feldspar (orthoclase, 11 percent) is found in antiperthitic intergrowths around plagioclase and as untwinned crystals. Muscovite (8 percent) is present as clear laths with mottled coloration. The muscovite is random in orientation and occurs as a secondary mineral after feldspar. Calcite (3 percent) occurs as an intergranular filling. Biotite (1 percent) is found as brown laths in lepidoblastic alignment and is partially altered to chlorite along grain margins. Kyanite (1 percent) occurs as fractured laths. Minerals that occur in trace amounts include graphite and pyrite as disseminated grains, monazite as clear crystals, and sphene.

P-2-120: Quartz-feldspar-biotite migmatite gneiss (Figures 28 and 29). Quartz (45 percent) occurs as large relict undulatory grains, as polygonal aggregates, and as inclusions within biotite, feldspar, and garnet. Some quartz has been recrystallized into elongate shapes (ribboned). Plagioclase feldspar, oligoclase (30 percent) is found as ovoid blasts that are stress-twinned and altered to sericite along cleavage planes. The feldspar blasts are surrounded by myrmekitic intergrowths of quartz and microcline. Biotite (10 percent) occurs as brown laths in lepidoblastic alignment. The biotite has altered to chlorite along grain margins and to amorphous masses of chlorite and rutile. Potassium feldspar

(orthoclase, 9 percent) is found as large poikiloblastic crystals that display antiperthitic vermicular intergrowths along grain margins. Lath-shaped exsolution lamella are common. Muscovite (5 percent) occurs as clear laths in random orientation. Elongate masses of intergrown chlorite, sericite, and biotite are thought to represent retrograded hornblende. Minerals that occur in trace amounts include pyrite as scattered grains and vein fillings, calcite as amorphous intergranular fillings, garnet as fractured poikiloblasts, kyanite as lath shaped crystals, and monazite and epidote as scattered equant grains.

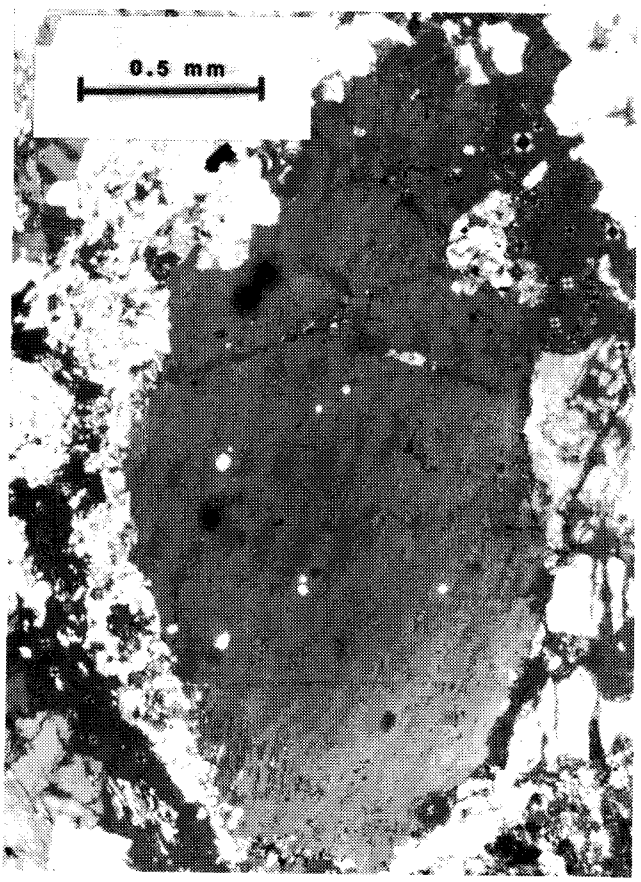

Figure 28. Photomicrograph of orthoclase crystal surrounded by rim of biotite and microcline (x-nicols).

P-2-134: Quartz-biotite-feldspar gneiss with a granoblastic elongate texture and a cataclastic overprint. Quartz (46 percent) occurs as equant crystals displaying undulatory extinction, recrystallized granular aggregates, and as inclusions within biotite, feldspar, and garnet. Recrystallized quartz has formed elongate crystals (ribbons). Garnet (23 percent) occurs as large poikiloblasts with quartz and biotite inclusions. Sericitization has occurred along fractured cleavage planes. Biotite (18 percent) is found as light-brown laths in lepidoblastic alignment and as an alteration product of hornblende. Plagioclase feldspar, oligoclase (9 percent) occurs as porphyroblasts with biotite and quartz inclusions. The porphyroblasts are fractured and have altered to sericite along cleavage planes. Kyanite (2 percent) is present as fractured lath-shaped grains typically intergrown with muscovite. Potassium feldspar (orthoclase, 1 percent) occurs as untwinned porphyroblasts with sericitization along cleavage planes. Minerals that occur in trace amounts include apatite, graphite, pyrite, and muscovite.

Figure 29. Photomicrograph of pyroxene (?) crystal with biotite inclusions; pyroxene replaced by chlorite and talc (plain light).

(orthoclase, 9 percent) is found as large poikiloblastic crystals that display antiperthitic vermicular intergrowths along grain margins. Lath-shaped exsolution lamella are common. Muscovite (5 percent) occurs as clear laths in random orientation. Elongate masses of intergrown chlorite, sericite, and biotite are thought to represent retrograded hornblende. Minerals that occur in trace amounts include pyrite as scattered grains and vein fillings, calcite as amorphous intergranular fillings, garnet as fractured poikiloblasts, kyanite as lath shaped crystals, and monazite and epidote as scattered equant grains.

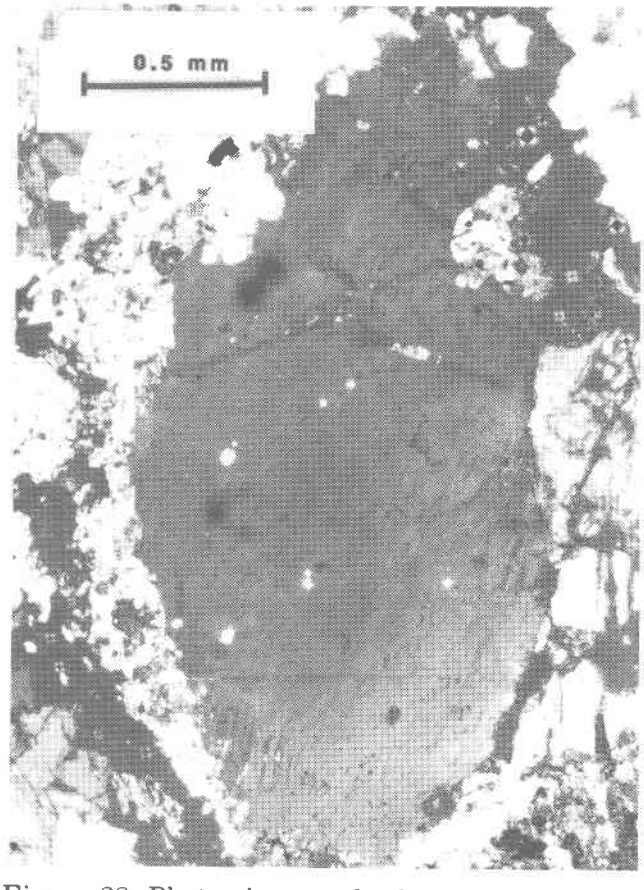

Figure 28. Photomicrograph of orthoclase crystal surrounded by rim of biotite and microcline (x-nicols).

P-2-134: Quartz-biotite-feldspar gneiss with a granoblastic elongate texture and a cataclastic overprint. Quartz (46 percent) occurs as equant crystals displaying undulatory extinction, recrystallized granular aggregates, and as inclusions within biotite, feldspar, and garnet. Recrystallized quartz has formed elongate crystals (ribbons). Garnet (23 percent) occurs as large poikiloblasts with quartz and biotite inclusions. Sericitization has occurred along fractured cleavage planes. Biotite (18 percent) is found as light-brown laths in lepidoblastic alignment and as an alteration product of hornblende. Plagioclase feldspar, oligoclase (9 percent) occurs as porphyroblasts with biotite and quartz inclusions. The porphyroblasts are fractured and have altered to sericite along cleavage planes. Kyanite (2 percent) is present as fractured lath-shaped grains typically intergrown with muscovite. Potassium feldspar (orthoclase, 1 percent) occurs as untwinned porphyroblasts with sericitization along cleavage planes. Minerals that occur in trace amounts include apatite, graphite, pyrite, and muscovite.

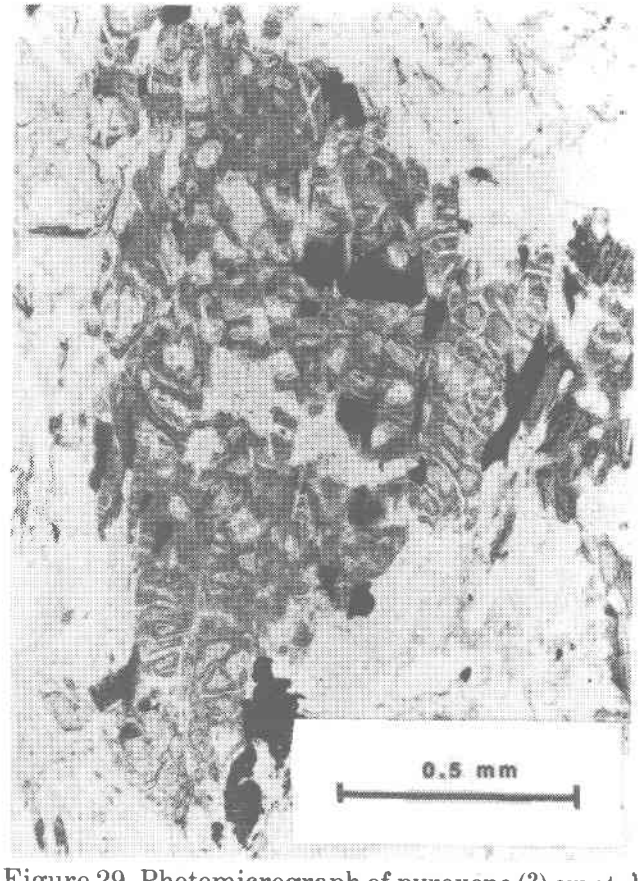

Figure 29. Photomicrograph of pyroxene (?) crystal with biotite inclusions; pyroxene replaced by chlorite and talc (plain light).

COMMONWEALTH OF VIRGINIA
DEPARTMENT OF MINES, MINERALS AND ENERGY
DIVISION OF MINERAL RESOURCES

PUBLICATION 78
GEOCHEMISTRY AND RADIOACTIVITY
IN THE POWHATAN AREA, VIRGINIA

PLATE 1

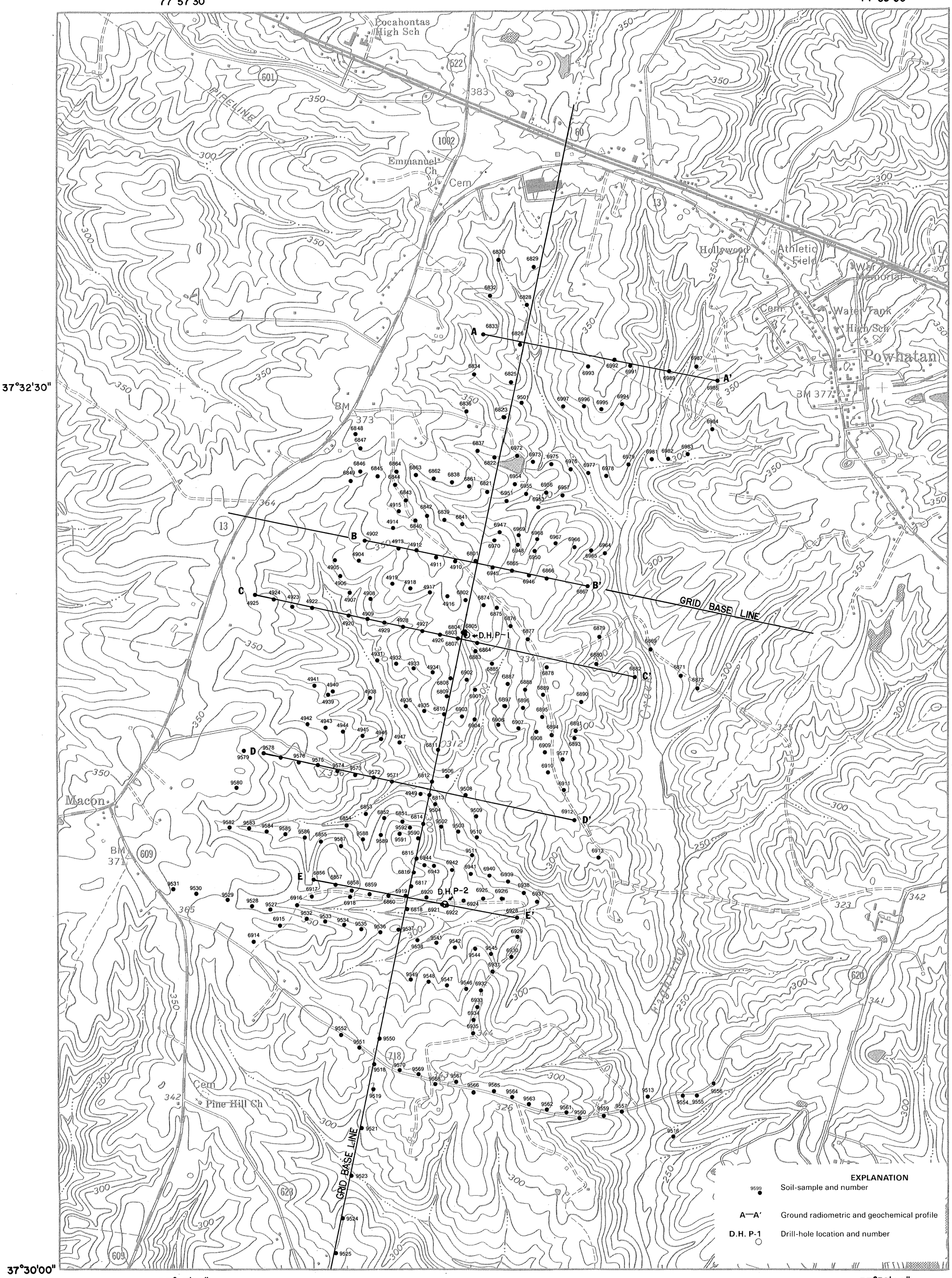

SOIL-SAMPLE AND DRILL-HOLE LOCATIONS IN THE POWHATAN AREA, VIRGINIA

JAN KRASON, STANLEY S. JOHNSON, PATRICK D. FINLEY, AND JOHN D. MARR, JR.

1988

COMMONWEALTH OF VIRGINIA
DEPARTMENT OF MINES, MINERALS AND ENERGY
DIVISION OF MINERAL RESOURCES

PUBLICATION 78
GEOCHEMISTRY AND RADIOACTIVITY
IN THE POWHATAN AREA, VIRGINIA

PLATE 2

77°57'30" 77°55'00" 37°32'30" 37°30'00"

Pocahontas High Sch
Emmanuel Ch
Cem
Hollywood Ch
Athletic Field
War Memorial
Water Tank
High Sch
Powhatan
BM 373
BM 377
Macon
BM 371
Pine Hill Ch
Cem
PIPELINE
GRID BASE LINE
Creek
Highland

EXPLANATION

- 9578 ● Coarse stream sediment and gravel-sample locations and number
- SS17 W10 ⊗ Special coarse, black-coated gravel and water samples and numbers
- W3 × Water sample location and number
- SS10 ○ Special coarse, black-coated gravel samples and number
- SS-1 Special bulk soil sample

SCALE
1 ½ 0 1 MILE
1000 0 1000 2000 3000 4000 5000 6000 7000 FEET

LOCATION OF SUPPLEMENTAL, GRAVEL, BEDROCK, AND WATER SAMPLES IN THE POWHATAN AREA, VIRGINIA

JAN KRASON, STANLEY S. JOHNSON, PATRICK D. FINLEY, AND JOHN D. MARR, JR.
1988

COMMONWEALTH OF VIRGINIA
DEPARTMENT OF MINES, MINERALS AND ENERGY
DIVISION OF MINERAL RESOURCES

PUBLICATION 78
GEOCHEMISTRY AND RADIOACTIVITY
IN THE POWHATAN AREA, VIRGINIA

PLATE 3

77°57'30" 77°55'00" 37°32'30" 37°30'00"

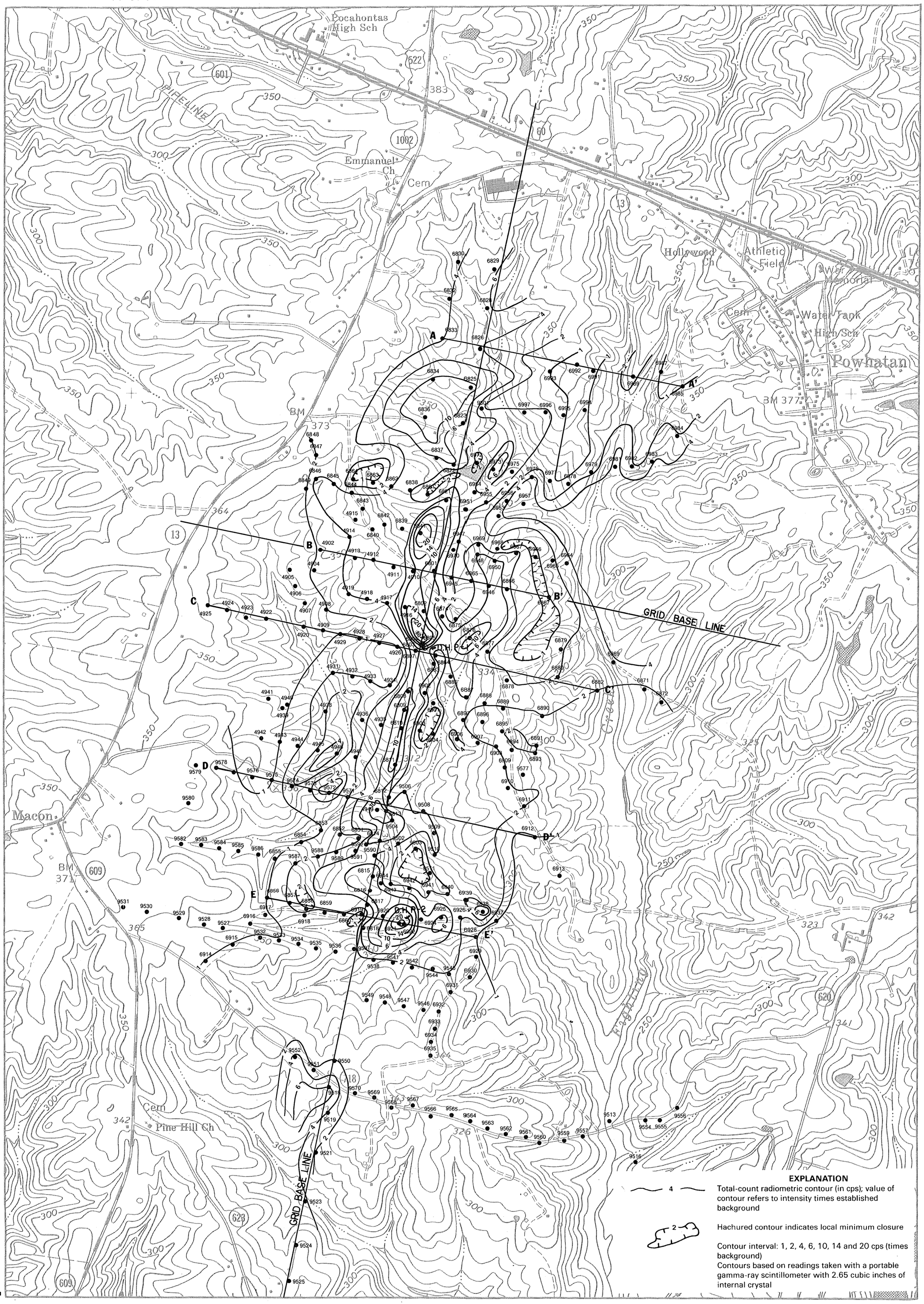

SCALE

1 ½ 0 1 MILE

1000 0 1000 2000 3000 4000 5000 6000 7000 FEET

CONTOUR MAP OF TOTAL-COUNT GROUND RADIOACTIVITY IN THE POWHATAN AREA, VIRGINIA

JAN KRASON, STANLEY S. JOHNSON, PATRICK D. FINLEY, AND JOHN D. MARR, JR.

1988

COMMONWEALTH OF VIRGINIA
DEPARTMENT OF MINES, MINERALS AND ENERGY
DIVISION OF MINERAL RESOURCES

PUBLICATION 78
GEOCHEMISTRY AND RADIOACTIVITY
IN THE POWHATAN AREA, VIRGINIA

PLATE 4

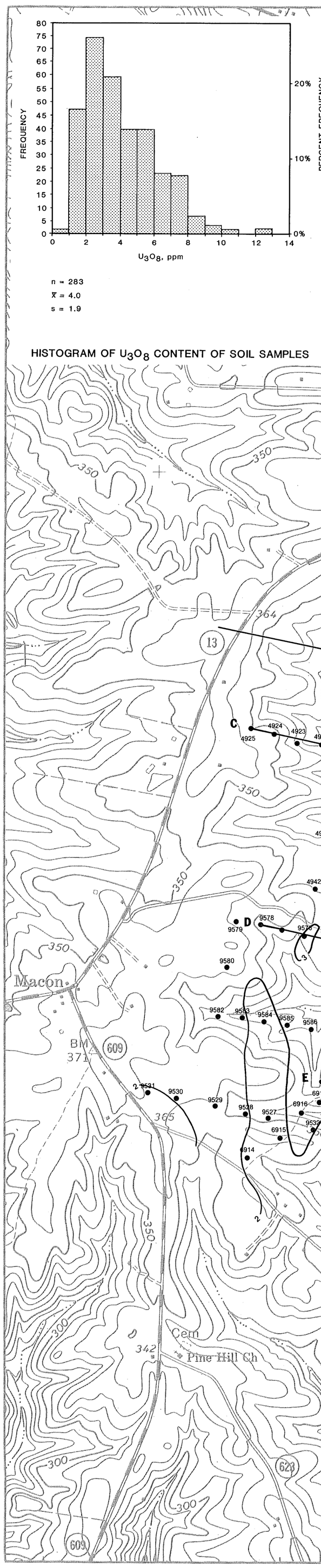

HISTOGRAM OF U_3O_8 CONTENT OF SOIL SAMPLES

77°57'30" 77°55'00" 37°32'30" 37°30'00"

Pocahontas High Sch · Emmanuel Ch · Cem · Hollywood Ch · Athletic Field · War Memorial · Water Tank · High Sch · Powhatan · BM 377 · BM 373 · Macon · BM 371 · Cem · Pine Hill Ch · Highland

A A' B B' C C' D D' E E' D.H.P-1 D.H.P-2 GRID BASE LINE

EXPLANATION

4 — Contour indicating value in ppm (soil values only)

2 — Hachured contour indicates local minimum closure

Contour interval: 1 ppm

SCALE

1 1/2 0 1 MILE

1000 0 1000 2000 3000 4000 5000 6000 7000 FEET

CONTOUR MAP OF URANIUM (U_3O_8) CONCENTRATION IN THE POWHATAN AREA, VIRGINIA

JAN KRASON, STANLEY S. JOHNSON, PATRICK D. FINLEY, AND JOHN D. MARR, JR.

1988

COMMONWEALTH OF VIRGINIA
DEPARTMENT OF MINES, MINERALS AND ENERGY
DIVISION OF MINERAL RESOURCES

PUBLICATION 78
GEOCHEMISTRY AND RADIOACTIVITY
IN THE POWHATAN AREA, VIRGINIA

PLATE 5

HISTOGRAM OF THORIUM CONTENT OF SOIL SAMPLES

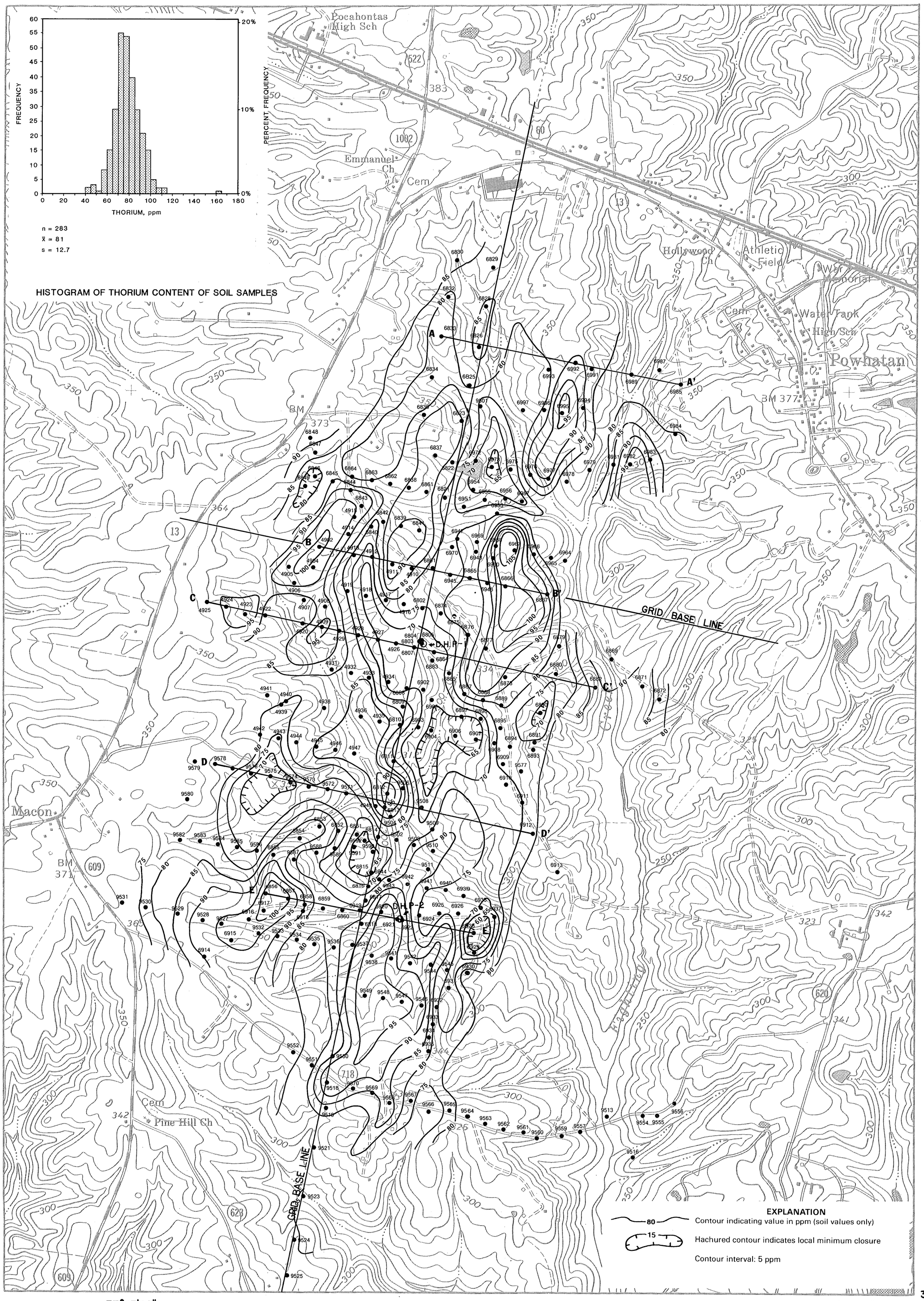

EXPLANATION

80 — Contour indicating value in ppm (soil values only)

15 — Hachured contour indicates local minimum closure

Contour interval: 5 ppm

SCALE

1 ½ 0 1 MILE

1000 0 1000 2000 3000 4000 5000 6000 7000 FEET

CONTOUR MAP OF THORIUM CONCENTRATION IN THE POWHATAN AREA, VIRGINIA

JAN KRASON, STANLEY S. JOHNSON, PATRICK D. FINLEY, AND JOHN D. MARR, JR.

1988

COMMONWEALTH OF VIRGINIA
DEPARTMENT OF MINES, MINERALS AND ENERGY
DIVISION OF MINERAL RESOURCES

PUBLICATION 78
GEOCHEMISTRY AND RADIOACTIVITY
IN THE POWHATAN AREA, VIRGINIA

PLATE 6

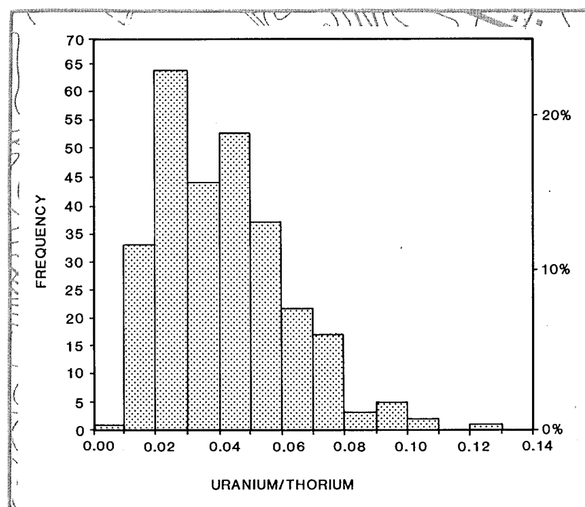

HISTOGRAM OF URANIUM TO THORIUM RATIO OF SOIL SAMPLES

77°57'30" 77°55'00" 37°32'30" 37°30'00"

Pocahontas High Sch
Emmanuel Ch
Cem
Hollywood Ch
Athletic Field
War Memorial
Water Tank
High Sch
Powhatan
BM 377
Macon
BM 371
Cem
Pine Hill Ch
Falling Creek

A A' B B' C C' D D' E E'
D.H.P-1
D.H.P-2
GRID BASE LINE

EXPLANATION
.05 Contour indicating ratio value
.02 Hachured contour indicates local lowest ratio values
Contour interval: .01

SCALE
1 MILE
7000 FEET

CONTOUR MAP OF THE RATIO OF URANIUM TO THORIUM IN THE POWHATAN AREA, VIRGINIA

JAN KRASON, STANLEY S. JOHNSON, PATRICK D. FINLEY, AND JOHN D. MARR, JR.
1988

COMMONWEALTH OF VIRGINIA
DEPARTMENT OF MINES, MINERALS AND ENERGY
DIVISION OF MINERAL RESOURCES

PUBLICATION 78
GEOCHEMISTRY AND RADIOACTIVITY
IN THE POWHATAN AREA, VIRGINIA

PLATE 7

HISTOGRAM OF THORIUM TO URANIUM RATIO OF SOIL SAMPLES

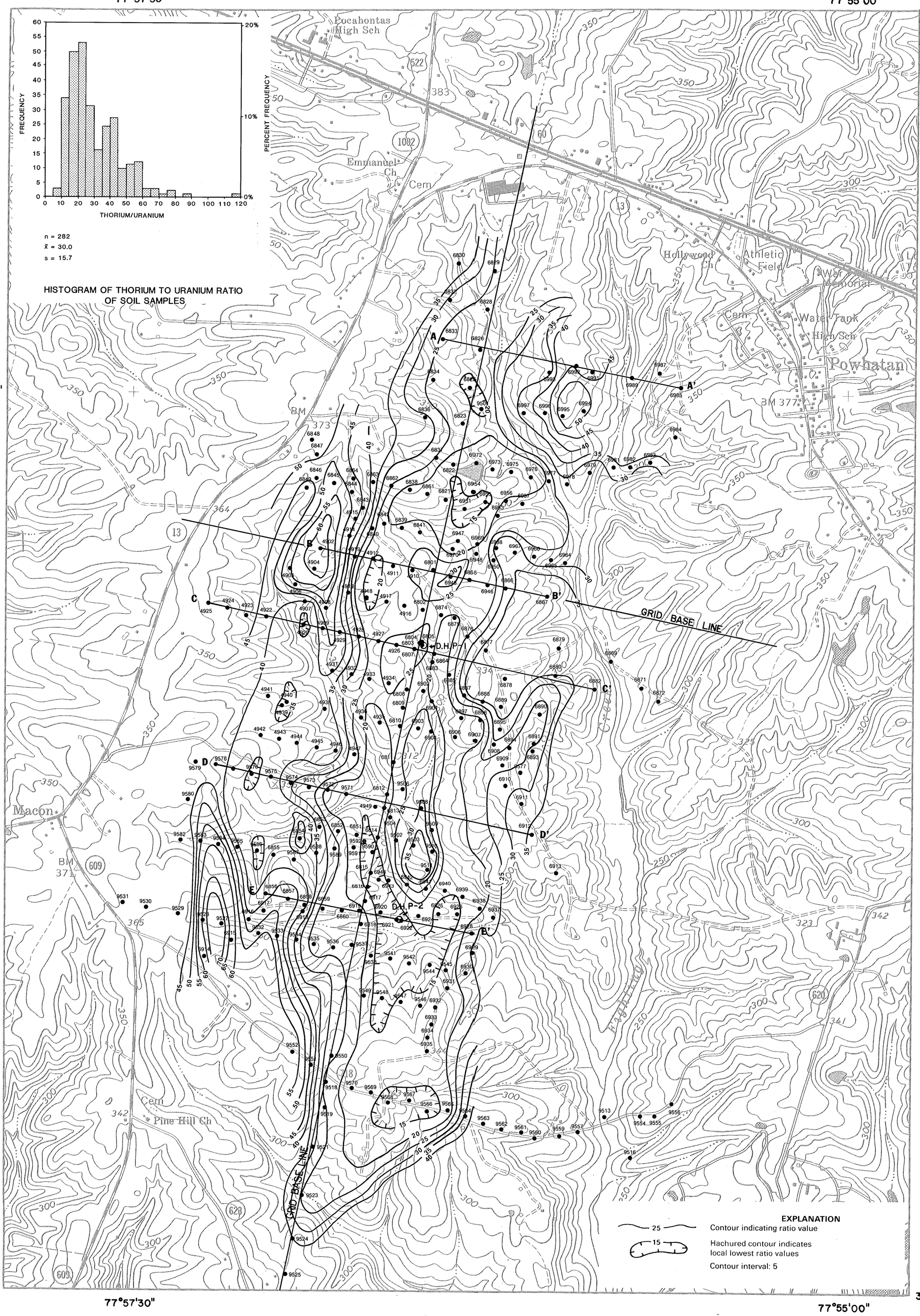

SCALE

1 MILE

1000 0 1000 2000 3000 4000 5000 6000 7000 FEET

CONTOUR MAP OF THE RATIO OF THORIUM TO URANIUM IN THE POWHATAN AREA, VIRGINIA

JAN KRASON, STANLEY S. JOHNSON, PATRICK D. FINLEY, AND JOHN D. MARR, JR.

1988

COMMONWEALTH OF VIRGINIA
DEPARTMENT OF MINES, MINERALS AND ENERGY
DIVISION OF MINERAL RESOURCES

PUBLICATION 78
GEOCHEMISTRY AND RADIOACTIVITY
IN THE POWHATAN AREA, VIRGINIA

PLATE 8

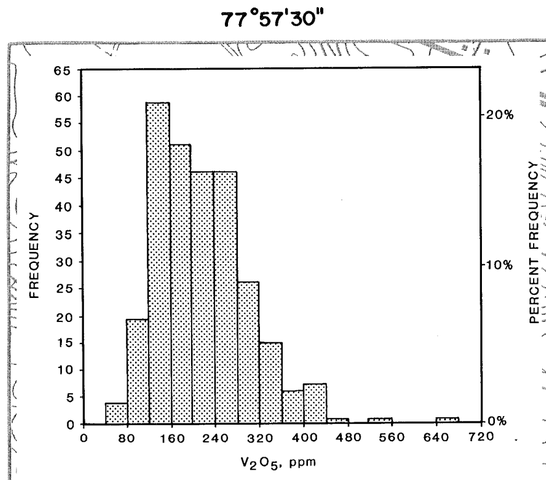

HISTOGRAM OF V_2O_5 CONTENT OF SOIL SAMPLES

77°57'30" 77°55'00" 37°32'30" 37°30'00"

Pocahontas High Sch · Emmanuel Ch · Cem · Hollywood Ch · Athletic Field · War Memorial · Water Tank · High Sch · Powhatan · Macon · Pine Hill Ch · Cem · BM 373 · BM 377 · BM 371 · Creek · Highland

A A' B B' C C' D D' E E' D.H.P-1 D.H.P-2

GRID BASE LINE

EXPLANATION

80 — Contour indicating value in ppm (soil values only)

40 — Hachured contour indicates local minimum closure

Contour interval: 40 ppm

SCALE

1 MILE 0 1/2 1

1000 0 1000 2000 3000 4000 5000 6000 7000 FEET

CONTOUR MAP OF VANADIUM (V_2O_5) CONCENTRATION IN THE POWHATAN AREA, VIRGINIA

JAN KRASON, STANLEY S. JOHNSON, PATRICK D. FINLEY, AND JOHN D. MARR, JR.

1988

COMMONWEALTH OF VIRGINIA
DEPARTMENT OF MINES, MINERALS AND ENERGY
DIVISION OF MINERAL RESOURCES

PUBLICATION 78
GEOCHEMISTRY AND RADIOACTIVITY
IN THE POWHATAN AREA, VIRGINIA

PLATE 9

HISTOGRAM OF COBALT CONTENT OF SOIL SAMPLES

77°57'30" 77°55'00" 37°32'30" 37°30'00"

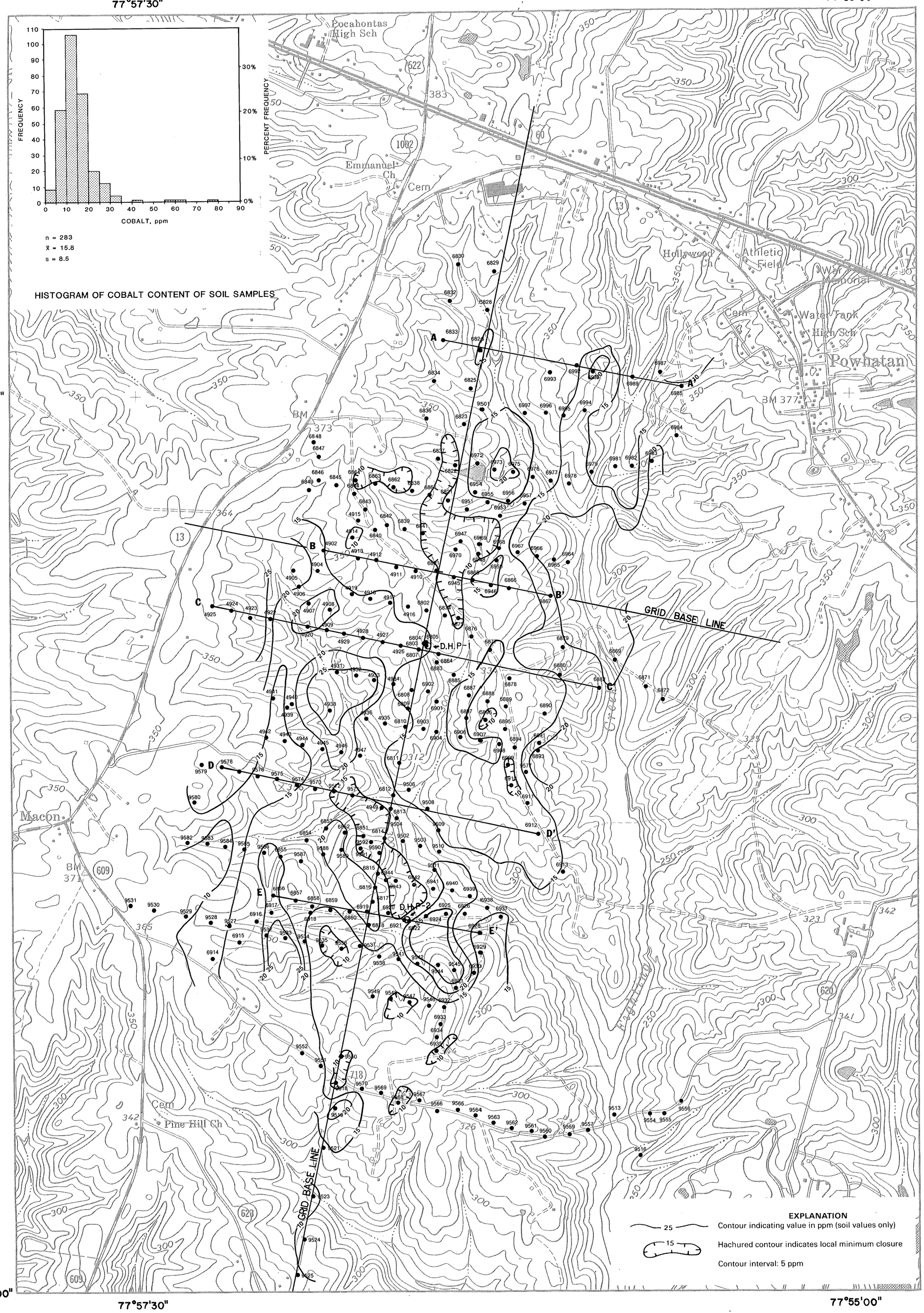

EXPLANATION

25 — Contour indicating value in ppm (soil values only)

15 — Hachured contour indicates local minimum closure

Contour interval: 5 ppm

SCALE

1 MILE 0 1/2 1

1000 0 1000 2000 3000 4000 5000 6000 7000 FEET

CONTOUR MAP OF COBALT CONCENTRATION IN THE POWHATAN AREA, VIRGINIA

JAN KRASON, STANLEY S. JOHNSON, PATRICK D. FINLEY, AND JOHN D. MARR, JR.

1988